MSC-PA-R-69-1
SUPPLEMENT 2

NATIONAL AERONAUTICS AND SPACE ADMINISTRATION

APOLLO 8 MISSION REPORT
SUPPLEMENT 2

GUIDANCE, NAVIGATION, AND CONTROL SYSTEM PERFORMANCE ANALYSIS

MANNED SPACECRAFT CENTER
HOUSTON, TEXAS
NOVEMBER 1969

MSC-PA-R-69-1
Supplement 2

APOLLO 8 MISSION REPORT

SUPPLEMENT 2

GUIDANCE, NAVIGATION, AND CONTROL SYSTEM PERFORMANCE ANALYSIS

PREPARED BY

TRW Systems Group

APPROVED BY

James A. McDivitt
Manager, Apollo Spacecraft Program

NATIONAL AERONAUTICS AND SPACE ADMINISTRATION
MANNED SPACECRAFT CENTER
HOUSTON, TEXAS
November 1969

PROJECT TECHNICAL REPORT

TASK E-38B

APOLLO VIII GUIDANCE, NAVIGATION AND CONTROL SYSTEM PERFORMANCE ANALYSIS FINAL REPORT

NAS 9-8166

15 APRIL 1969

Prepared for
NATIONAL AERONAUTICS AND SPACE ADMINISTRATION
MANNED SPACECRAFT CENTER
HOUSTON, TEXAS

Approved by 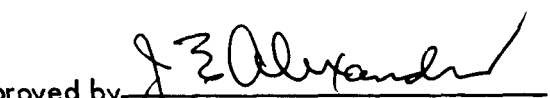

J. E. Alexander, Manager
Guidance and Control
Systems Department

TRW
SYSTEMS GROUP

CONTENTS

		Page
1.0	INTRODUCTION	1-1
	1.1 General	1-1
	1.2 Background	1-2
2.0	SUMMARY	2-1
3.0	IMU PERFORMANCE	3-1
	3.1 Ascent and TLI Velocity Comparisons	3-1
	3.2 Free Flight Performance of Gyros and Accelerometers	3-17
4.0	GNCS TVC DAP Performance	4-1
	4.1 Pitch and Yaw Attitude Errors	4-1
	4.2 Velocity Residuals	4-1
	4.3 Engine Gimbal Trim	4-2
	4.4 Roll TVC DAP Activity	4-2
	4.5 Time Determination	4-3
5.0	DAP ATTITUDE CONTROL	5-1
	5.1 RCS Translation (Translunar)	5-1
	5.2 Auto Maneuvers	5-2
6.0	PASSIVE THERMAL CONTROL	6-1
7.0	ONBOARD NAVIGATION/OPTICS	7-1
	7.1 Midcourse Navigation	7-1
	7.2 Lunar Landmark Tracking	7-3
8.0	ENTRY EVALUATION	8-1
	8.1 Entry DAP Performance	8-1
	8.2 Entry Monitor System	8-3
APPENDIX A		
	ANALYTIC METHODOLOGY	A-1
REFERENCES		R-1

TABLES

		Page
3.1-1	IMU System Errors	3-2
3.2-1	Gyro Torquing Angles	3-19
3.2-2	Gyro Drift Summary	3-21
3.2-3	Gyro Torquing Residuals	3-22
3.2-4	PIPA Bias Summary	3-29
4-1	Ullage Rates and Attitude Errors for SPS Burns	4-4
4-2	Velocity-to-be-gained and Velocity Residuals for SPS Burns	4-5
4-3	Engine Gimbal Trims	4-6
4-4	SPS Burn Data	4-7
7-1	Star-Horizon Sightings	7-5
8-1	RCS Fuel Consumption for Apollo 8 Entry	8-5
A-1	IMU Error Sources	A-12

FIGURES

		Page
3.1.1	Ascent Velocity Comparison GNCS Minus Edited S-IVB IU/TM X-Axis	3-3
3.1.2	Ascent Velocity Comparison GNCS Minus Edited S-IVB IU/TM Y-Axis	3-4
3.1.3	Ascent Velocity Comparison GNCS Minus Edited S-IVB IU/TM Z-Axis	3-5
3.1.4	TLI Velocity Comparison GNCS Minus Edited S-IVB IU/TM X-Axis	3-6
3.1.5	TLI Velocity Comparison GNCS Minus Edited S-IVB IU/TM Y-Axis	3-7
3.1.6	TLI Velocity Comparison GNCS Minus Edited S-IVB IU/TM Z-Axis	3-8
3.1.7	Ascent Velocity Residual Errors; Corrected GNCS Minus Edited S-IVB IU/TM X-Axis	3-9
3.1.8	Ascent Velocity Residual Errors; Corrected GNCS Minus Edited S-IVB IU/TM Y-Axis	3-10
3.1.9	Ascent Velocity Residual Errors; Corrected GNCS Minus Edited S-IVB IU/TM Z-Axis	3-11
3.1-10	TLI Velocity Residual Errors; Corrected GNCS Minus Edited S-IVB IU/TM X-Axis	3-12
3.1-11	TLI Velocity Residual Errors; Corrected GNCS Minus Edited S-IVB IU/TM Y-Axis	3-13
3.1-12	TLI Velocity Residual Errors; Corrected GNCS Minus Edited S-IVB IU/TM Z-Axis	3-14
3.2-1	Accumulated X PIPA Counts During Free Flight	3-23
3.2-2	Accumulated Y PIPA Counts During Free Flight	3-25
3.2-3	Accumulated Z PIPA Counts During Free Flight	3-27
4-1	LOI 1; AK0 (roll attitude error)	4-8
4-2	LOI 1; AK1 (pitch attitude error)	4-9

FIGURES (Continued)

		Page
4-3	LOI 1; AK2 (yaw attitude error)	4-10
4-4	LOI 1; PACTOFF (pitch trim angle)	4-11
4-5	LOI 1; PCMD and CH3517H (pitch gimbal position)	4-12
4-6	LOI 1; YACTOFF (yaw trim angle)	4-13
4-7	LOI 1; YCMD and CH3518H (yaw gimbal position)	4-14
4-8	TEI; AK0 (roll attitude error)	4-15
4-9	TEI; AK1 (pitch attitude error)	4-16
4-10	TEI; AK2 (yaw attitude error)	4-17
4-11	TEI; PACTOFF	4-18
4-12	TEI; PCMD and CH3517H (pitch gimbal position)	4-19
4-13	TEI; YACTOFF (yaw trim angle)	4-20
4-14	TEI; YCMD and CH3518H (pitch gimbal position)	4-21
4-15	LOI 1; Pitch Gimbal Position (CH3517H)	4-22
4-16	LOI 1; Yaw Gimbal Position (CH3518H).	4-23
4-17	TEI; Pitch Gimbal Position (CH3517H)	4-24
4-18	TEI; Yaw Gimbal Position (CH3518H).	4-25
5-1	X-Axis Attitude Hold - Trimming of MCC1 ΔV Residuals	5-5
5-2	Y-Axis Attitude Hold - Trimming of MCC1 ΔV Residuals	5-7
5-3	Z-Axis Attitude Hold - Trimming of MCC1 ΔV Residuals	5-9
5-4	X-Axis Attitude Hold - Transearth Mid-course Correction	5-11

FIGURES (Continued)

		Page
5-5	Y-Axis Attitude Hold - Transearth Mid-course Correction	5-13
5-6	Z-Axis Attitude Hold - Transearth Mid-course Correction	5-15
5-7	Automatic Maneuver; 0.5 deg/sec, CDU Angle	5-17
5-8	Automatic Maneuver, 0.5 deg/sec Body Rates	5-18
5-9	Automatic Maneuver, 0.2 deg/sec, CDU Angles	5-19
5-10	Automatic Maneuver, 0.2 deg/sec Body Rates	5-20
5-11	DAP Attitude Hold - X Axis (Narrow Deadband)	5-21
5-12	DAP Attitude Hold - Y Axis (Narrow Deadband)	5-22
5-13	DAP Attitude Hold - Z Axis (Narrow Deadband)	5-23
6-1	Coning Angles During PTC, Pitch and Yaw Axes Free	6-3
6-2	Coning Angles During PTC, Pitch and Yaw Axes Free	6-4
6-3	Coning Angles During PTC, Pitch and Yaw Axes Maximum Deadband, High Rate Attitude Hold	6-5
8-1	Roll Command/Roll Angle Histories for Apollo 8	8-6
8-2	Pitch Rate Measurements and Jet Activity - Apollo 8 Entry.	8-7
8-3	Entry Monitor System G/V Trace for Apollo 8	8-9
A-1	Configuration for Processing Basic Data Sources	A-2
A-2	Configuration for Correcting, Comparing and Analyzing Boost Guidance Data	A-5
A-3	Configuration for Correcting, Comparing and Analyzing Burn Data	A-9

1.0 INTRODUCTION

1.1 GENERAL

This report presents the final analyses of the inflight performance of the Guidance, Navigation and Control system of the AS-503/CSM-103/ Apollo 8 spacecraft and is intended as a supplement to the MSC Mission Report for Apollo 8. Preparation and submittal of this report were accomplished under MSC/TRW Task E-38B, "Guidance and Control Test Analysis." Contributions to the analyses were made under MSC/TRW Task E-72, "Guidance and Control Analysis" and MSC/TRW TAsk A-50, "Trajectory Reconstruction." Specifically, Sections 4.0; GNCS TVC Performance, Section 5.0; DAP Attitude Control, and Section 8.0; Entry Analysis were prepared by Task E-72 personnel. In addition, some of the E-72 analysis was included in Section 7.0; Onboard Navigation/Optics. The inertial system evaluation and trajectory reconstruction tasks are highly interdependent, and Task A-50 personnel contributed significantly to Section 3.0.

Section 3.0 includes the determination of error sources present in the Apollo 8 Inertial Measurement Unit (IMU) during the flight. A description of the IMU error parameters considered appear in Table A-1. The parameters examined include platform misalignments, gyro and accelerometer errors and accelerometer mounting errors. The error values were derived from comparing the CSM navigation state vectors with the S-IVB IU guidance data during boost and TLI.

Sections 4.0 and 5.0 present detailed analyses of the TVC DAP and the Attitude Control DAP.

Section 6.0 contains an analysis of Passive Thermal Control vehicle stability during translunar and transearth coasting flight.

Section 7.0 contains analyses of midcourse navigation based on SXT sightings and lunar landmark tracking using the SXT and SCT.

Section 8.0 contains final analyses of the Entry DAP and EMS.

1.2 BACKGROUND

The purpose of the Apollo 8 mission was to satisfy CSM development and verification objectives not accomplished on previous missions and to gain experience in manned operations in deep space and lunar orbit. Overall spacecraft performance data and mission event times are presented in the MSC Mission Report for Apollo 8.

2.0 SUMMARY

The inertial subsystem performance was excellent throughout the mission. The IMU remained powered up during translunar and transearth flight and considerable data was obtained on IMU free flight drift characteristics and PIPA bias stability. Numerous realignments were accomplished providing a sample of data points adequate for statistical analysis of the alignment process. Analysis indicated an RMS error of approximately 0.03 degrees per axis which is a 3 sigma MEI specification values (40 sec = 1σ). No impact on mission performance was observable as a result of these errors. PIPA bias data was extremely stable with detectable shifts in the order of 1/7 to 1/10 of the MEI flight stability specification (1σ = 0.2 cm/sec^2).

The inertial subsystem performance parameters during powered flight were determined by standard velocity comparison techniques using boost and translunar injection data. A set of error terms for each phase was derived which provided a satisfactory fit to the observed performance of the system.

Midcourse navigation using optics was successfully demonstrated in cislunar flight (star-horizon) and lunar landmark tracking was successfully accomplished. Although midcourse navigation was not required during the transearth phase of flight, uninterrupted MSFN coverage being available, postflight studies have established that the sightings were sufficiently accurate to allow the crew to autonomously navigate to safe entry conditions. Numerous SXT measurements were conducted using the earth and lunar horizons. Star-earth horizon data indicated bias errors of 10 sec and random errors of 18 sec, both within the 3 sigma MEI system specifications. Bias errors for star-lunar horizon sightings were considerably higher, approximately 72 sec, apparently the result of one or a combination of the following: (1) error in

assumed lunar radius; (2) inability of the observer to define a true horizon due to terrain irregularities. Analysis of this lunar horizon bias is continuing. As expected, the random errors for star-lunar sightings were generally the same as the star-earth horizon measurements. Although approximately 200 measurements were made, there was not enough data to establish any positive trends as in correlation of measurement accuracy with star brightness, distance from the body being viewed, etc. Without any editing of the measurements, the residuals indicate that the accuracy of measurements using stars of 1.5 magnitude and brighter was twice that using stars less bright. However, many accurate measurements were still made using dim stars. There was also indication of growing inaccuracy with time which could be attributed to astronaut fatigue, however, some accurate measurements were accomplished later in the mission.

Performance of all phases of DAP were excellent. During SPS thrusting, attitude errors in the pitch and yaw axes were never greater than one-half degree. An unexplained roll disturbance torque was present during the LOI and TEI burns possibly the result of cg migration, however, the specific cause has not yet been established. The roll torque (3.5 ft/lb)resulted in 0.45 lbs of RCS propellant usage during LOI 1 and 0.36 lb of propellant during TEI. Attitude Control DAP Performance during attitude maneuvers and attitude hold was excellent. Automatic control of the spacecraft for, entry stabilization was successfully accomplished. As has been experienced on previous flights, the number of jet firings at low mach numbers was significantly higher than predicted by preflight entry simulations. Propellant margins were adequate for the flight considering the disparity between expected and actual flight performance.

Passive Thermal Control using the X-axis roll up with the spacecraft in SCS minimum impulse mode (no continuous control system) was initiated during both the translunar and transearth periods. In the

translunar configuration the "coning" built up to an intolerable angle after 30 minutes, and in the transearth configuration limits were approached after 40 minutes. Additional RCS propellant was required to re-initialize the mode. For the majority of the PTC, the attitude control mode was configured for SCS maximum deadband high rate attitude hold in pitch and yaw. Based on the data reviewed, it appears that the SCS free drift mode has little or no advantage over the SCS attitude hold.

3.0 IMU PERFORMANCE

Analysis of the Apollo 8 IMU is contained in Sections 3.1 and 3.2. Section 3.1 presents the results of an error analysis performed for the ascent phase and the translunar insertion phase. The analysis was accomplished in part using the methodology outline in Appendix A. Section 3.2 presents PIPA bias data and platform drift data evaluated from the long periods of coasting flight available from Apollo 8.

3.1 ASCENT AND TLI VELOCITY COMPARISONS

Analysis of the Apollo 8 GεC system accuracy was based on the determination of a common set of errors which resulted in small residuals for both the boost to orbit phase and the translunar insertion phase. At the same time, several constraints were imposed on the errors used. The bias values for accelerometers and gyros were forced to be in close agreement with inflight determined values and other error terms which were preflight calibrated, were chosen to agree favorably with calibration histories. Due to various physical factors such as actual acceleration sensitive parameter shifts during the boost phase and some degradation of the reference data between the two flight phases (3 hours of drift between ascent and TLI) it was recognized that all of the above conditions could not be met at all times. Based on engineering judgement the approach pursued was to determine two sets of error sources with minimum variations between the two flight phases. The error terms derived from the analyses are presented in Table 3.1-1, and using these values, the GεN corrected trajectories fit the respective external measurement trajectories.

For each of the two flight phases, two trajectories were generated by MSFN as a basis for comparison. One boost/TLI trajectory was the "Edited S-IVB IU TM" trajectory and the other was the "Final S-IVB Observed Mass Point Trajectory" (OMPT). The trajectory designated "Final S-IVB OMPT" is normally considered the best estimate trajectory for the boost and TLI phases but was rejected due to inconsistencies in the trajectory characteristics throughout the boost phase. Similar problems have been encountered with the OMPT on previous flights and in all cases no reasonable set of errors was found which effected a good boost comparison.

Table 3.1-1. IMU System Errors

Error Source	Preflight Data Mean	Flight Load	Expected Error*	Standard Deviation	Preflight Expected 1σ Bounds Maximum	Minimum	Ascent Output Error Value	TLI Output Error Value	|(Ascent Output Error Value) − (TLI Output Error Value)| / σ	Comments
VOX (ft/sec)	NA	NA	NA	NA	NA	NA	-0.665	-0.169	NA	Not comparable due to state vector update between ascent and TLI.
VOY (ft/sec)	NA	NA	NA	NA	NA	NA	0.558	0.085	NA	
VOZ (ft/sec)	NA	NA	NA	NA	NA	NA	4.26	0.165	NA	
DT (sec)	NA	NA	NA	NA	NA	NA	0.011	0.0102	NA	
ACBX (cm/sec^2)	-0.0013	0	-0.0013	0.20	0.199	-0.201	-0.017	-0.017	NA	Values established from inflight measurements.
ACBY (cm/sec^2)	0.803	0.80	0.003	0.20	0.203	-0.197	0.028	0.028	NA	
ACBZ (cm/sec^2)	0.631	0.60	0.031	0.20	0.231	-0.169	0.0058	0.0058	NA	
SFEX (ppm)	-76	-144	68	116	184	-48	-132	-133	0.0068 σ	
SFEY (ppm)	-329	-329	0	116	116	-116	-11	58	0.6 σ	Insensitive in ascent
SFEZ (ppm)	-200	-201	1	116	117	-115	-53	-65	0.1 σ	
MXAZ (arc sec)	NA	NA	NA	20	20	-20	0	-8	0.32 σ	
MXAY (arc sec)	NA	NA	NA	20	20	-20	-8	20.0	0.6 σ	
MYAZ (arc sec)	NA	NA	NA	20	20	-20	0	-10	0.57 σ	
MYAX (arc sec)	NA	NA	NA	20	20	-20	20	20	0	
MZAY (arc sec)	NA	NA	NA	20	20	-20	6	18	0.6 σ	
MZAX (arc sec)	NA	NA	NA	20	20	-20	-14	-14	0.6 σ	
NBDX (meru)	-0.51	-0.80	0.29	2	2.29	-1.71	-1.33	-1.33	NA	Values established from inflight measurements.
NBDY (meru)	0.34	0.60	-0.26	2	1.74	-2.26	-0.167	-0.167	NA	
NBDZ (meru)	-2.73	-2.7	-0.03	2	1.97	2.03	1.67	1.67	NA	
ADIAX (meru/g)	5.99	-4.1	10.09	8	18.09	2.09	7.6	7.6	0	
ADIAY (meru/g)	-13.88	-12.0	-1.88	8	6.12	-9.88	-1.2	-8.2	0.87 σ	Insensitive in ascent
ADIAZ (meru/g)	27.05	21.7	5.32	8	13.35	-2.65	-9.5	-6.73	0.35 σ	
ADSRAX (meru/g)	-0.95	2.0	-2.95	5.0	2.05	-7.95	-2.45	-2.58	0.026 σ	
ADSRAY (meru/g)	3.94	3.0	0.94	5.0	5.94	-4.06	10.03	6.85	0.64 σ	Insensitive in TLI
ADSRAZ (meru/g)	26.2	30.0	-3.8	5.0	1.2	-8.8	-2.9	-4.23	0.27 σ	
ADOAX (meru/g)	2.52	NA	2.52	2-5**	7.52**	-2.48**	-0.094	-0.136	0.008 σ	
ADOAY (meru/g)	2.28	NA	2.28	2-5**	7.88**	-2.72**	3.86	3.2	0.13 σ	
ADOAZ (meru/g	0.36	NA	0.36	2-5**	5.36**	-4.64**	-11.2	-10.3	0.22 σ	
MLMX (arc sec)	NA	NA	NA	50***	50***	-50***	93	102	NA	Not comparable. TLI values based on platform misalignment and 2 hours drift before TLI.
MLMY (arc sec)	NA	NA	NA	50***	50***	-50***	-40	-261	NA	
MLMZ (arc sec)	NA	NA	NA	500***	500***	-500***	-10	235	NA	

*Data mean minus flight load.

**Recent unofficial measurements by MIT.

***Boost phase only.

NA = not applicable

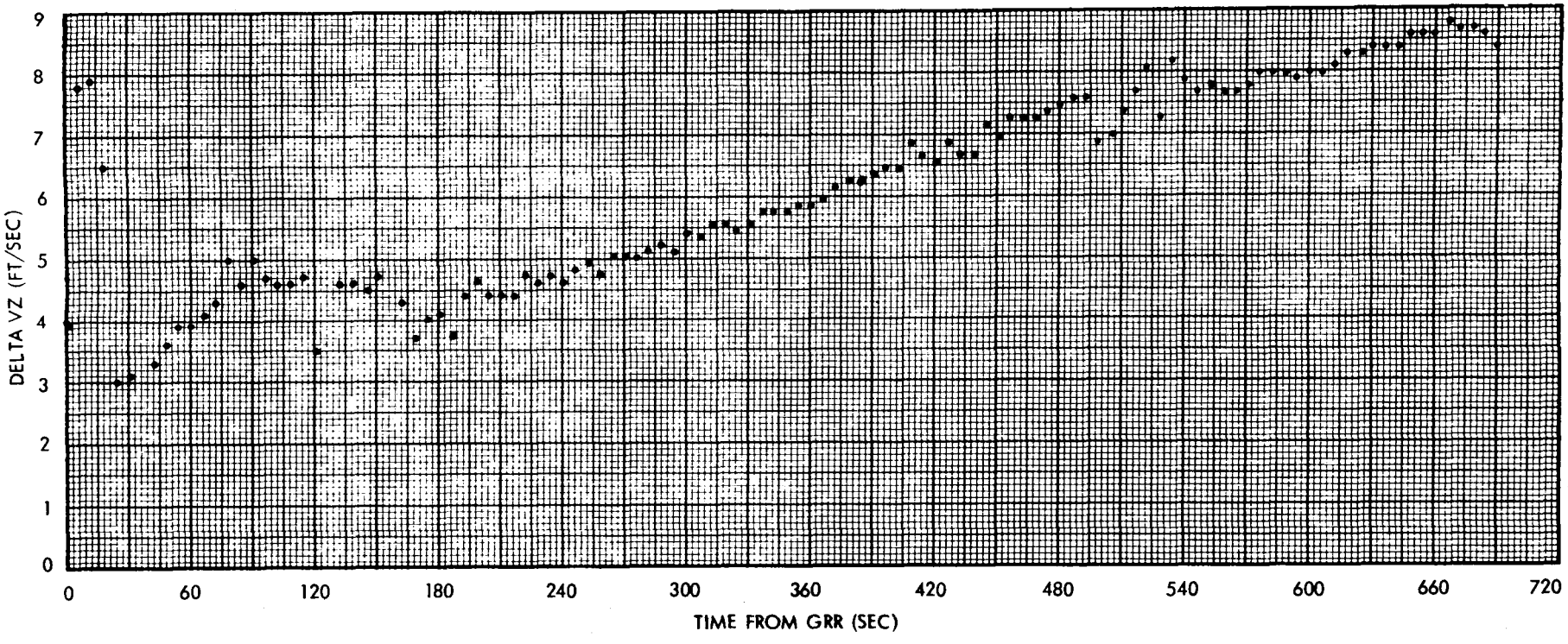

Figure 3.1-1. Ascent Velocity Comparison GNCS Minus Edited S-IVB IU/TM X-Axis

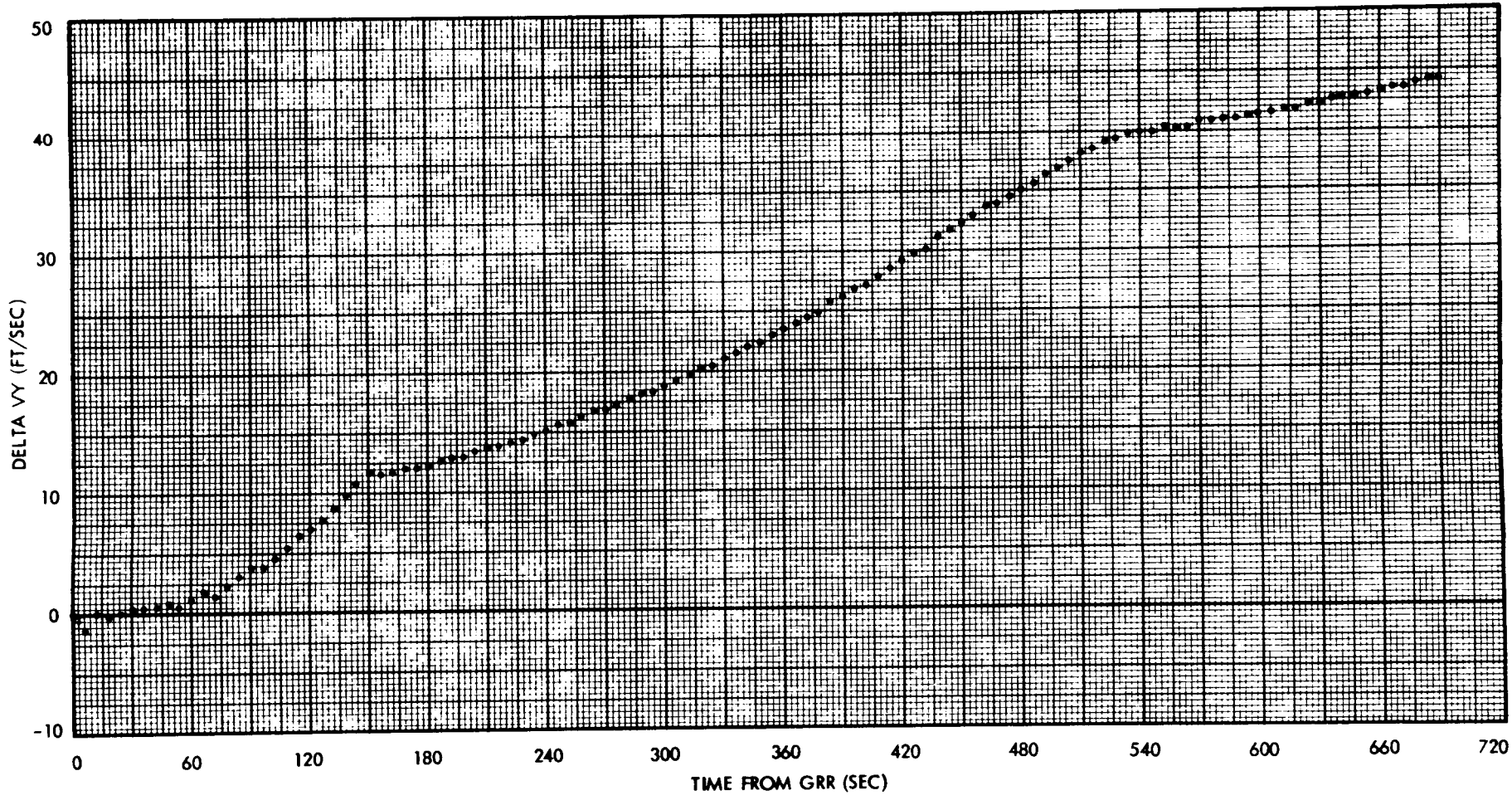

Figure 3.1-2. Ascent Velocity Comparison GNCS Minus Edited S-IVB IU/TM Y-Axis

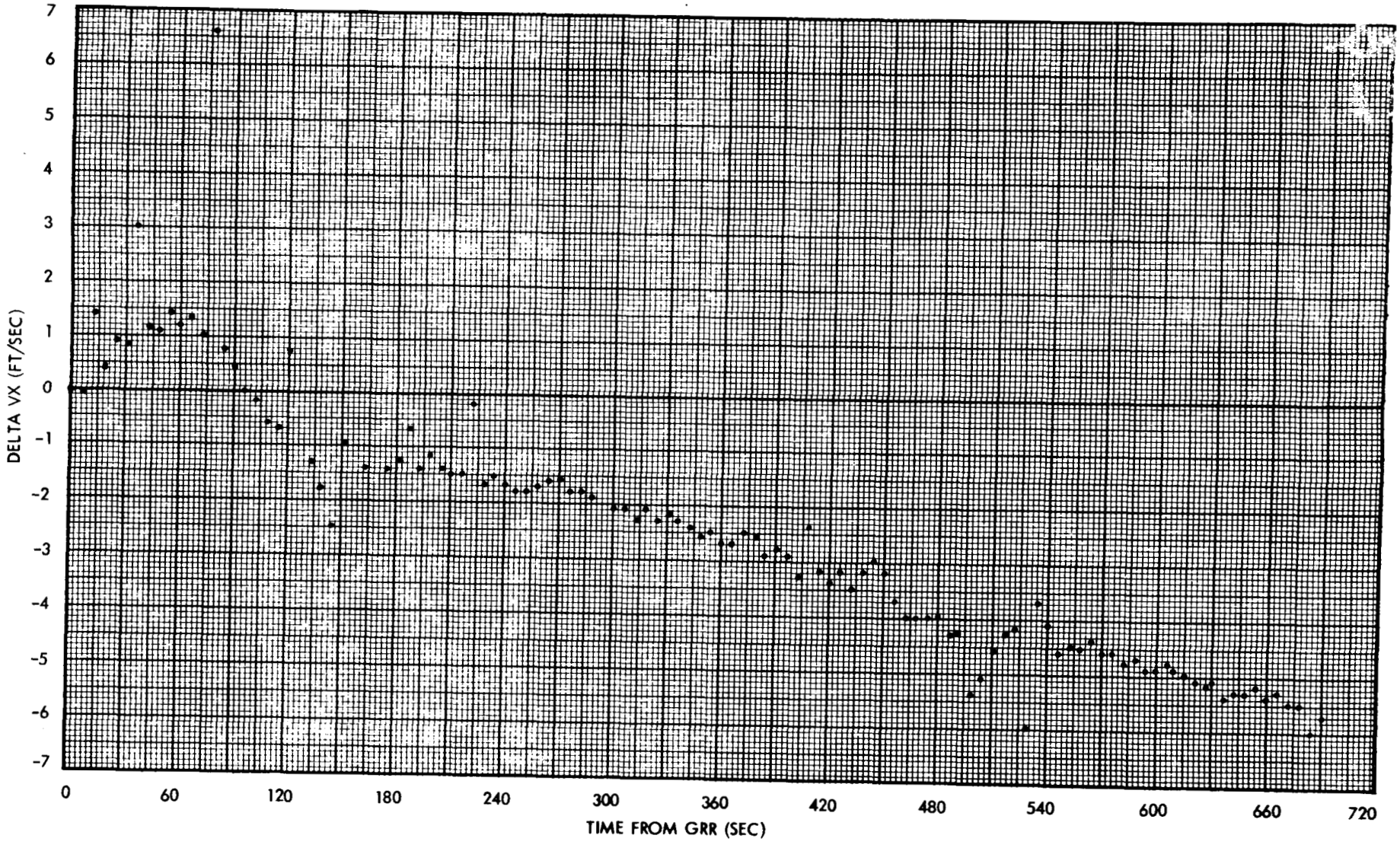

Figure 3.1-3. Ascent Velocity Comparison GNCS Minus Edited S-IVB IU/TM Z-Axis

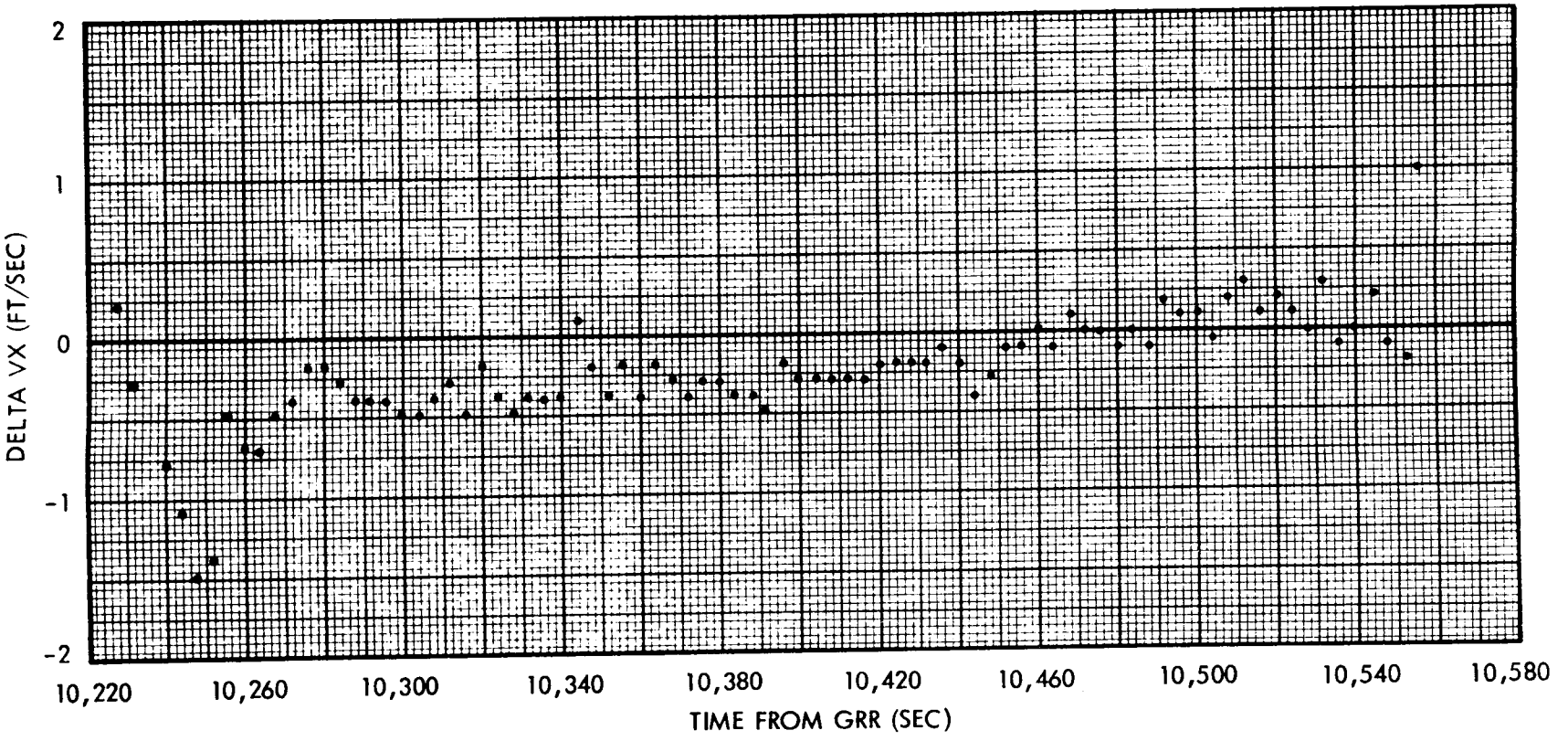

Figure 3.1-4. TLI Velocity Comparison GNCS Minus Edited S-IVB IU/TM X-Axis

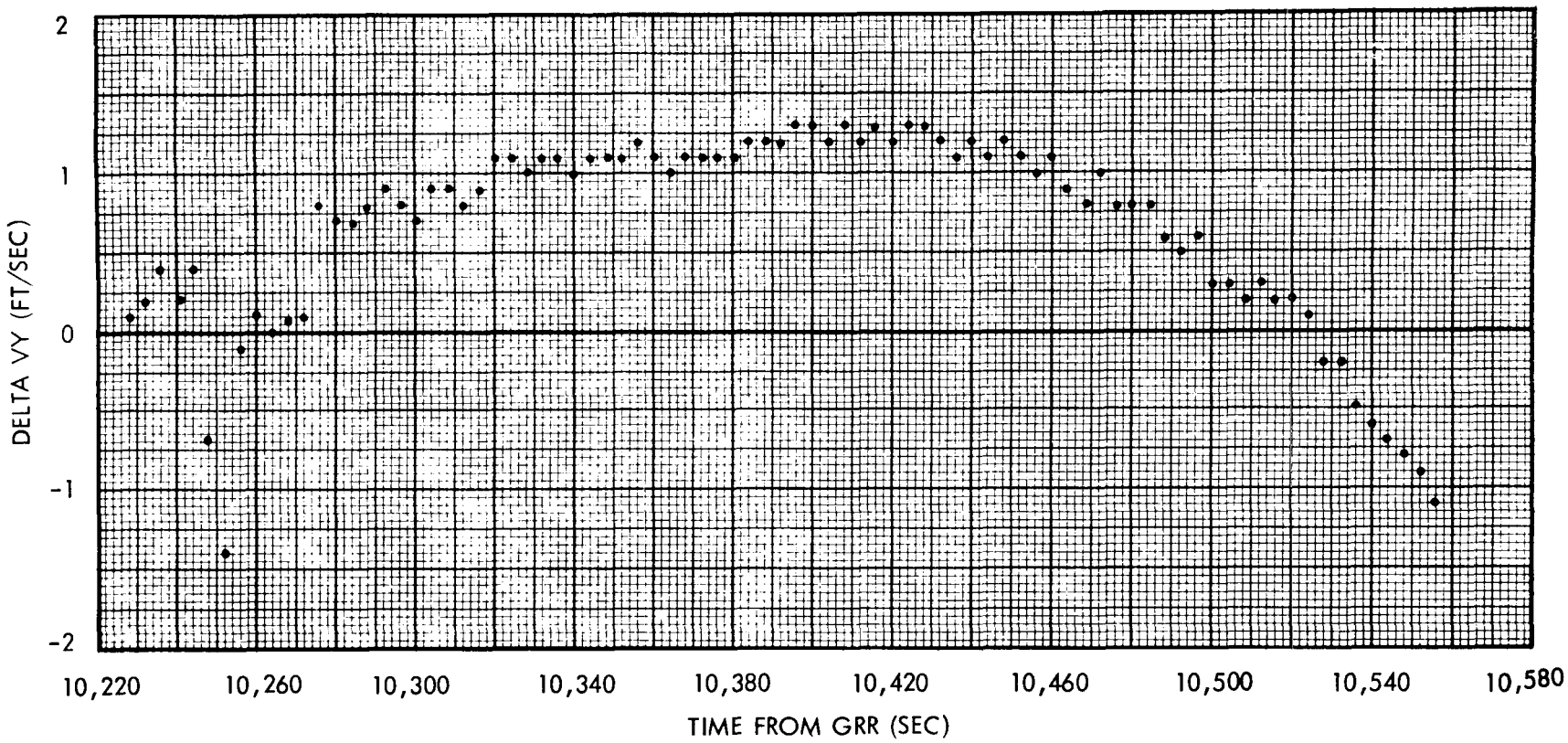

Figure 3.1-5. TLI Velocity Comparison GNCS Minus Edited S-IVB IU/TM Y-Axis

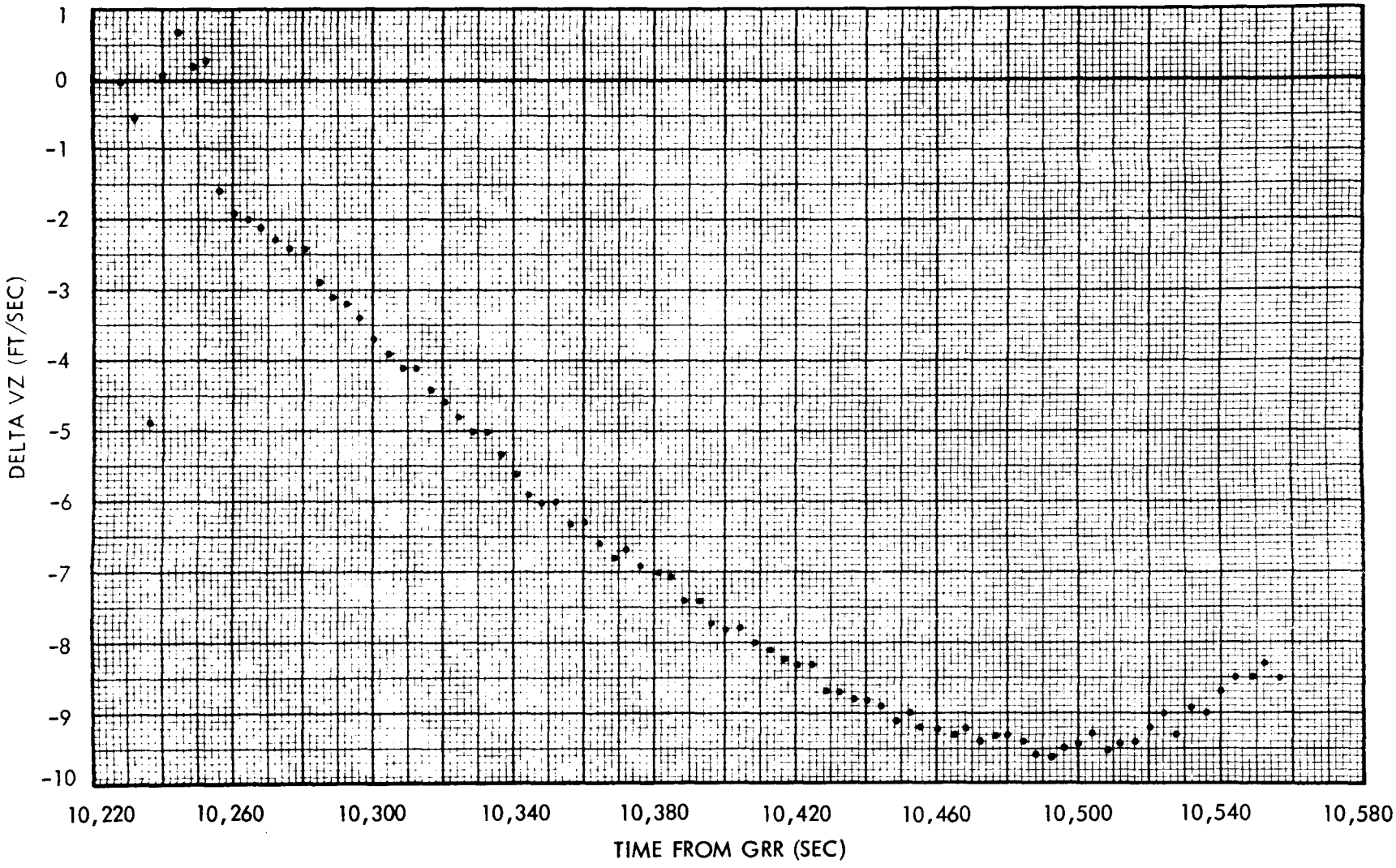

Figure 3.1-6. TLI Velocity Comparison GNCS Minus Edited S-IVB IU/TM Z-Axis

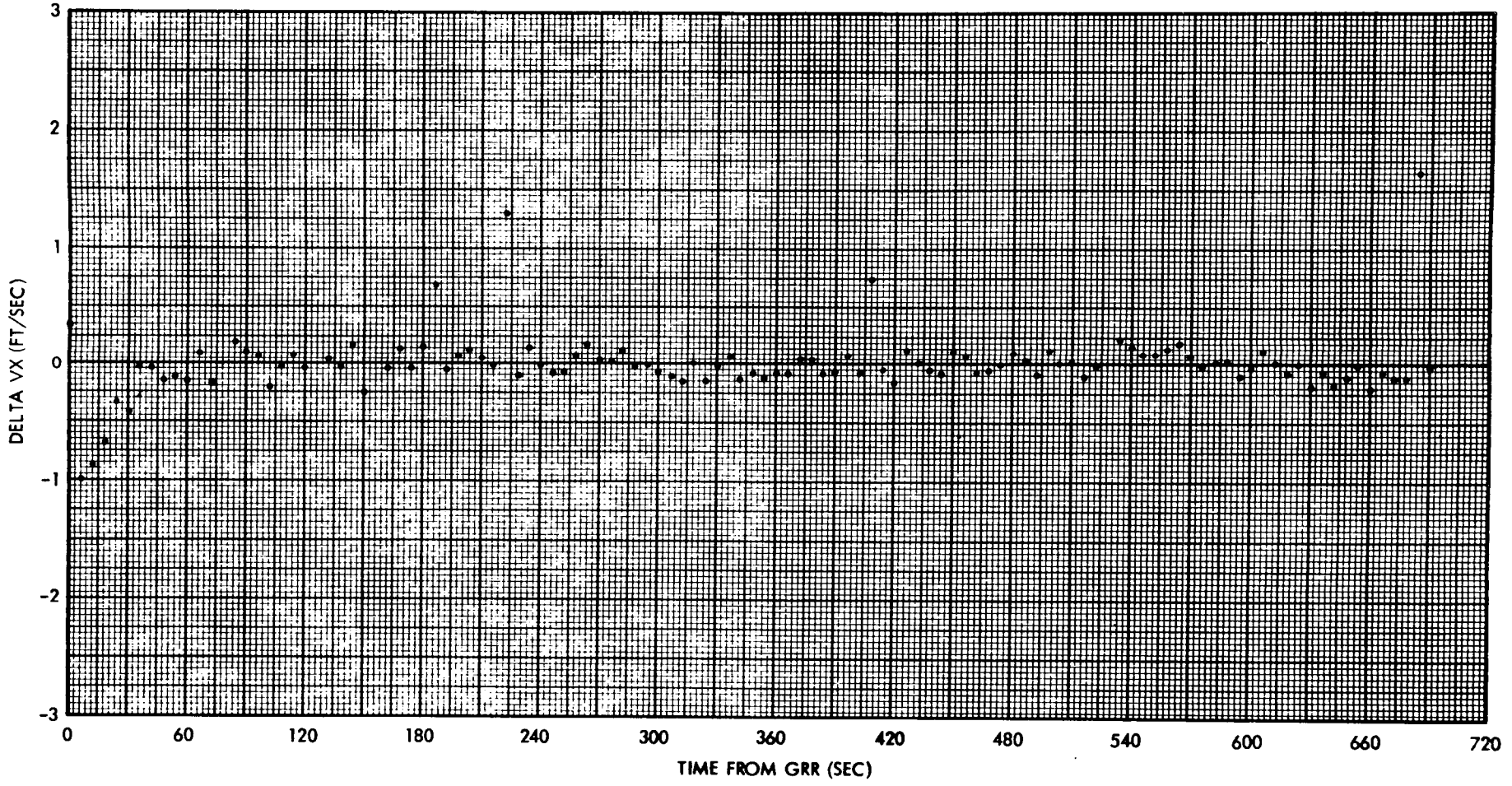

Figure 3.1-7. Ascent Velocity Residual Errors; Corrected GNCS Minus Edited S-IVB IU/TM X-Axis

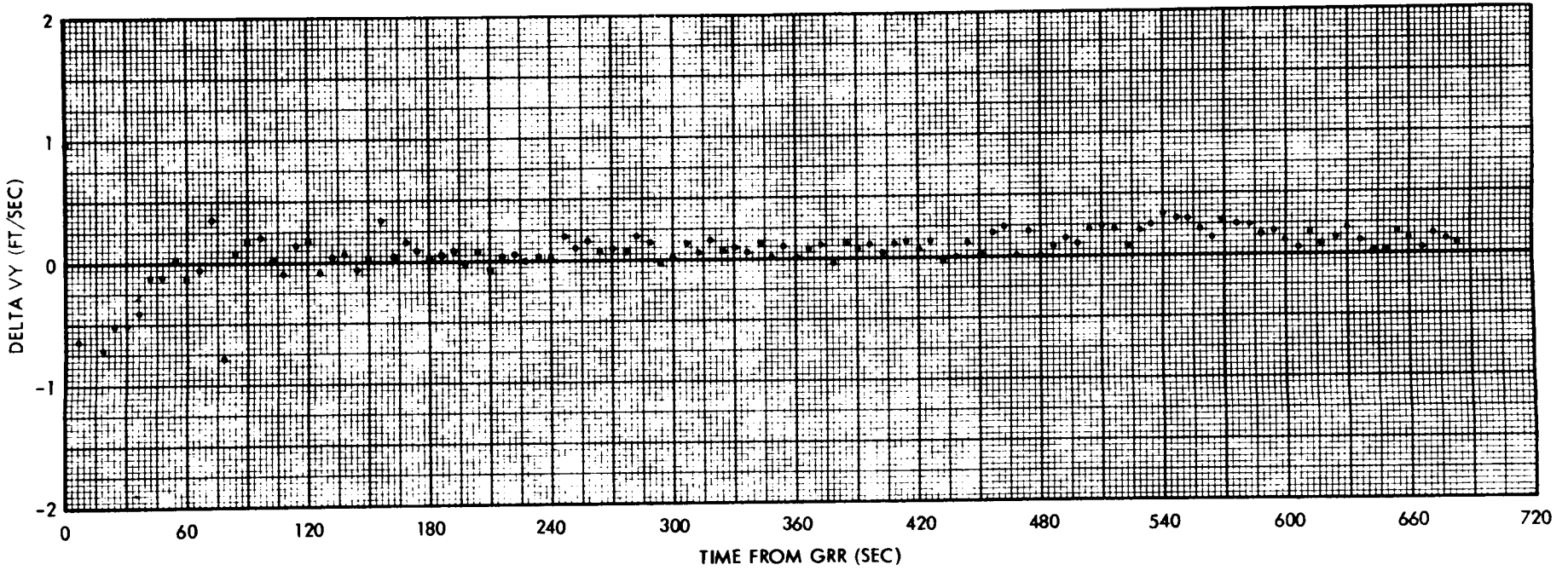

Figure 3.1-8. Ascent Velocity Residual Errors; Corrected GNCS Minus Edited S-IVB IU/TM Y-Axis

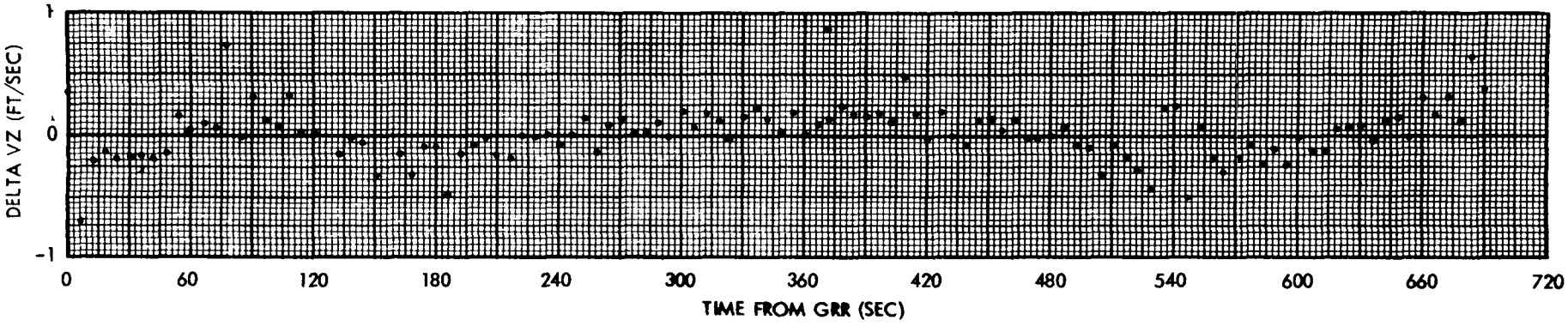

Figure 3.1-9. Ascent Velocity Residual Errors; Corrected GNCS Minus Edited S-IVB IU/TM Z-Axis

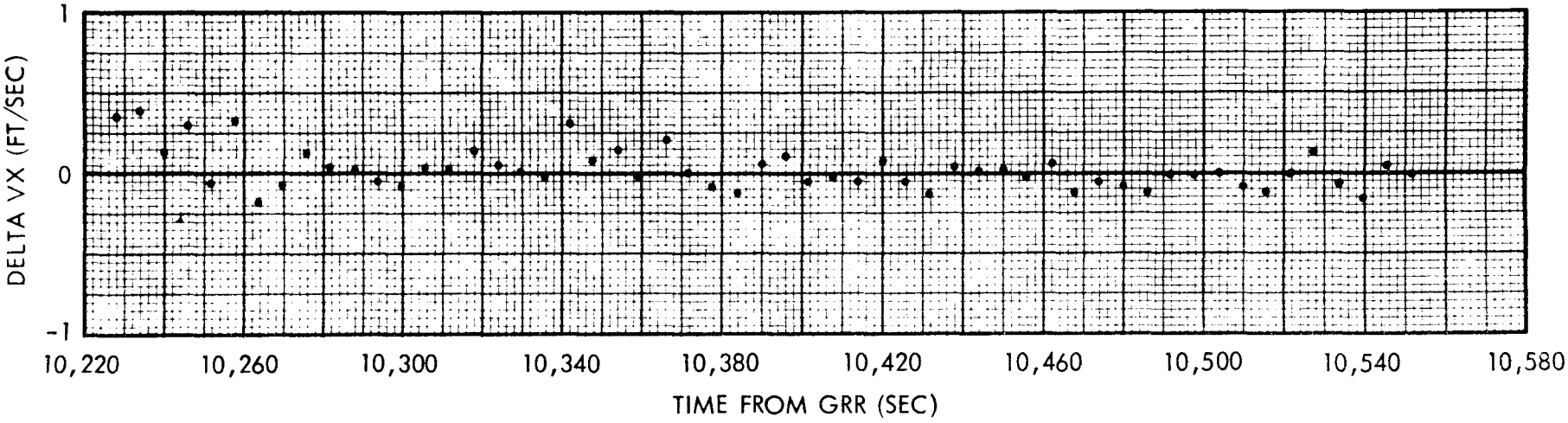

Figure 3.1-10. TLI Velocity Residual Errors; Corrected GNCS Minus Edited S-IVB IU/TM X-Axis

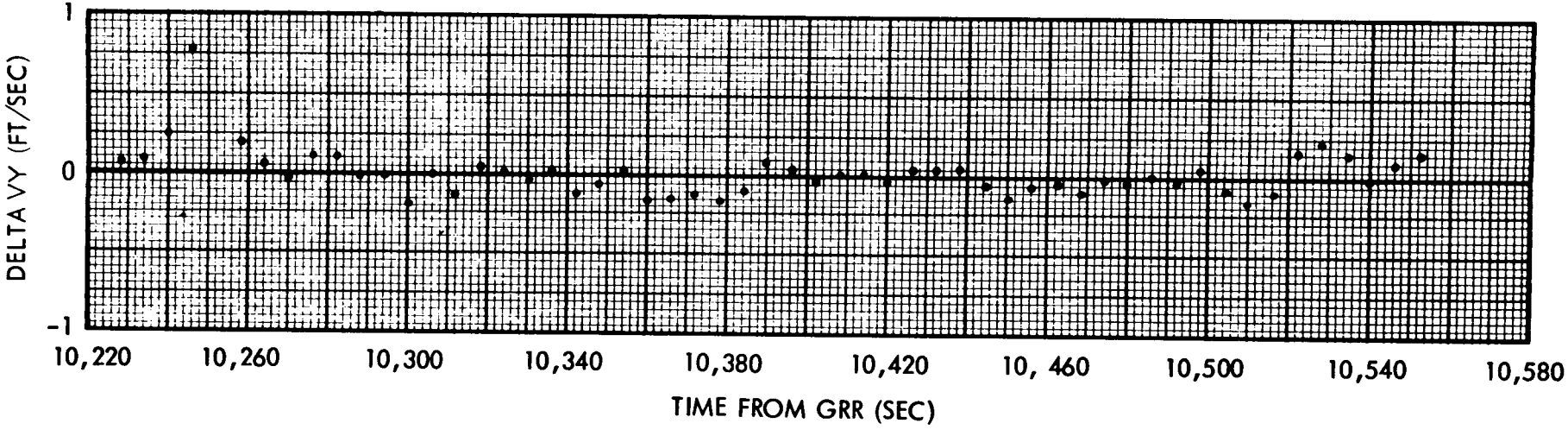

Figure 3.1-11. TLI Velocity Residual Errors, Corrected GNCS Minus Edited S-IVB IU/TM Y-Axis

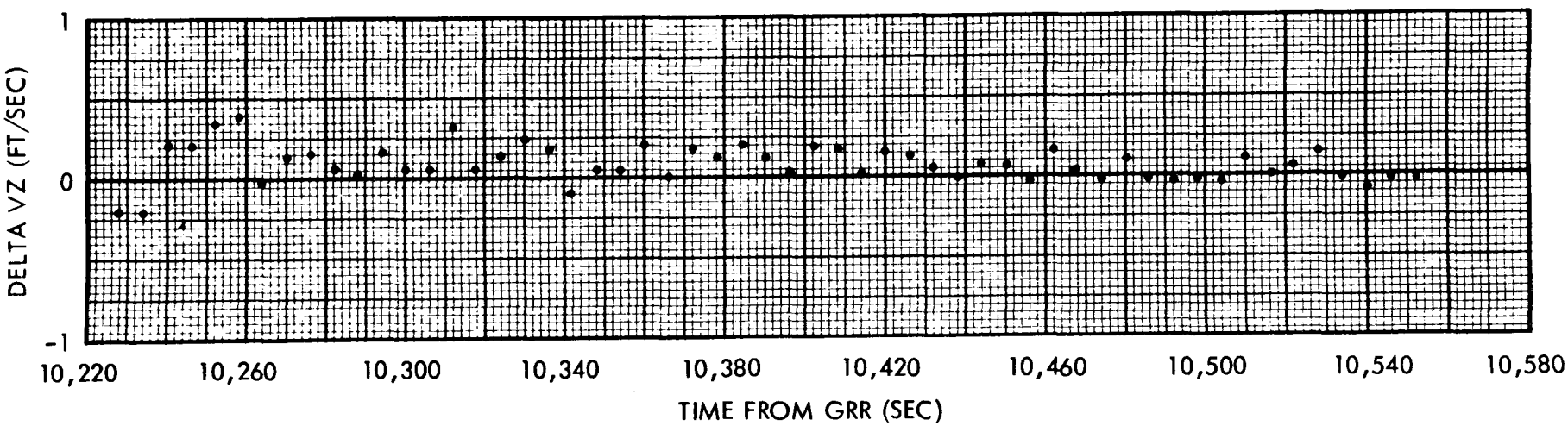

Figure 3.1-12. TLI Velocity Residual Errors Corrected GNCS Minus Edited S-IVB IU/TM Z-Axis

(Reference 1 and 3.) As was done in the past, the "Edited S-IVB IU TM" trajectory was accepted as the most realistic.

The major difference expected between the OMPT and "Edited S-IVB IU TM" is that the OMPT has been corrected for booster guidance errors. No allowance has been made for these errors; any that exist are included in the Apollo GεN errors. Analysis has shown, however, that these errors have less effect on the indicated performance of the Apollo GεN than the "corrections" included in the OMPT. (Reference 3.)

3.1.1 ISS Errors

The velocity differences before any compensation for errors appear in Figures 3.1-1 through 3.1-6 for the boost phase and TLI phase. The error set derived to fit the boost errors and the error set derived to fit the TLI errors are presented in Table 3.1-1. The velocity residuals resulting from a comparison of the Apollo GεN data, corrected for these errors, compared to the "Edited S-IVB IU TM," are shown in Figures 3.1-7 through 3.1-12. Of the 34 error sources derived, none deviated by more than one standard deviation from each other for the two flight phases evaluated. (See Table 3.1-1.) Based on the approach established at the onset of this analysis, satisfactory ISS performance has been established.

Since all previous mission IMU analysis has been based primarily on the ascent phase, the Apollo 8 ascent error set should be reviewed also for comparative purposes. During the ascent phase three error sources are considered worthy of noting and are discussed below.

3.1.1.1 Misalignment of the Platform About X (MLMX)

The value of MLMX was 92 arc secs. or 1.8 sigma. This error magnitude was constantly required to obtain fits during the evolution of the ascent solution and therefore has a high probability of being the correct value. PIPA Y bias which correlates directly with MLMX showed no erractic tendencies either in preflight testing or during flight measurements. No specific explanation exists for this error.

3.1.1.2 X PIPA Scale Factor (SFEX)

The X PIPA scale factor differed by 1.1 sigma from the flight load value. No specific cause for this apparent instrument S.F. shift

exists, however, it appears the error estimate is valid due to the close agreement between ascent and TLI phases. Preflight histories for KSC testing show rather large changes in this term during preflight calibrations (oscillating in a band from 0 to -120 ppm), however, no value as large as that established from flight data was experienced. Although numerous possibilities exist for the cause, this type of shift has been seen for other PIPA's (reference Apollo 6 results) and one is led to believe that an acceleration sensitive scale factor change exists, a phenomenon recently contended by MIT.

3.1.1.3 Acceleration Sensitive Drift of the Y Gyro Due to Acceleration Along the Spin Axis (ADSRA Y)

The ADSRAY term varied by 2 sigma from the flight load value. Nothing in the preflight test history of ADSRA Y satisfactorily explains the large deviation noted in the flight data, however, considerably less confidence exists for this term than MLMX and SFEX since ADSRA Y is insensitive during the TLI phase. This term was ultimately selected in order to achieve a good data fit to the boost trajectory.

3.2 FREE FLIGHT PERFORMANCE OF GYROS AND ACCELEROMETERS

Gyro non "g" sensitive bias drift (NBD) was evaluated based on IMU alignments accomplished to realign the platform to REFSMMAT. Data indicated that flight stability of the NBD terms for all gyros was well within the Master End Item (MEI) flight stability specification (1σ = 2 meru) with maximum measured deviations from the inflight NBD compensation of 0.57, 0.81 and 1.19 meru respectively for X, Y and Z. Due to the large number of realignments obtained it was possible to statistically evaluate the error in the alignment process. If the mean of the IMU trim angle corrections is assumed to be totally gyro drift (no systematic alignment errors and the gyro bias remains fixed) then the variations about this mean can be considered as uncertainties in the alignment process. Based on this hypothesis an average RMS error of 0.033 degrees per axis was determined. This is equivalent to a 3σ MEI error (40 sec = 1σ).

An abundance of PIPA bias data was avaliable from the mission, since the uncompensated ΔV pulses were accumulated in T/M sampled registers during the long periods that the CMC was in a coasting flight program. Data indicates that the PIPA stability was well within the MEI flight stability specification of 0.2 cm/sec^2, with maximum deviations from the prelaunch compensation load of 0.033, 0.044 and 0.015 cm/sec^2 for X, Y and Z respectively. The maximum deviation was measured from the first good bias determination after S-IVB separation. Shifts after S-IVB separation, once the inflight bias was established, were slight. This also indicates that the magnitude of the shifts across major burns was negligible. The only PIPA which indicated any instability in a relative sense was the PIPAX. This instrument had a near zero bias during prelaunch calibration and a compensation value of zero was loaded. From Figure 3.2-1 it can be seen that the bias shifts significantly in a relative sense, but the absolute magnitude of the shift is small. The reason for this shift is most probably the null coincidence phenomenon discussed in Reference 3. The only conclusions which can be deduced from this data is that the stability of the bias term in the vicinity of null is unpredictable and the choice of zero for a prelaunch load is a practical decision.

3.2.1 IMU Realignments

Each realignment time and corresponding set of gyro torquing angles is presented in Table 3.2-1. Based on these data points, a long term drift determination was made to minimize the effects of $\Delta\theta$ measurement error and timing errors. After each new IMU alignment (change REFSMMAT) a new drift interval was established. Mean platform drifts for the intervals evaluated are presented in Table 3.2-2. From these mean drifts, a calculated set of expected torquing angles were established for each realignment. These angles were differenced from the actual torquing angles and listed in Table 3.2-3 as residuals. The RMS of the residuals were 0.031°, 0.025° and 0.045° for X, Y and Z axis respectively. If the gyro drift is considered to be constant and no systematic alignment errors exists, the RMS values indicate the random uncertainty associated with the alignment process. This represents a 2.8, 2.3 and 4.1 sigma alignment uncertainty per X, Y and Z respectively, relative to the inflight alignment accuracy of 0.011° per axis specified in the MEI specification.

3.2.2 PIPA Bias Determination

PIPA ΔV accumulations during the translunar phase, after LOI and during the transearth phase are presented in Figures 3.2-1, 3.2-2 and 3.2-3 for ΔV_x, ΔV_y, and ΔV_z respectively. Bias was only calculated for periods where a group of PIPA counts correlated closely enough to establish a slope. In most cases enough data was available to establish biases preceding and following each major burn. The figures indicate that only the X PIPA slope changes significantly across burns, however, the absolute value of this shift is a negligible contributer to ΔV measuring error for the expected burn durations. A summary of the biases at different points along the mission are shown in Table 3.2-4. In all cases no significant shift across the burns is apparent and the shifts that do occur are in the range of 1/7 to 1/10 of the one sigma flight stability criteria (0.2 cm/sec^2) established in the MEI specification.

Table 3.2-1

Realign to REFSMMAT (g.e.t.)	θ Gyro Torquing (deg) X	Y	Z	Remarks
00:54:31	0.026	0.035	0.119	These values not used since they include correction for gyro compassing errors.
03:40:00	-0.012	0.000	0.001	
04:21:00	-0.034	-0.027	0.100	
10:12:40	--	--	--	Data not available
16:49:40	-0.122	-0.044	+0.172	
27:30:46	-0.242	+0.049	+0.295	
34:08:48	-0.136	-0.013	+0.192	
36:10:00	-0.157	-0.018	+0.216	
44:31:00	-0.201	-0.003	+0.255	
51:39:00	-0.143	+0.003	+0.164	
Sum	-1.047	-0.105	+1.395	
Drift (deg/hr)	-0.0206	-0.0021	+0.0275	
Drift	-1.37 meru	-0.138 meru	1.83 meru	
60:09:00	Align to new REFSMMAT			
66:21:00	-0.089	-0.007	+0.128	
70:09:00	-0.077	+0.017	+0.045	
72:17:00	-0.053	-0.007	+0.047	
74:34:00	-0.052	-0.007	+0.053	
76:25:00	-0.022	-0.006	+0.074	
78:27:00	-0.060	-0.013	+0.040	
80:28:00	-0.052	+0.002	+0.071	
82:28:00	-0.022	-0.004	+0.032	
86:30:00	-0.078	-0.006	+0.102	
Sum	-0.505	-0.050	+0.592	
Drift (deg/hr)	-0.0192	-0.0019	+0.0225	
Drift	-1.28 meru	-0.127 meru	+1.51 meru	
90:03:50	Align to new REFSMMAT			
99:44:00	-0.208	-0.010	+0.242	
106:54:56	(-0.148)	(-0.015)	(+0.198)	Fine align after inadvertent coarse align.
119:33:00	-0.262	-0.021	+0.302	
129:29:00	-0.161	-0.096	+0.254	

Realign to REFSMMAT (g.e.t.)		Gyro Torquing (deg) X	Y	Z	Remarks
139:23:48		-0.180	-0.011	+0.235	
143:03:00		-0.096	-0.020	+0.083	
144:50:00		-0.034	+0.001	+0.043	
	Sum	-1.089	-0.173	+1.357	
	Drift (deg/hr)	-0.0199	-0.0032	+0.0248	
	Drift	-1.33 meru	-0.21 meru	+165 meru	

( ) Torquing values estimated based on previous drift rates.

TABLE 3.2-2

	X Gyro		Y Gyro		Z Gyro	
Drift Period	Compensation load (meru)	Measured drift (meru)	Compensation load (meru)	Measured drift (meru)	Compensation load (meru)	Measured drift (meru)
03/40/00 - 51/39/00	-0.8	-1.37	0.6	-0.138	-(-2.7)*	1.83
60/09/00 - 86/30/00	-0.8	-1.28	0.6	-0.127	-(-2.7)*	1.51
90/03/50 - 144/50/00	-0.8	-1.33	0.6	-0.210	-(-2.7)*	1.65

*Positive drift about ZSM is equivalent to negative gyro drift because the Z gyro input axis is reversed.

Table 3.2-3

REALIGN TO REFSMMAT (GET)	θ_E ESTIMATED GYRO DRIFT ANGLE (DEG) X	Y	Z	RESIDUALS ($\theta_A - \theta_E$) DEG X	Y	Z
03:40:00	-0.055	-0.007	0.068	+0.043	+0.007	-0.067
04:21:00	-0.012	-0.002	0.015	-0.022	-0.025	+0.085
10:12:40	-	-	-	-	-	-
16:49:40	-0.132	-0.017	0.165	+ .010	-0.027	0.007
27:30:46	-0.2.2	-0.028	0.266	-0.030	+0.077	0.029
34:08:48	-0.132	-0.017	0.165	-0.004	+0.004	+0.027
36:10:00	-0.040	-0.005	0.050	-0.117	-0.013	+0.166
44:31:00	-0.166	-0.022	0.208	-0.035	+0.019	+0.047
51:39:00	-0.141	-0.018	0.177	-0.002	+0.021	-0.013
66:21:00	-0.123	-0.016	0.154	+0.034	+0.009	-0.026
70:09:00	-0.076	-0.010	0.095	-0.001	-0.027	-0.050
72:17:00	-0.042	-0.005	0.052	-0.011	-0.002	-0.005
74:34:00	-0.046	-0.006	0.057	-0.006	-0.001	-0.004
76:25:00	-0.037	-0.005	0.046	+0.015	-0.001	+0.028
78:27:00	-0.040	-0.005	0.050	-0.020	-0.008	-0.010
80:28:00	-0.040	-0.005	0.050	-0.012	+0.007	0.021
82:28:00	-0.040	-0.005	0.050	+0.018	+0.001	-0.018
86:30:00	-0.080	-0.010	0.100	+0.002	+0.004	0.002
99:44:00	-0.191	-0.025	0.239	-0.017	+0.015	0.003
106:54:56	-0.143	-0.019	0.179	-0.005	+0.004	0.019
119:33:00	-0.251	-0.033	0.314	-0.011	+0.012	-0.012
129:29:00	-0.198	-0.026	0.247	+0.037	-0.070	0.007
139:23:48	-0.197	-0.026	0.247	+0.017	+0.015	-0.012
143:03:00	-0.073	-0.009	0.091	-0.023	-0.011	-0.008
144:50:00	-0.035	-0.005	0.044	+0.001	+0.006	-0.001
				RMS = 0.031	RMS= 0.025	RMS= 0.045

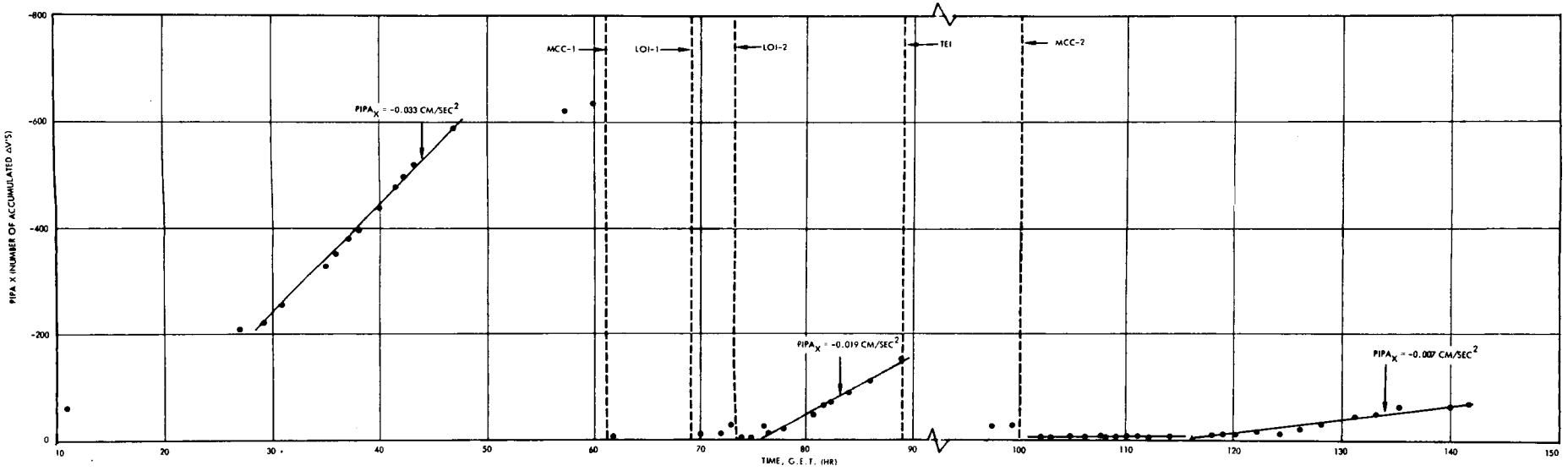

Figure 3.2-1. Accumulated X PIPA Counts During Free Flight

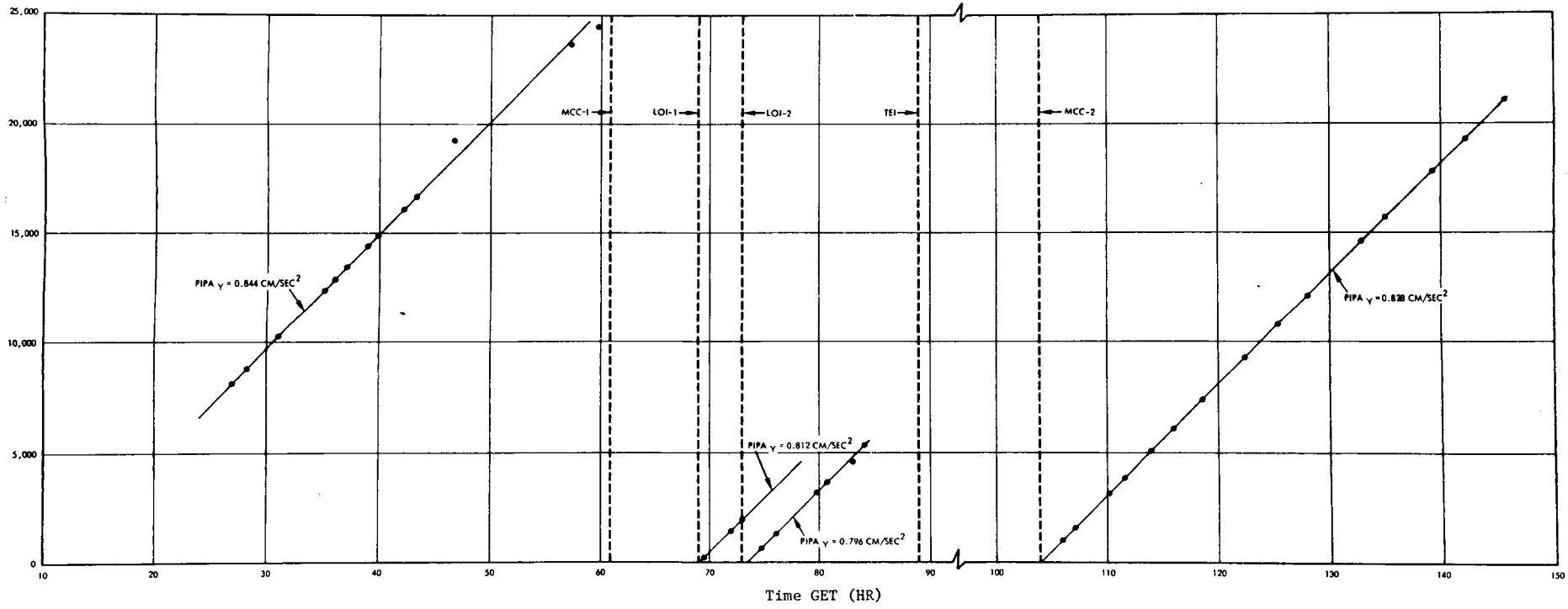

Figure 3.2-2. Accumulated Y PIPA Counts During Free Flight

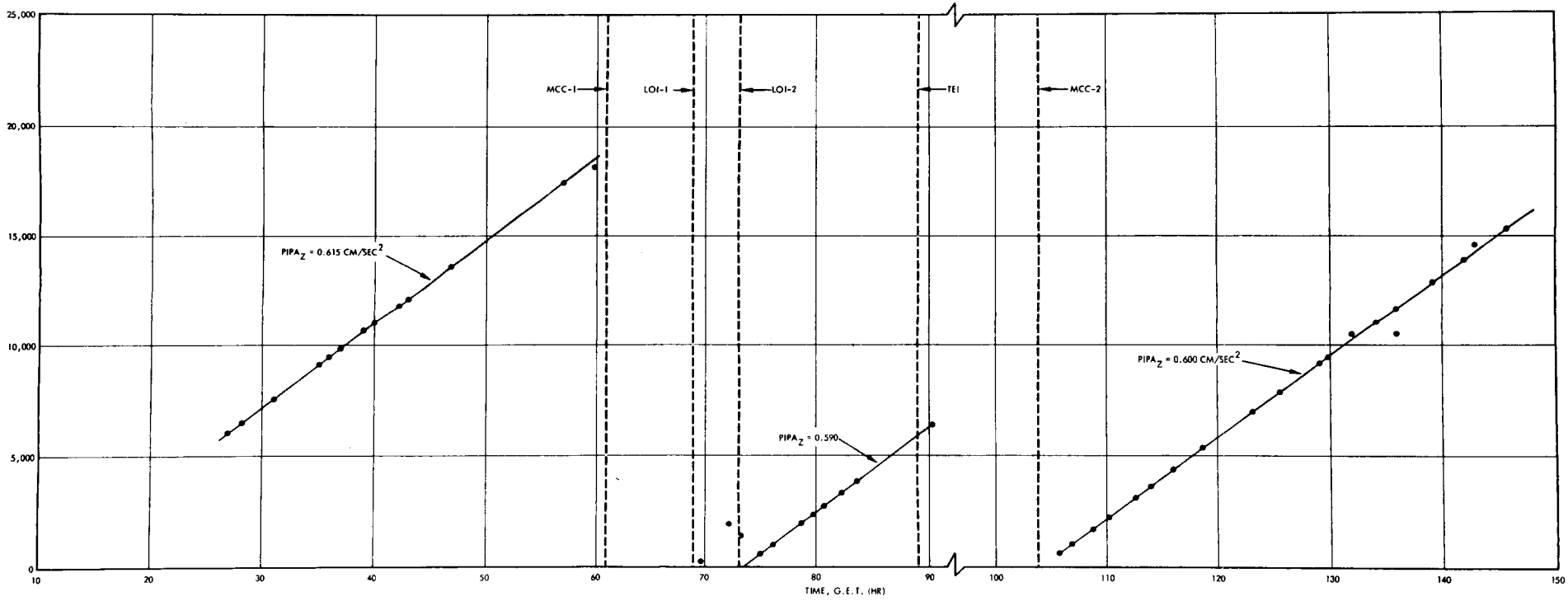

Figure 3.2-3. Accumulated Z PIPA Counts During Free Flight

Table 3.2-4

PIPA BIAS SUMMARY (cm/sec^2)

PIPA	PRELAUNCH LOAD	AFTER SIVB SEPARATION	AFTER LOI 1	AFTER LOI 2	AFTER TEI
X	0	-0.033	-0.019	*	-0.007
Y	+0.80	+0.844	+0.812	+0.796	+0.828
Z	+0.60	+0.615	+0.590	*	+0.600

* Insufficient data to establish accurate bias level.

4.0 GNCS TVC DAP PERFORMANCE

Four SPS controlled burns occurred during the Apollo 8 mission; the first midcourse correction (MCC1), the Lunar Orbit Injection Burn (LOI 1), the Lunar Orbit Circularization Burn (LOI 2) and the Transearth Injection Burn (TEI). TVC DAP operation during all these burns was excellent.

4.1 PITCH AND YAW ATTITUDE ERRORS

During SPS thrusting, attitude errors in the pitch and yaw axes were less than one-half degree. When steering and mistrim transients had subsided, pitch and yaw attitude errors remained within $\pm$.1 degree of zero.

In Table 4-1 the attitude errors are tabulated along with peak ullage rates for the TEI burn. Plots of some of the important parameters used in evaluating TVC DAP for the LOI 1 and TEI burns are presented in Figures 4-1 through 4-18. Attitude errors at ignition were within the .5 degree deadband on the MCC 1 and LOI 1 burns where no ullage maneuvers were performed. On the TEI burn an ullage maneuver was performed and the attitude errors were close to the deadband. The attitude errors were also within a few hundredths of a degree of the attitude errors predicted during ullage by preflight simulations. The changes in COLOSSUS RCS DAP filter gains used during translation account for the improvement in attitude errors during ullage over the SUNDISK Program. (That is, attitude errors of approximately 1 degree were expected with SUNDISK.)

4.2 VELOCITY RESIDUALS

Table 4-2 lists velocity residual information for the Apollo 8 SPS burns. The only large velocity residual occurred after the MCC 1 burn where a velocity-to-be-gained of 4.4 ft/sec remained in the X control axis. This was subsequently trimmed out with an RCS burn using the THC.

The first midcourse correction burn was a short burn (i.e., duration was 2.4 seconds which is less than the 6 seconds time duration used to differentiate short from long burns) and as a result, no steering occurred. The large residual after this burn has been accounted for by the fact that helium bubbles formed in the SPS engine fuel lines and resulted in a slow thrust build up following the engine ON command. Since this was a short burn, the cutoff time was never recomputed and the engine was shut down using the

initial computed burn duration, leaving a large velocity-to-be-gained residual along the X body axis. Functioning of the TVC DAP was nominal during this burn.

4.3 ENGINE GIMBAL TRIM

Estimated initial mistrims are presented in Table 4-3. The largest mistrim was approximately -0.3 degree in the pitch axis for the LOI 1 burn. These values were computed by comparing the initial trim and single-shot trim values. An examination of Figures 4-15 through 4-18 indicates that after the migration of the C.G. has been subtracted from the difference between the initial SPS engine gimbal trim and the trim value reached after slosh oscillations have subsided, an initial mistrim value within "one bit" ($\approx$ 87 $\widehat{sec}$) of the single-shot value is obtained.

SPS gimbal support compliance causes the sharp transient evident at ignition time in the plots of gimbal position (Figures 4-15 through 4-18). The transient oscillation which follows is partly due to the thrust vector being repostioned to remove the initial mistrim and slosh disturbance. Comparison of engine gimbal transients on the LOI 1 burn (no ullage) and the TEI burn (15 second 4-jet ullage) show that the TEI transients were much more subdued immediately following ignition. This may be the result of the higher mistrim values encountered on LOI 1 rather than the lack of an ullage maneuver prior to ignition.

Tracking of the migrating C.G. during extended SPS burns is apparent for both LOI 1 and TEI burns. Figures 4-4 through 4-7 and Figures 4-11 through 4-14 show this clearly.

4.4 ROLL TVC DAP ACTIVITY

During the LOI 1 and TEI burns there was considerable roll TVC DAP activity. All of the jet firings applied a negative roll control torque to the vehicle. The design of the Roll TVC DAP provides that jet pairs should be alternated if the roll control torque on successive jet firings has the same sign. On the Apollo 8 mission, roll control jets on quads B and D (jets 10 and 12 were used to apply all the roll control torques; the astronaut disabled quads AC roll control during these SPS burns.

Figures 4-1 and 4-8 indicate that a positive steady state roll disturbance torque was present during the LOI 1 and TEI burns. The approximate magnitude of this torque was computed assuming a constant value, was 3.5 ft/lb.

During the LOI 1 burn this torque resulted in a total roll control torque ON time of approximately .6 seconds and the use of approximately .45 lb of RCS fuel. During the TEI burn approximately .5 seconds of roll control was commanded using .36 lb of RCS fuel. In both cases 9 roll control jet firings were commanded.

4.5 TIME DETERMINATION

Values for the SPS engine ignition time and burn duration were computed (Table 4-4) from the best available CMC clock information and the bi-level tab engine-on discrete where available. These values differed by more than the $\pm$.1 second uncertainty allowed for the bi-level sampling rate for the MCC 1 burn. For this burn the difference was 0.358 seconds. The relationships between Ground Elapsed Time (g.e.t.) and CMC clock time used to compute time of ignition from the computer stored TIG are:

1. MCC 1

   g.e.t. (seconds) = CMC clock (seconds) -.0084 seconds drift
   +.89 seconds bias

2. LOI 1

   g.e.t. (seconds) = CMC clock (seconds)+.0089 second drift
   +.89 seconds bias

3. LOI 2

   g.e.t. (seconds) = CMC clock (seconds) +.004 seconds drift
   +.89 seconds bias

4. TEI

   g.e.t. (seconds) = CMC clock (seconds) -.0113 seconds drift
   +.89 seconds bias

TABLE 4-1
Ullage Rates and Attitude
Errors for SPS Burns

SPS Burn	Peak Ullage Rates (deg/sec)			Ignition Attitude Error (control axes-deg)			Burn Peak Attitude Error (body axes-deg)			Final Attitude Error (body axes-deg)		
	Roll	Pitch	Yaw	Roll	Pitch	Yaw	Roll	Pitch	Yaw	Roll	Pitch	Yaw
MCC 1	NA	NA	NA	-.4065	.2197	-.0879	.1099	.2637	.4944	-.0110	.0330	.4944
LOI 1	NA	NA	NA	-.3625	.2307	-.4175	5.0757	.4395	.4504	4.9878	.0220	.0659
LOI 2	NA	NA	NA	-.1978	-.2637	.2527	-.4834	.1634	.1318	.2527	.1318	.1318
TEI	-.0602	+.0559	+.1226	.3076	-.6152	.5713	5.0867	.2417	.3955	5.0208	-.1978	-.0439

All data obtained from computer words.

TABLE 4-2
Velocity-to-be-gained and
Velocity Residuals for SPS Burns

SPS Burn	Noun 85 DSKY Display (Control Axes)						V_G in reference coordinates						Noun 40 DSKY Display Register 2		EMS ΔV Monitor
	V_{GX} Residual		V_{GY} Residual		V_{GZ} Residual		V_{GX}		V_{GY}		V_{GZ}		V_G Magnitude		
	Initial	Trimmed	Initial	Trimmed	Initial	Trimmed	Initial	Final	Initial	Final	Initial	Final	Initial	Final	
MCC 1	4.4	0.0	- .1	-.1	+.1	+.1	-8.347	-1607	23.268	4.271	-2.298	-.237	24.8	4.4	
LOI 1	-1.4+	no trim	0.0+	no trim	+.2+	no trim	1303. 163	-.381	2089. 227	-.787	1705. 460	-.828	+2999.53	+1.2	-20.2+
LOI 2	X	X	X	X	X	X	102.529	.405	77.418	.874	41.544	-.387	+ 134.8	+1.0	- 9.4+
TEI	-.5	no trim	+ .4	no trim	-.1	no trim	-1911. 494*	.238	-2471. 187*	.565	-1620. 035*	-.003	+3519.8	+,6	-26.4+

X - No data available

* - Sampled just prior to SPS burn during ullage

\+ - Value noted by astronaut during flight

TABLE 4-3

ENGINE GIMBAL TRIMS

Pitch Angle-degrees									
SPS Burn	R03 Display		Initial Trim		Single-shot		Final Value		Mistrim
	First	Final	PACTOFF	Measured	PACTOFF	Change	PACTOFF	Measured	
MCC 1	-1.64	-1.64	-1.6767	X	None	None	-1.5795	X	-.0972
LOI 1	-	-	-1.6524	-1.6634	-1.3365	+.3159	- .4374	-.4899	-.3159
LOI 2	-	-	- .5346	X	X	X	- .4131	X	X
TEI	-	-	- .4131	- .4899	- .3159	+.0972	- .7047	-.8379	-.0972

Yaw Angle-degrees									
SPS Burn	R03 Display		Initial Trim		Single-shot		Final Value		Mistrim
	First	Final	YACTOFF	Measured	YACTOFF	Change	YACTOFF	Measured	
MCC 1	+1.28	+1.28	1.3122	X	None	None	1.4094	X	-.0972
LOI 1	-	-	1.3122	1.2367	1.5795	+.2673	1.5795	1.4058	-.2673
LOI 2	-	-	1.4337	X	X	X	1.6038	X	X
TEI	-	-	1.6038	1.5326	1.7982	+.1944	.8262	.6450	-.1944

X-Data not available

TABLE 4-4
SPS Burn Data

SPS Burn	Ullage				Burn		
	No. Jets	Start GET	Duration	Overlap	CMC	Start GET SPS Engine ON Bilevel	Duration
MCC 1	-	No ullage	-	-	10:59:59.18	10:59:59.539	0:02.4*
LOI 1	-	No ullage	-	-	69:08:20.41	69:08:20.43	4:06.90*
LOI 2	-	No ullage	-	-	73:35:06.584	X	X
TEI	4	89:19:02.108	16.40	1.923	89:19:16.55	89:19:16.635	3:23.76*

X - Data not available

* - Computed from SPS solenoid driver discrete

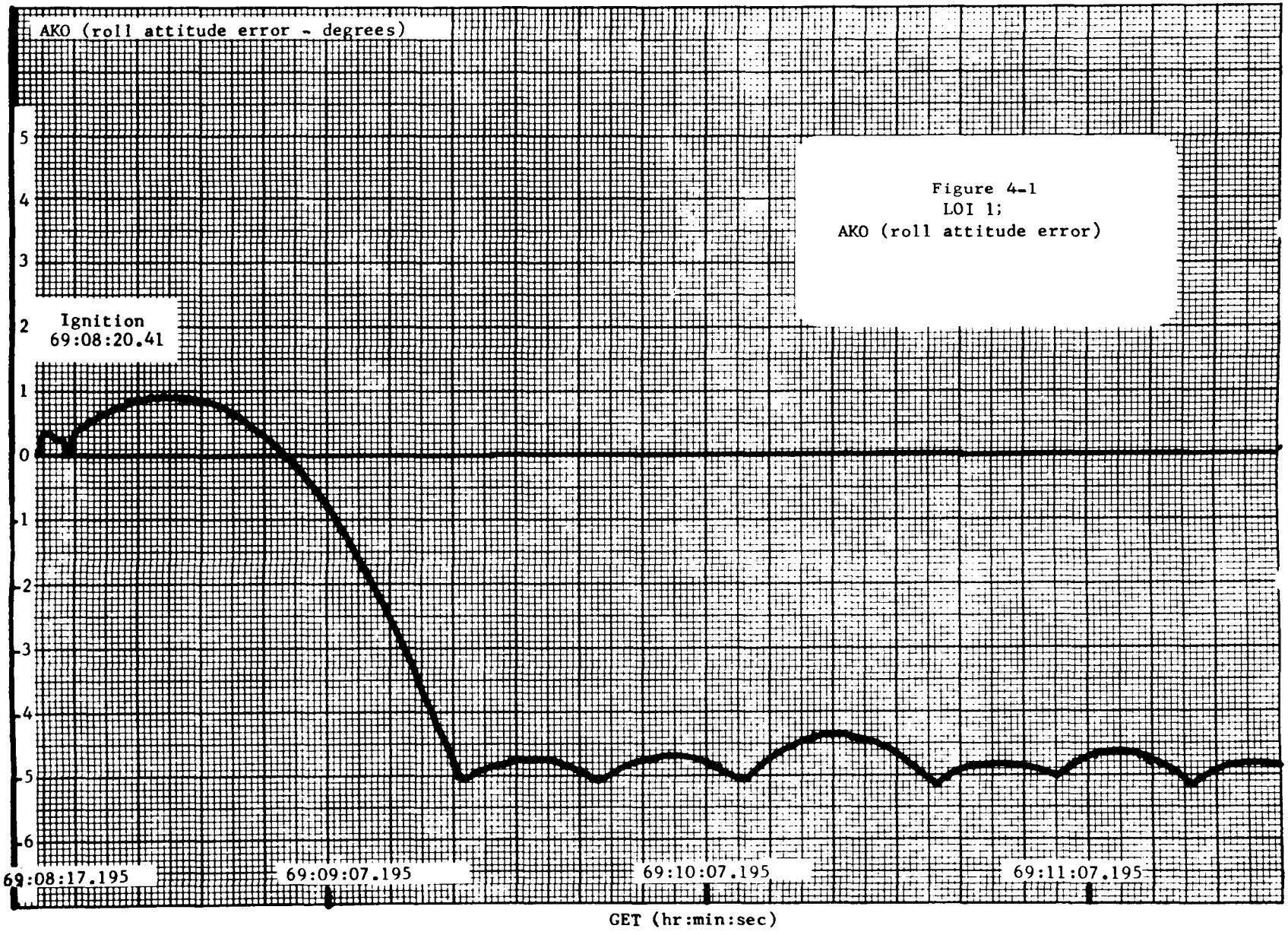

Figure 4-1
LOI 1;
AKO (roll attitude error)

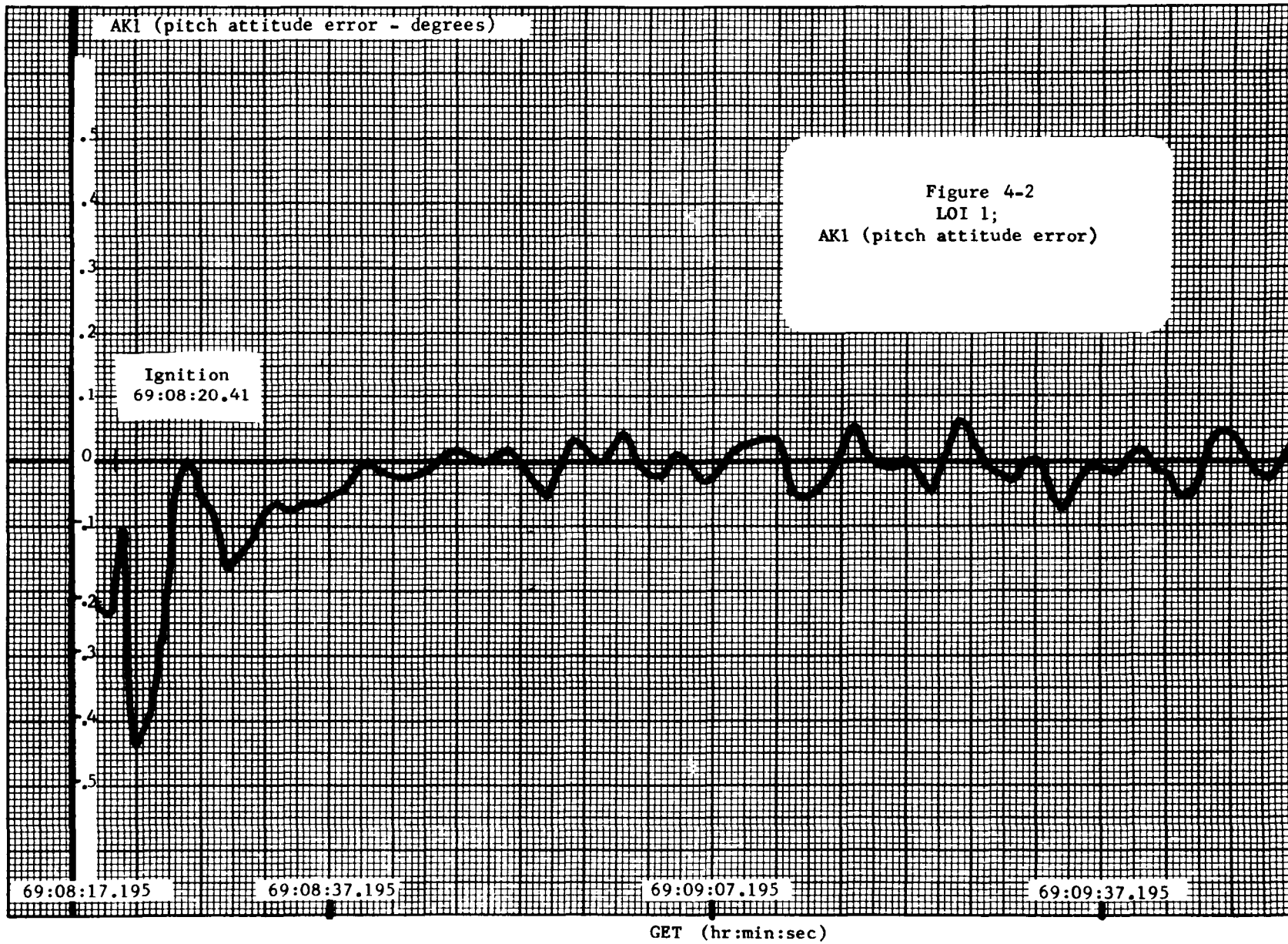

Figure 4-2
LOI 1;
AK1 (pitch attitude error)

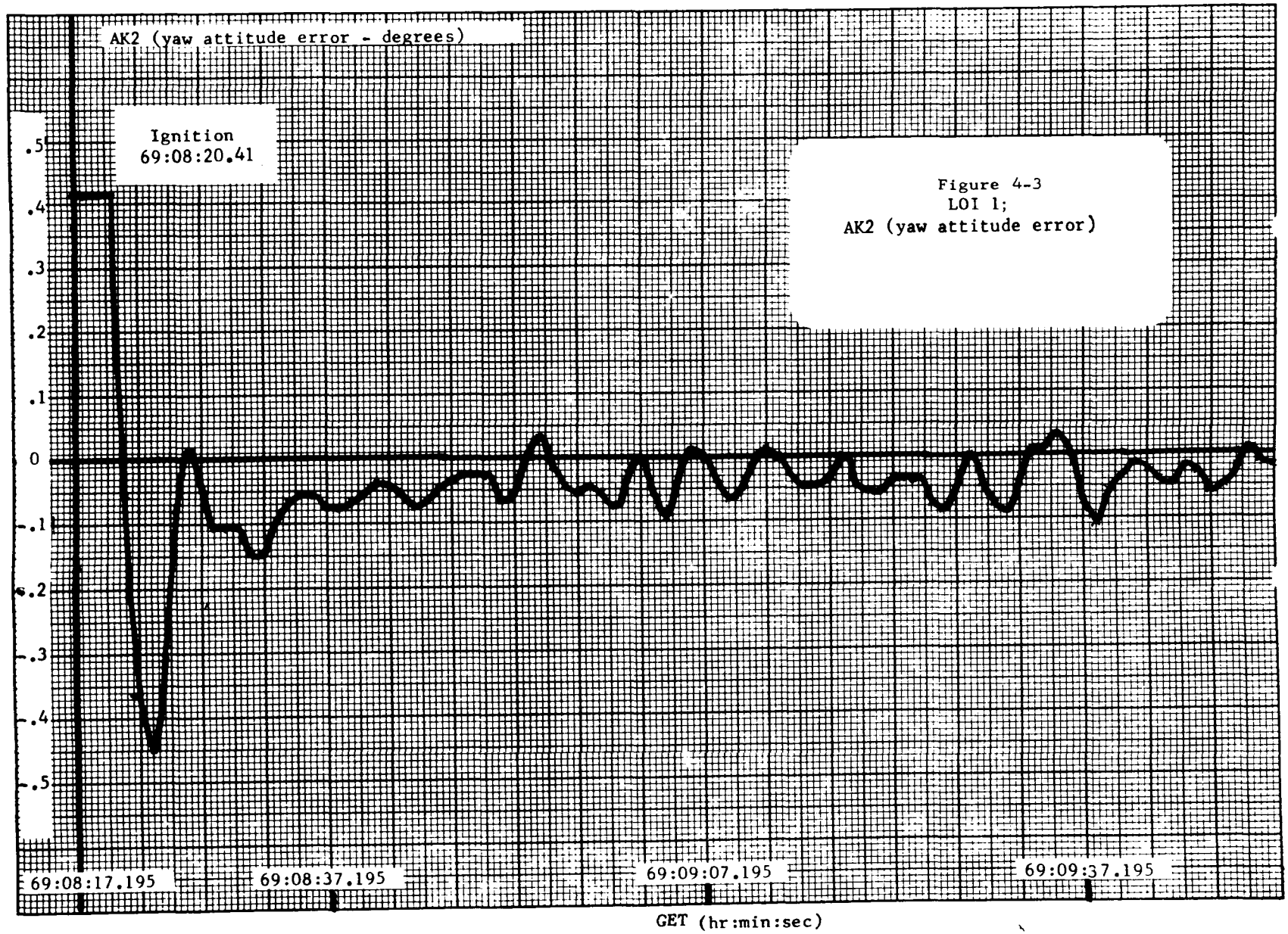

Figure 4-3
LOI 1;
AK2 (yaw attitude error)

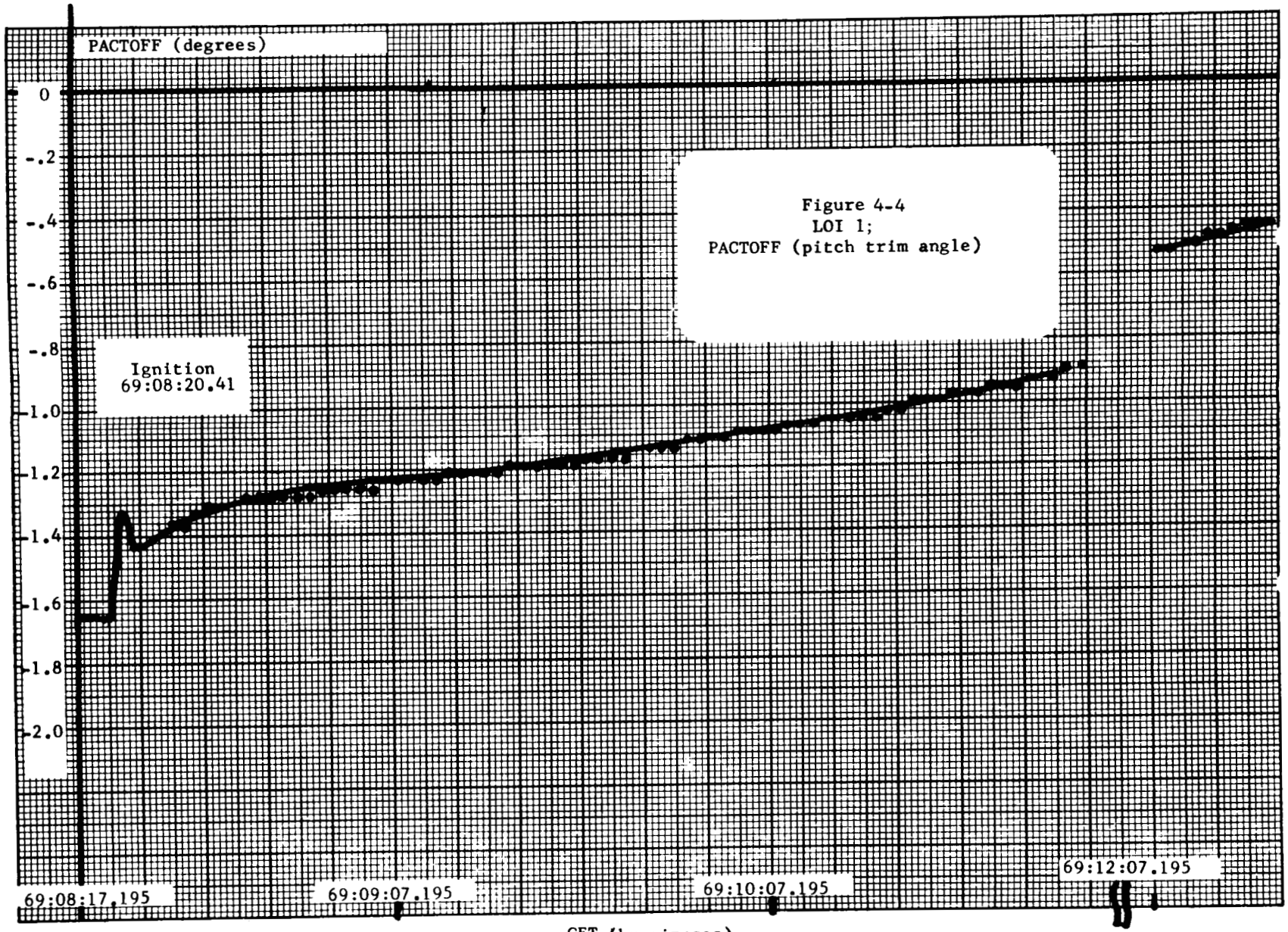

Figure 4-4
LOI 1;
PACTOFF (pitch trim angle)

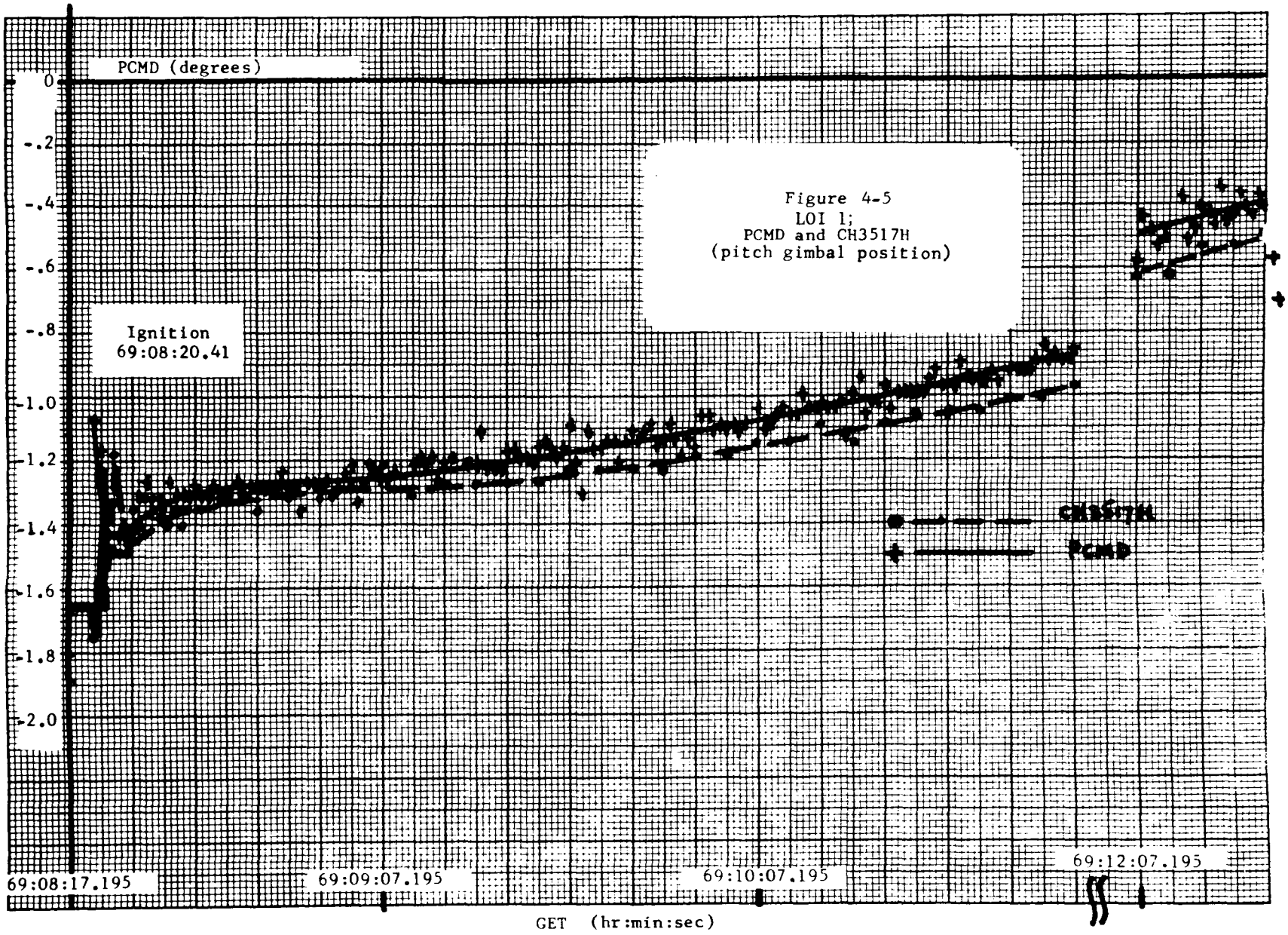

Figure 4-5
LOI 1;
PCMD and CH3517H
(pitch gimbal position)

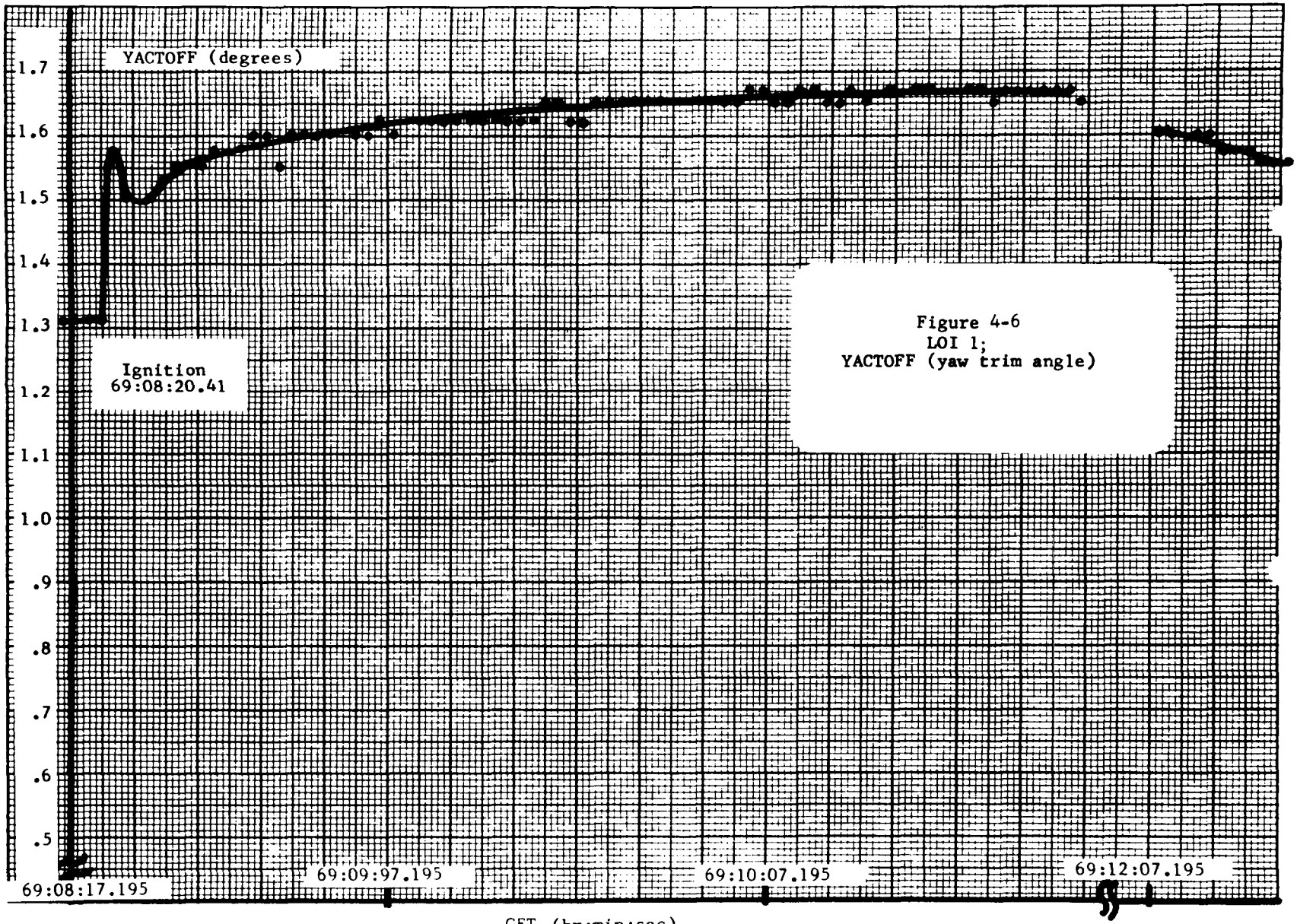

Figure 4-6
LOI 1;
YACTOFF (yaw trim angle)

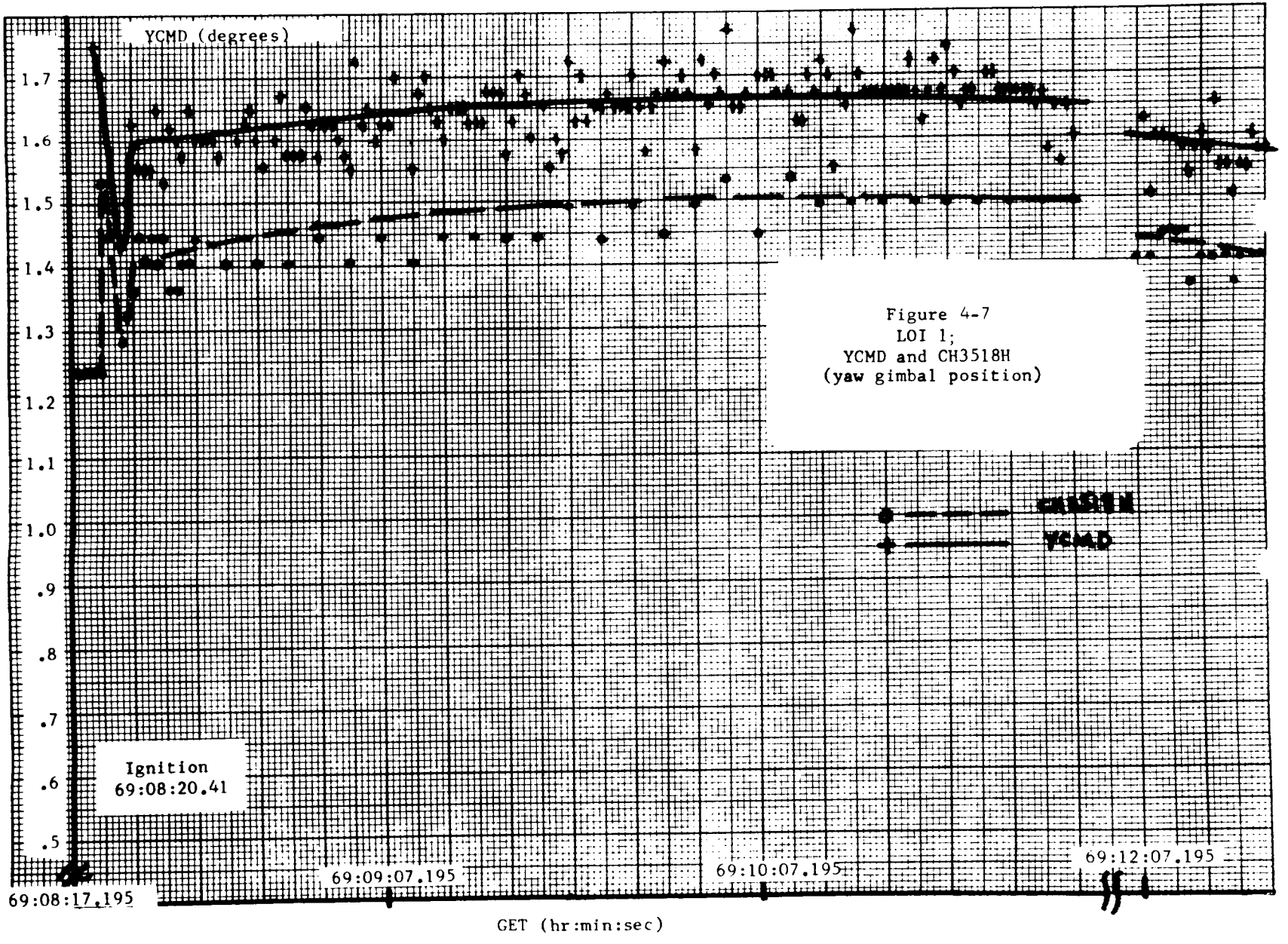

Figure 4-7
LOI 1;
YCMD and CH3518H
(yaw gimbal position)

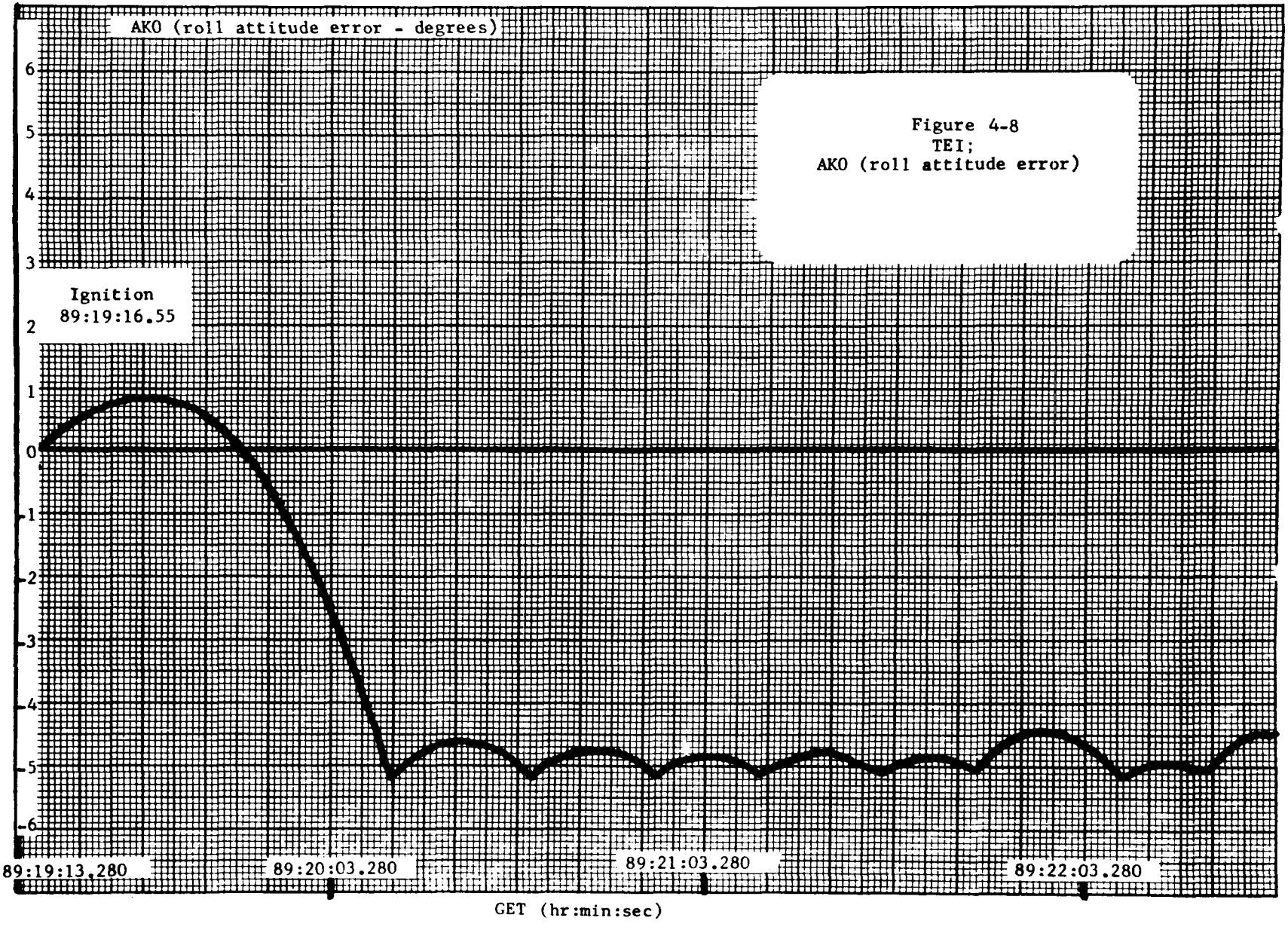

Figure 4-8
TEI;
AKO (roll attitude error)

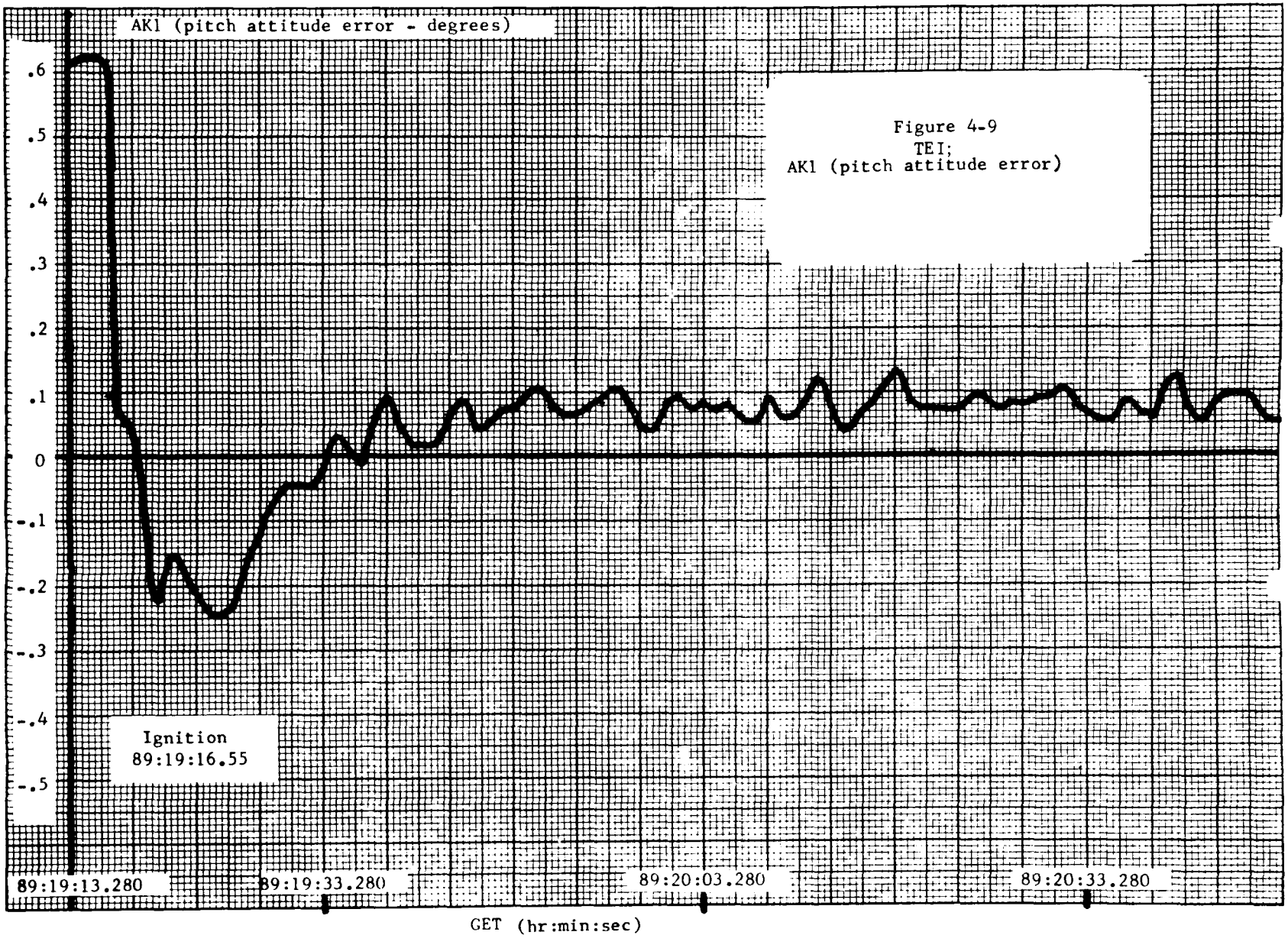

Figure 4-9
TEI;
AK1 (pitch attitude error)

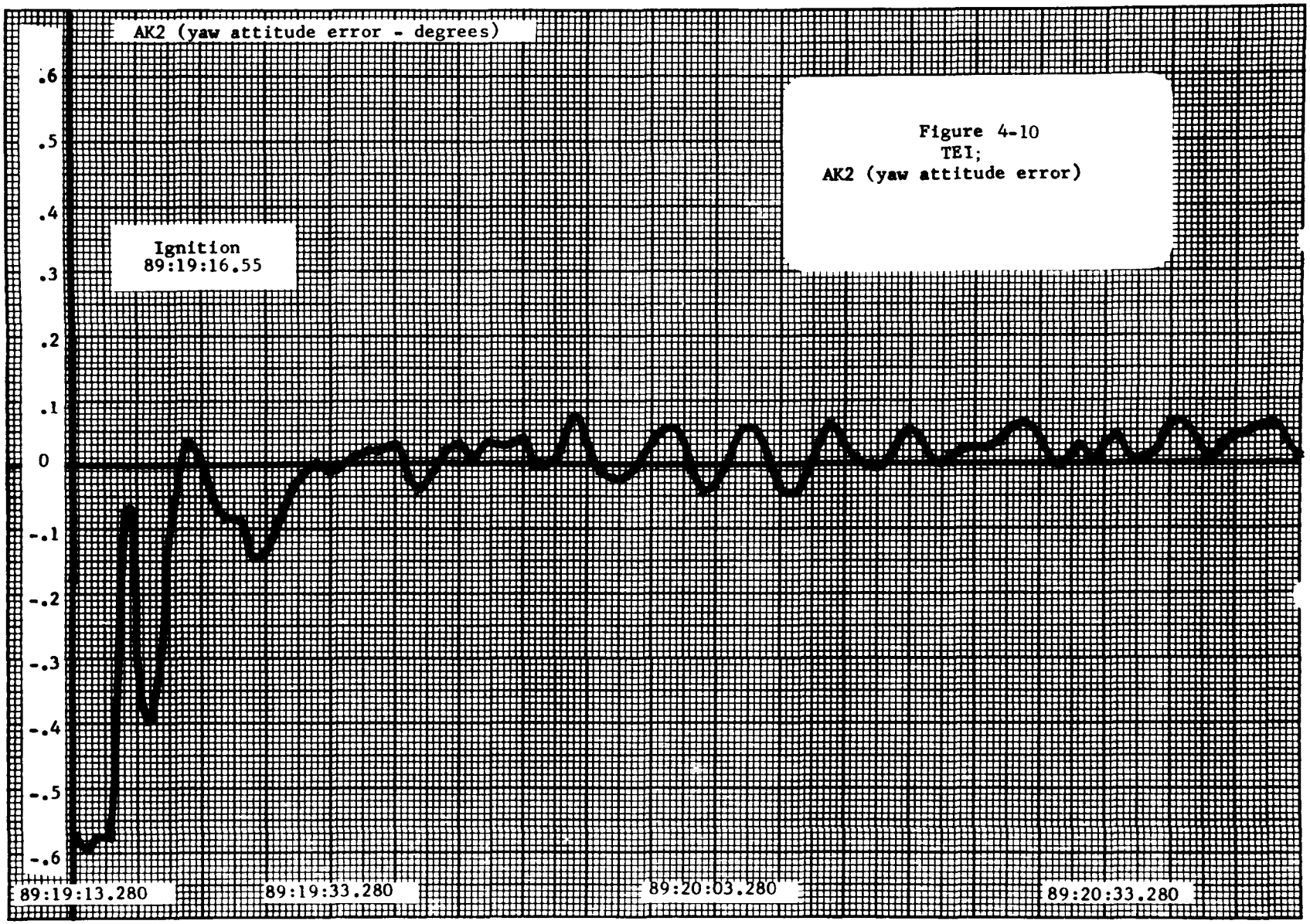

Figure 4-10
TEI;
AK2 (yaw attitude error)

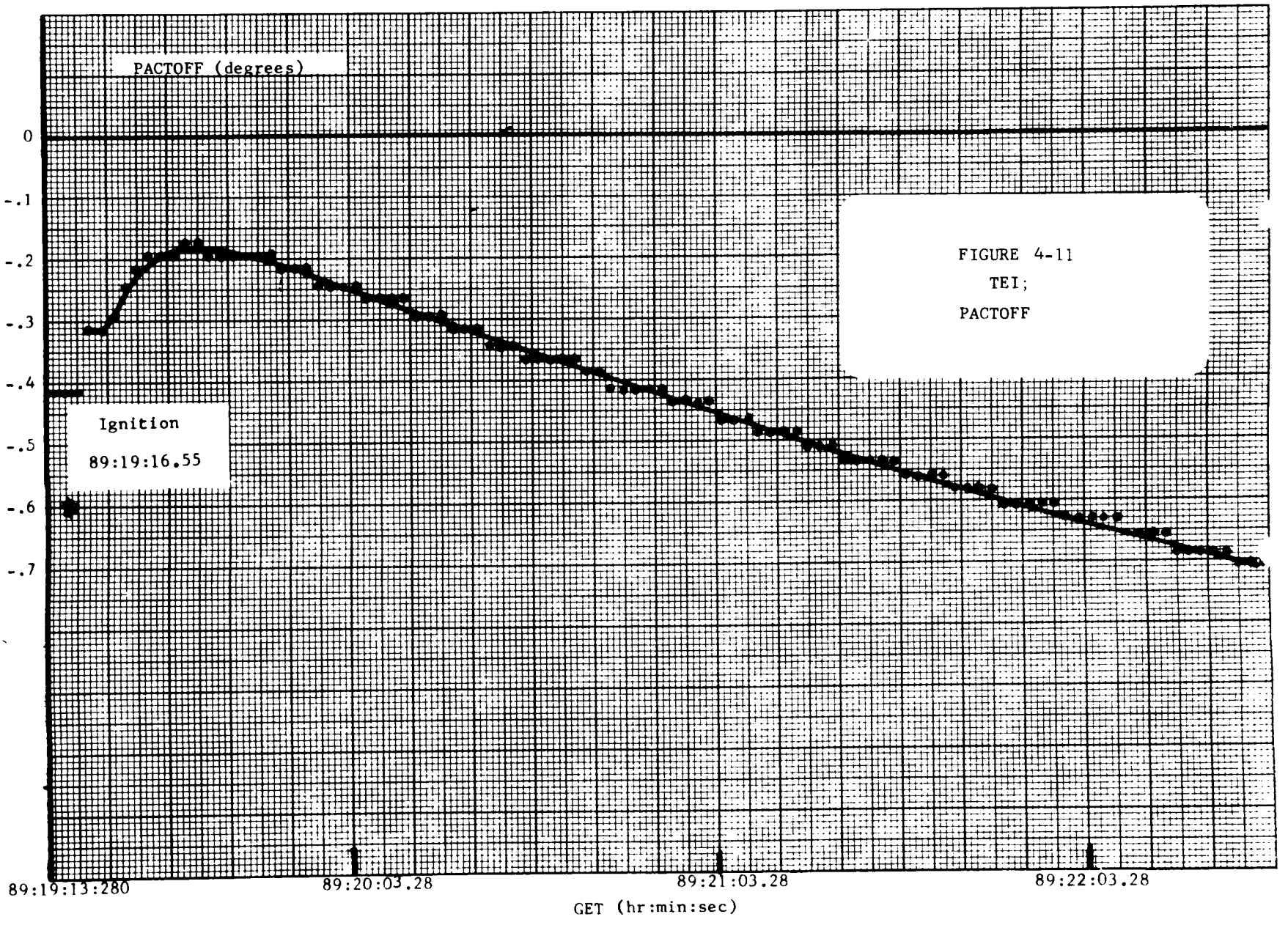

FIGURE 4-11
TEI;
PACTOFF

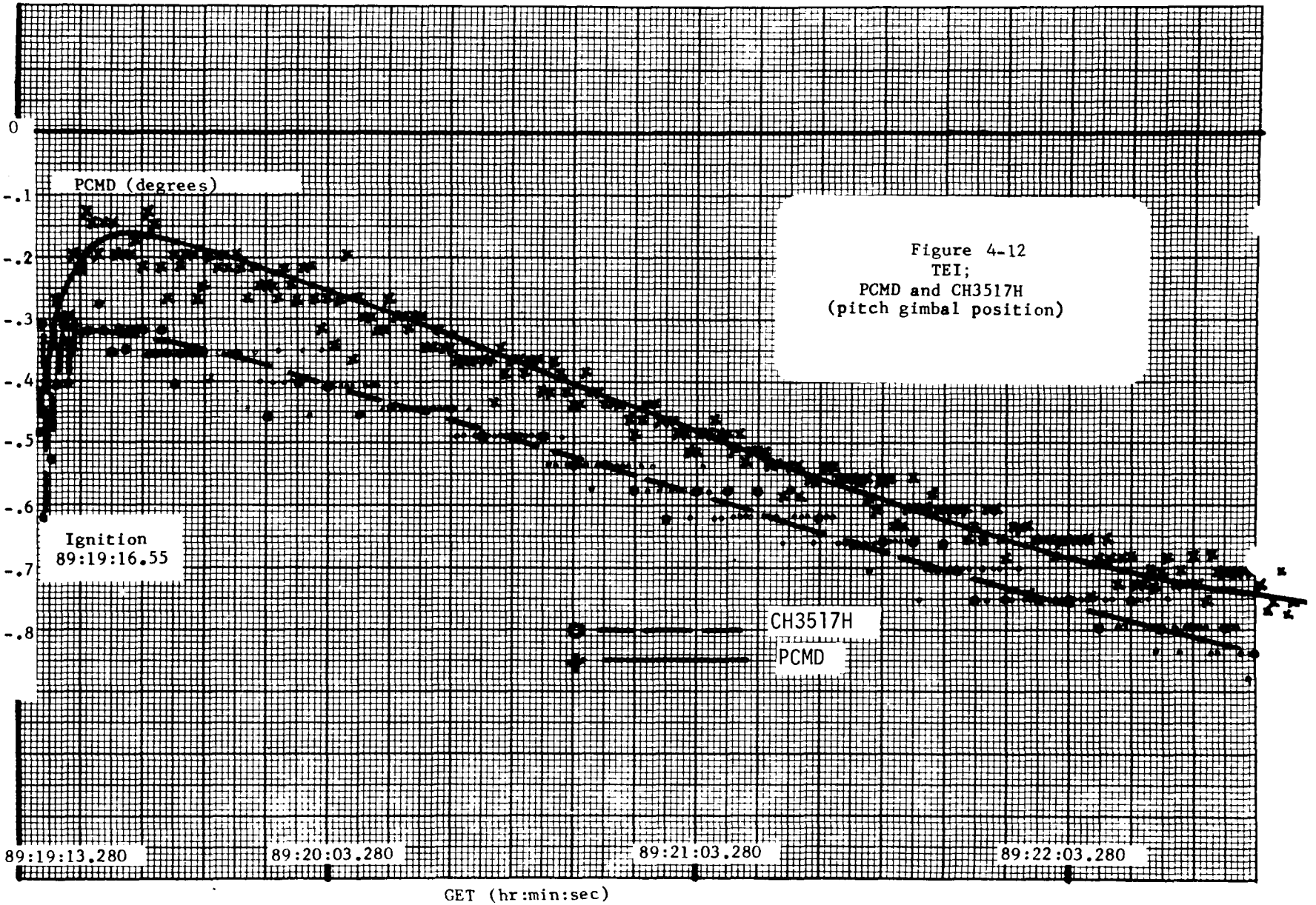

Figure 4-12
TEI;
PCMD and CH3517H
(pitch gimbal position)

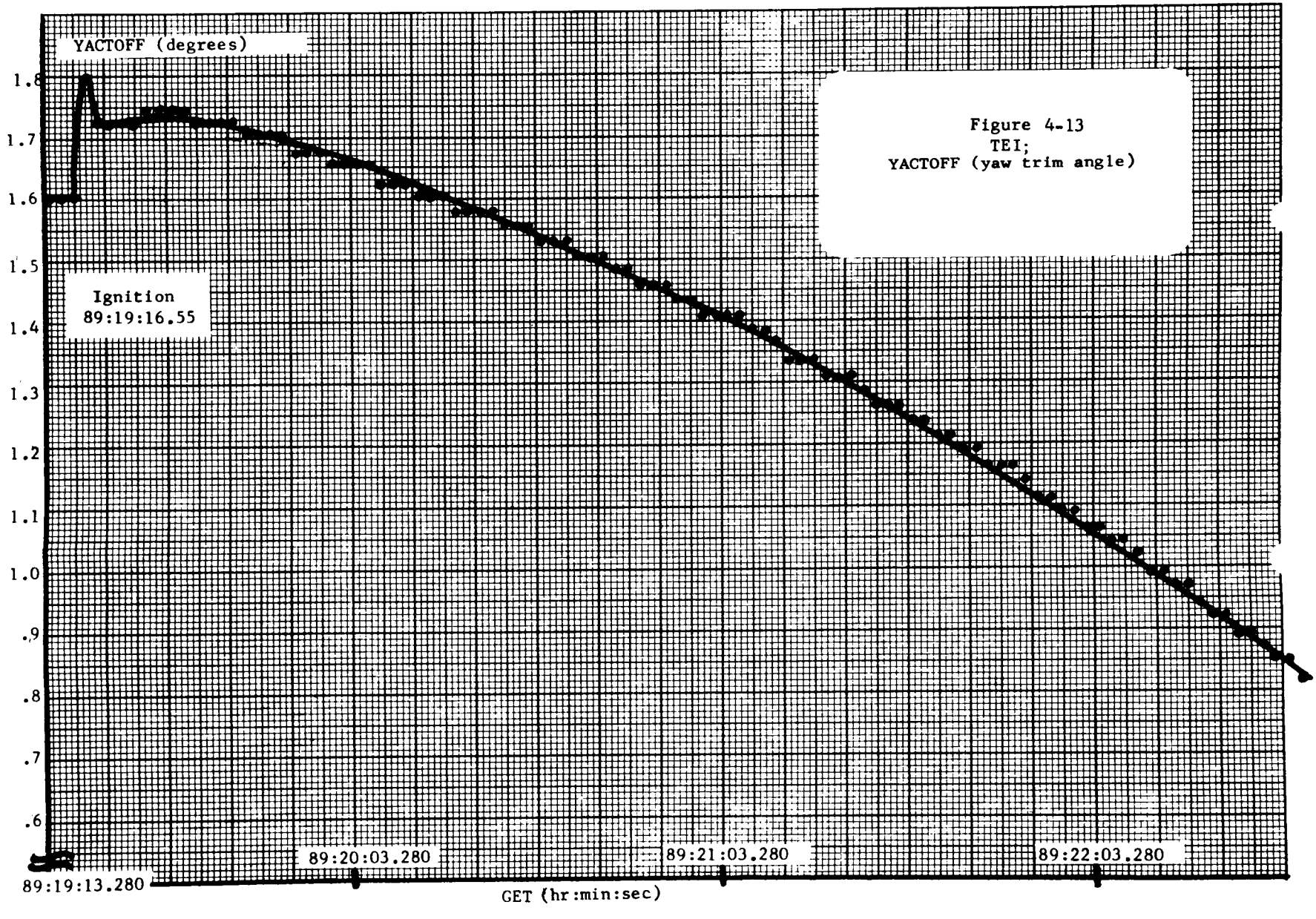

Figure 4-13
TEI;
YACTOFF (yaw trim angle)

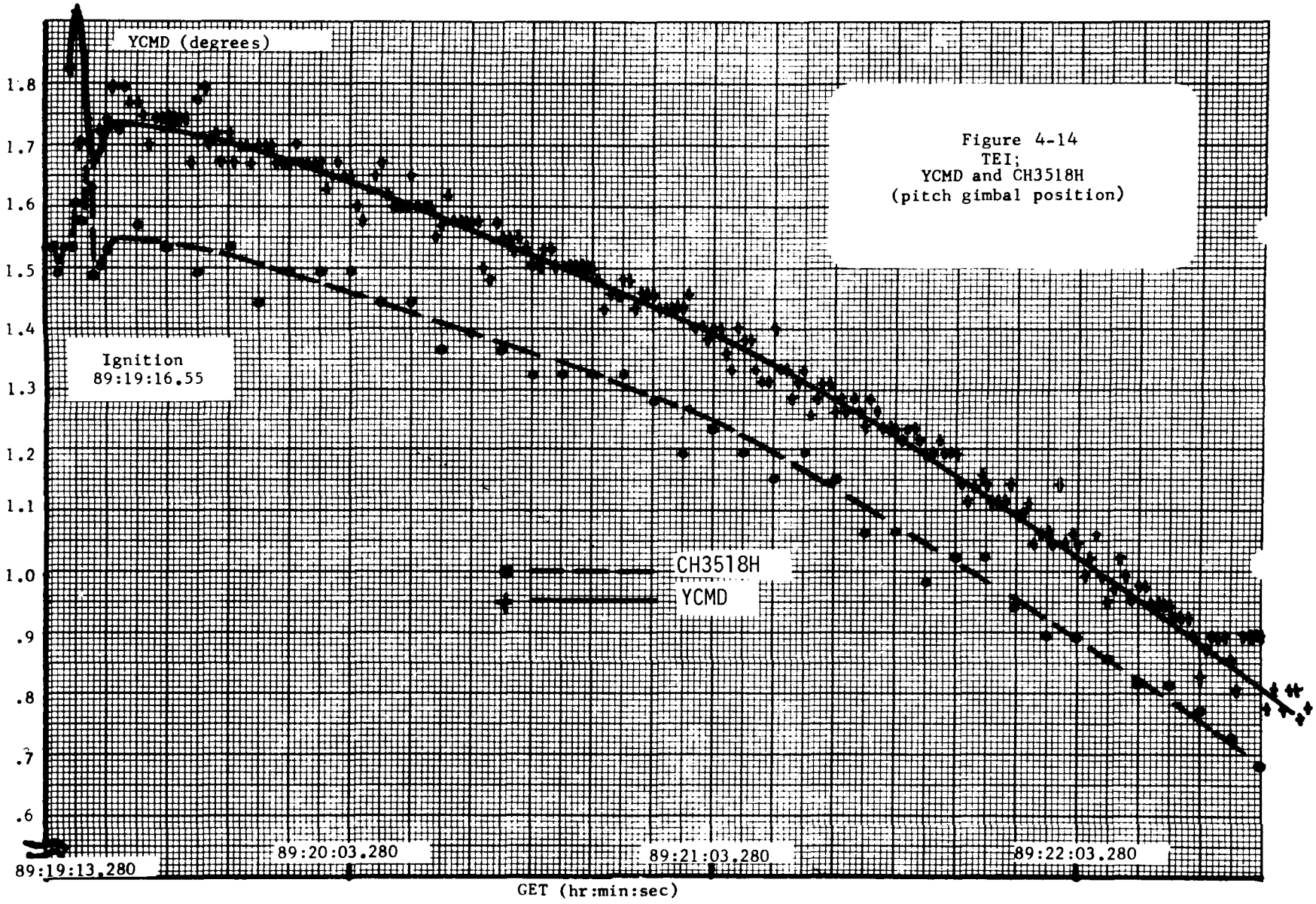

Figure 4-14
TEI;
YCMD and CH3518H
(pitch gimbal position)

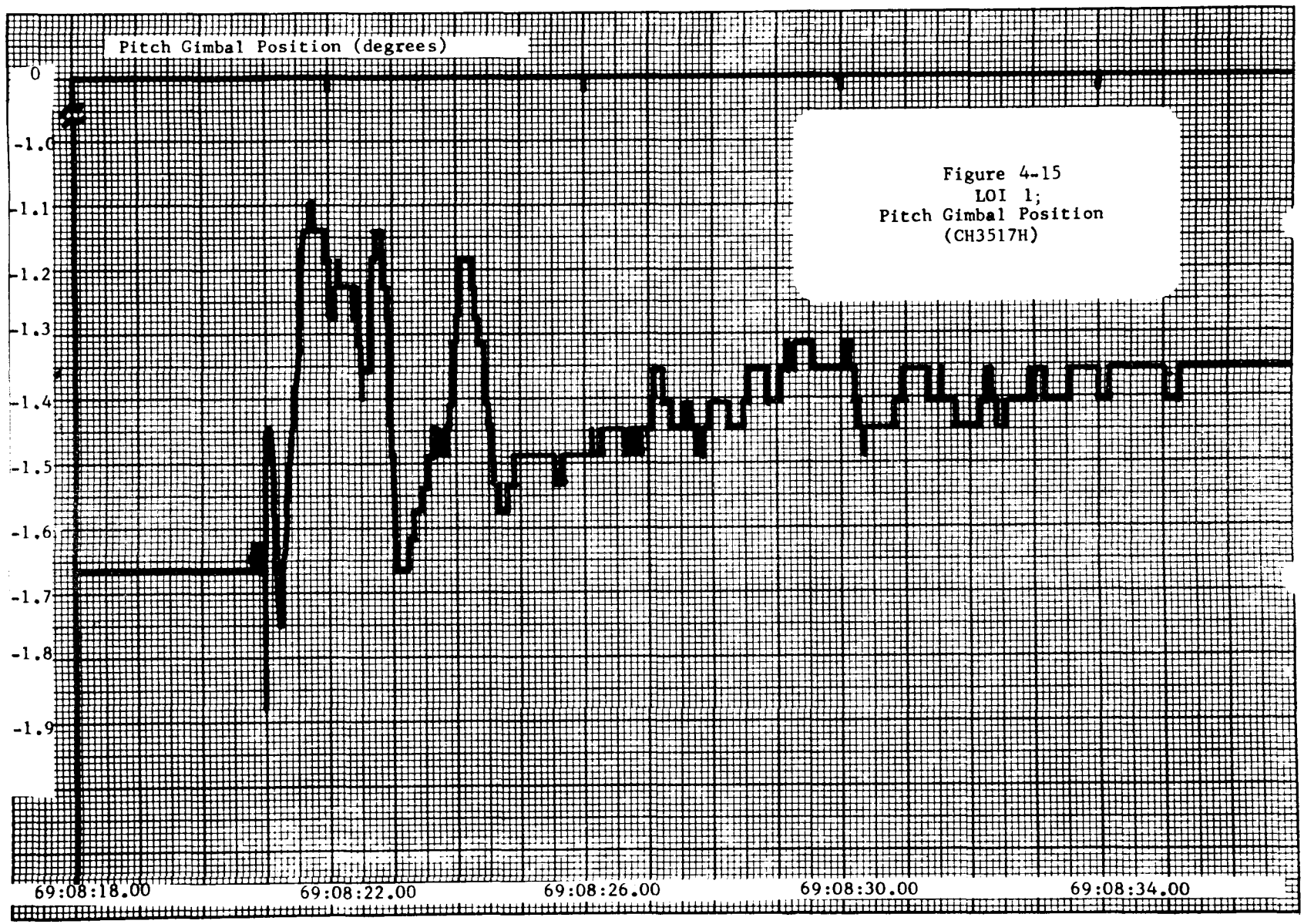

Figure 4-15
LOI 1;
Pitch Gimbal Position
(CH3517H)

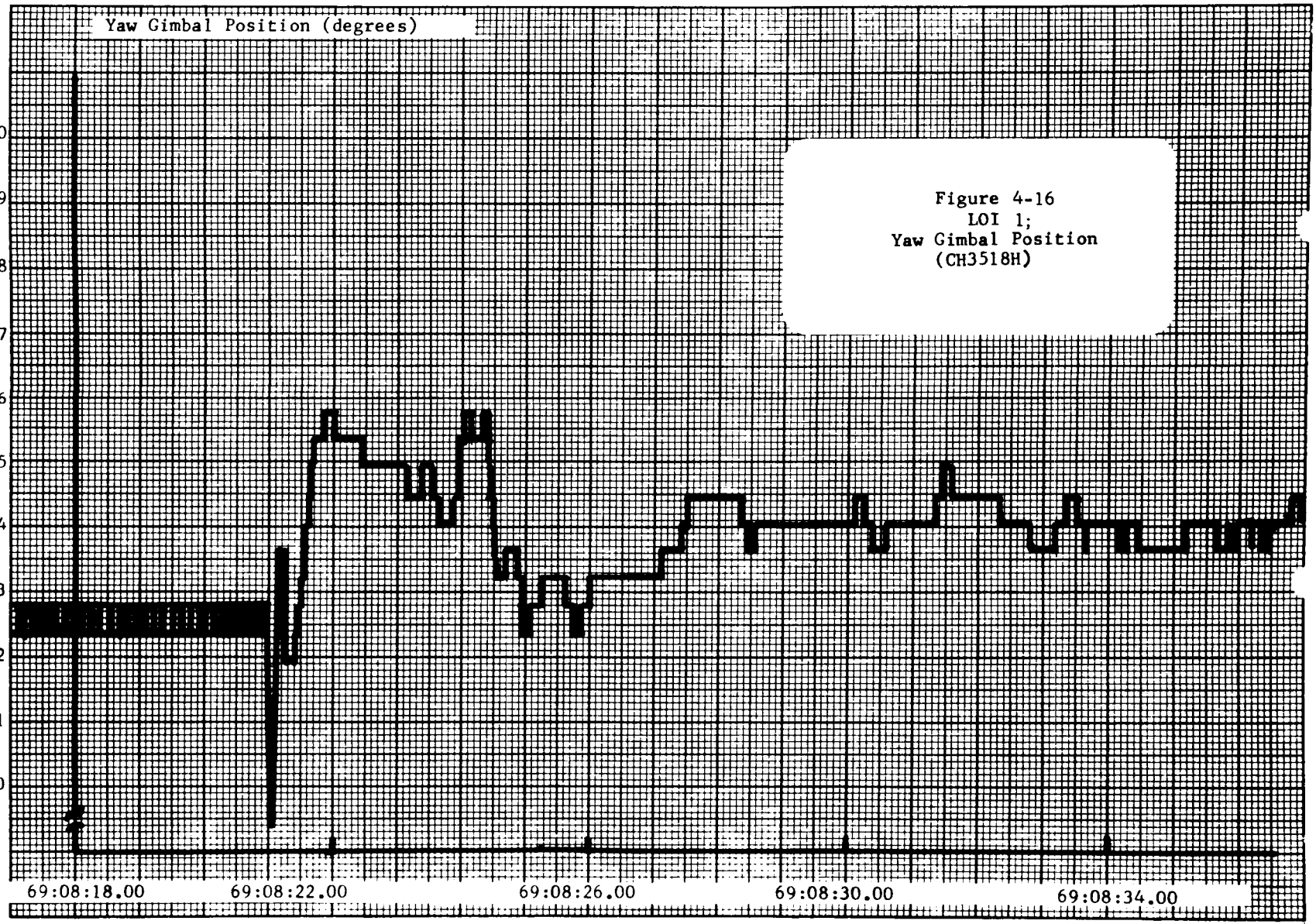

Figure 4-16
LOI 1;
Yaw Gimbal Position
(CH3518H)

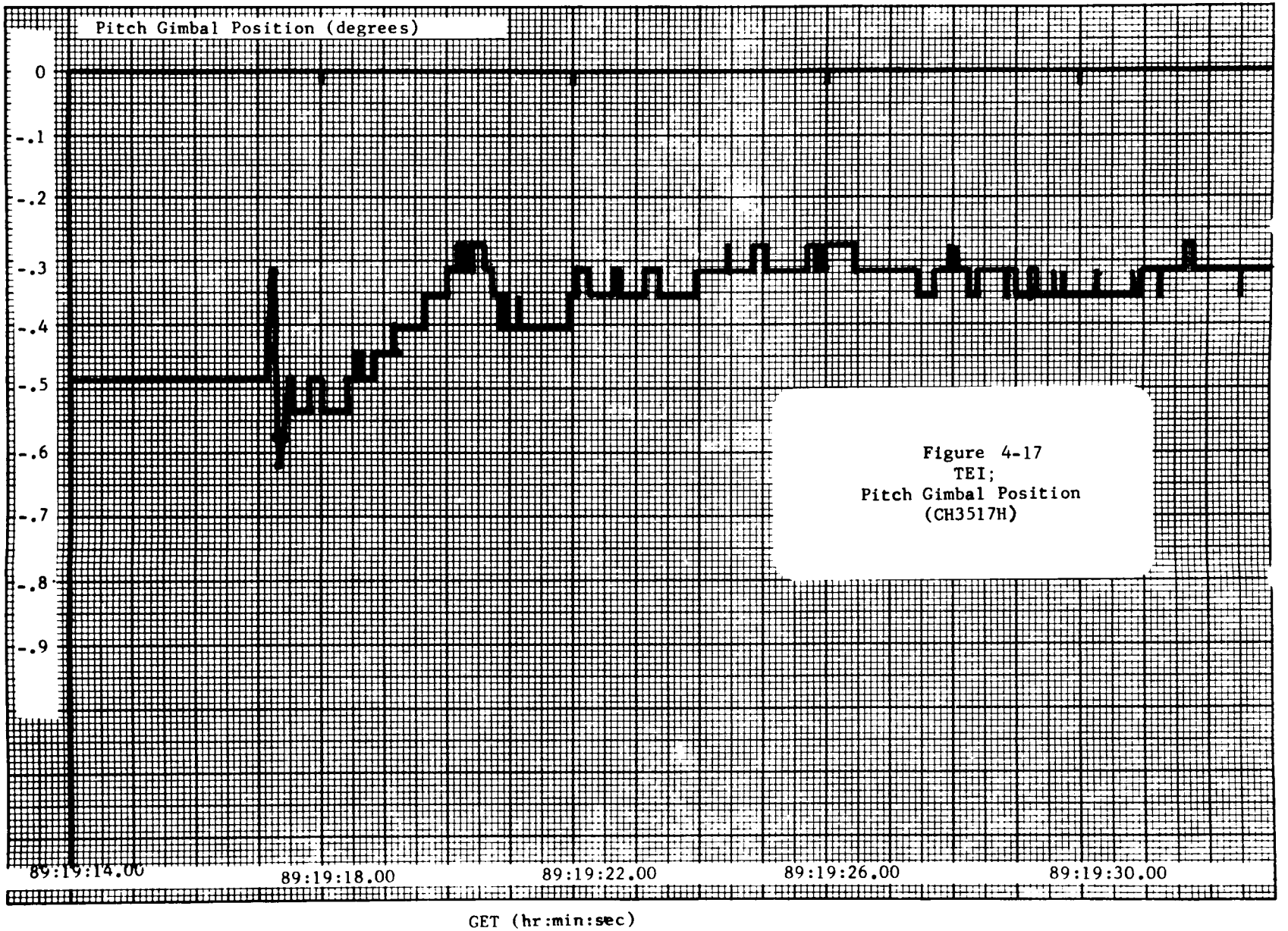

Figure 4-17
TEI;
Pitch Gimbal Position
(CH3517H)

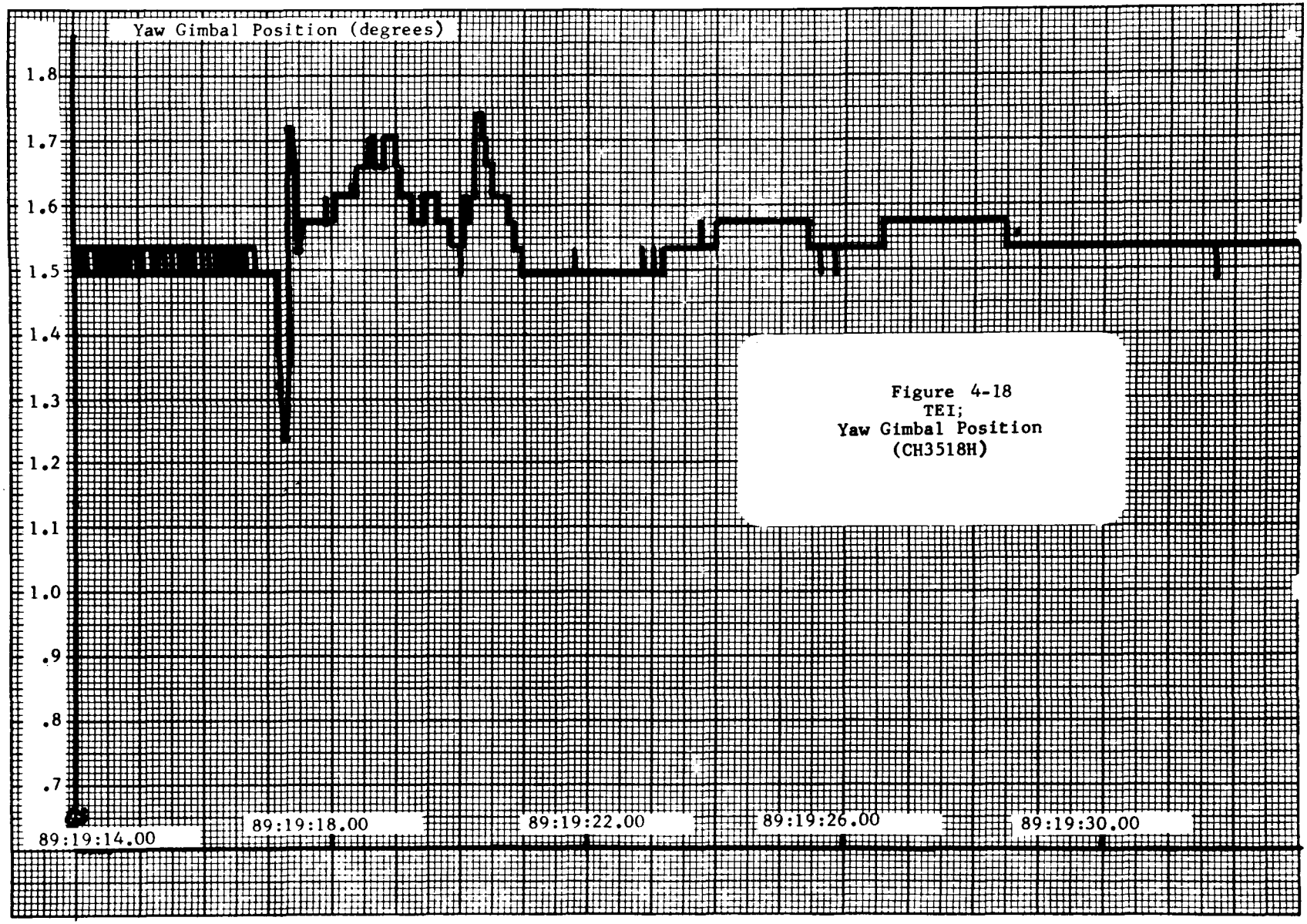

Figure 4-18
TEI;
Yaw Gimbal Position
(CH3518H)

5.0 DAP ATTITUDE CONTROL

This section presents results of analyses of various RCS DAP functions during the Apollo 8 mission. Narrow deadband attitude hold was investigated during periods of THC activity; specifically, during the nulling of MCC 1 ΔV residuals and the transearth MCC, which was an RCS burn. The AUTO maneuver to various burn attitudes was examined. Also, periods of DAP attitude hold limit cycling in the narrow deadband were examined.

5.1 RCS TRANSLATION (TRANSLUNAR)

ΔV residuals resulting from the Apollo 8 translunar MCC were nulled by approximately 22 seconds of +X THC activity. This was accomplished with 4 X-jets active for the translation burn.

Figures 5-1 through 5-3 present phase plane profiles for the period during and following this THC activity. Because these data were only available at 2 second intervals, the plots can only indicate trends; they cannot be used for detailed verification of RCS DAP functions. For example, firing time computations cannot be accurately verified although, considering the lack of data, they appear to be reasonable.

Figures 5-1 through 5-3 are plotted on identical scales to facilitate comparisons of control activity in the three axes. Initial vehicle roll accelerations in Figure 5-1 arise from jet firings about the pitch and yaw axes, which couple into the X- direction via product of inertia terms. This necessitates several firings for X- rotation control; however, Figures 5-1 through 5-3 show that X-axis activity is of a low level compared to requirements in the other axes.

Y and Z axes rates result primarily from vehicle c.g. offsets in the Z and Y directions respectively. During the time period analyzed, the c.g. position was approximately +4 inches in the Y direction and +6.5 inches in Z. The figures show that the RCS DAP performed well in maintaining the vehicle state within the control deadzone during the period of translation. Upon termination of THC activity, the DAP control began to evolve toward steady state minimum impulse limit cycles in all three axes.

Two DAP error resets (to zero) are indicated in Figures 5-1 through 5-3. These are normal operations performed by the automatic program exit

routine (R00). In Figure 5-1, the vehicle state trace between 11:02:25 and 11:04:11 g.e.t. verifies the DAP's ability to adequately measure a minute S/C roll rate of approximately .003 deg/sec.

Only one transearth MCC was required during Apollo 8. It occurred approximately 15 hours after TEI. This was an RCS burn consisting of approximately 16 seconds of +X THC activity followed by about 2 seconds of -X THC firings.

Figures 5-4 through 5-6 illustrate the RCS DAP's attitude hold performance during this MCC. The X and Y rate excursions induced during this period were significantly greater than during ΔV nulling after the translunar MCC. This occurred because the vehicle mass and inertia values had decreased considerably: Ixx by 45 percent and Iyy by 25 percent. Rates induced about the Z axis during the transearth MCC were not as great as during MCC 1 ΔV trimming because, while Izz decreased by approximately 25 percent, the Y c.g. offset value more than compensated by decreasing approximately 65 percent. Even with the larger overall induced spacecraft rates, Figures 5-4 through 5-6 verify that the RCS DAP adequately maintained the vehicle state within the control deadzone.

Figure 5-5 illustrates a period of 24 seconds (104:00:53 to 104:01:17 g.e.t.) during which the DAP correctly measured an S/C pitch rate of .026 deg/sec. During the period from 104:00:43 to 104:00:52, Figure 5-4 shows the DAP's rate measurement function being slightly in error. The attitude error change during this time implies a rate of -.041 deg/sec, while the DAP computed value is -.035 deg/sec, a difference of approximately 15 percent. This is not a problem, because the rates involved are so low. The error appears to be a cross-coupling effect, resulting from Y-jet activity during this time period. This small error is not significant; it merely shows that the DAP lags behind rate changes induced by off-axis jet firings. This is especially true for light vehicle weights.

5.2 AUTO MANEUVERS

A crew-defined automatic maneuver to the TEI burn attitude was performed approximately 1 lunar revolution before the actual TEI burn. This was primarily a roll maneuver. It lasted for approximately 12 minutes and consisted of a 140 degree change in outer gimbal angle together with small

changes of 10 degrees or less in pitch and yaw. A 0.2 deg/sec maneuver rate was employed. Downlink data show that most of this (0.198 deg/sec, was commanded about the X-control axis. Data for this period is only available at low bit rate; however, comparisons of commanded and actual CDU values show excellent agreement, with errors less than .01 degree.

Two large angle pitch and yaw automatic maneuvers at 0.5 deg/sec and 0.2 deg/sec were analyzed in detail in the post flight analysis. After the 0.5 deg/sec maneuver at g.e.t., 10 hr 48 min, the DAP was configured for the 0.2 deg/sec maneuver rate and subsequent maneuvers during the flight were performed at the lower rate. The automatic maneuver to MCC1 burn attitude was performed at 0.5 deg/sec. Desired X, Y and Z axis body rates for the maneuver were calculated by the CMC as .344, .0538 and -.3589 deg/sec respectively for a total desired angular rate of 0.5 deg/sec. The maneuver was initiated at g.e.t., 10 hr 27 min 57 sec and terminated at g.e.t., 10 hr 31 min 18 sec. Final CDU desired and CDU actual angles during the maneuver are shown in Figure 5-7. DAP estimated and desired body rates during the maneuver are shown in Figure 5-8. Figures show that DAP operation during the maneuver was entirely nominal. The DAP successfully maneuvered the CSM at the desired body rates to the desired CDU angles and terminated the maneuver with little or no overshoot. The following DAP functions for automatic maneuver were thus verified.

1) The maneuver rate of 0.5 deg/sec was resolved into desired rates in each body axis, WBODY X, Y and Z.

2) Desired CDU angles were correctly incremented during the maneuver resulting in actual body rates achieving desired body rates.

3) At termination of the maneuver, CDU-CDUD errors resolved into body axis errors were within the DAP deadband and attitude hold was initiated.

The maneuver to LOI burn attitude was performed by the DAP at 0.2 deg/sec. Desired X, Y, and Z axis body rates calculated by the CMC were .0088, -.1651, and .1126 deg/sec respectively for a total angular rate of 0.2 deg/sec. The maneuver was initiated at g.e.t., 66 hr 56 min 40 sec and terminated at g.e.t., 67 hr 07 min 10 sec. Final CDU desired and CDU actual angles during the maneuver are shown in Figure 5-9. DAP estimated rates and desired body rates during the maneuver are shown in Figure 5-10.

X, Y, and Z axis phase plane plots are shown in Figures 5-11, 5-12 and 5-13 for DAP narrow deadband attitude hold. DAP operation was entirely according to the phase plane design. What appears to be an overshoot of the DAP switching line corresponds to the IMU gimbal angle resolution of .011 degrees.

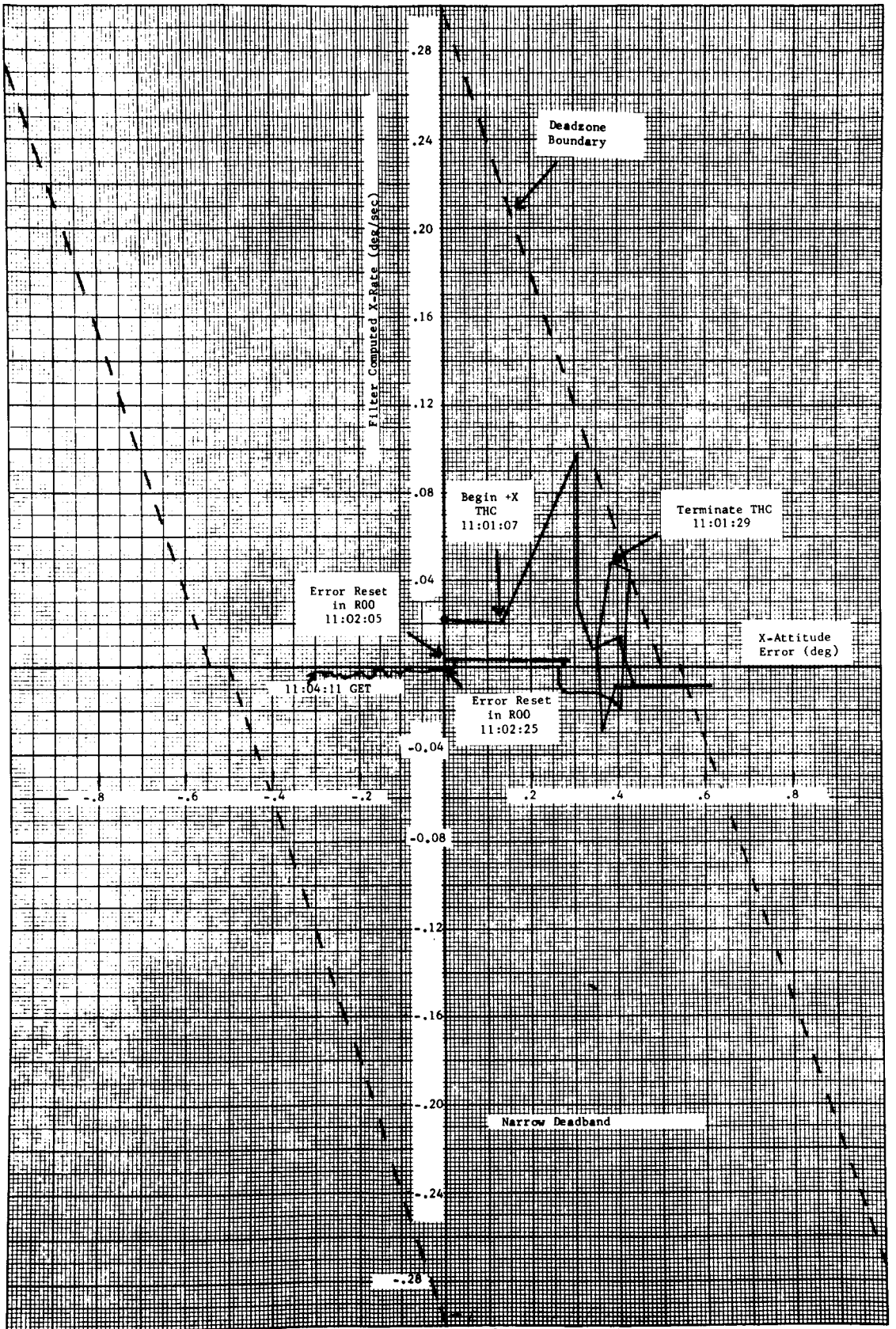

Figure 5-1 X-Axis attitude Hold - Trimming of MCC1 ΔV Residuals

5-5

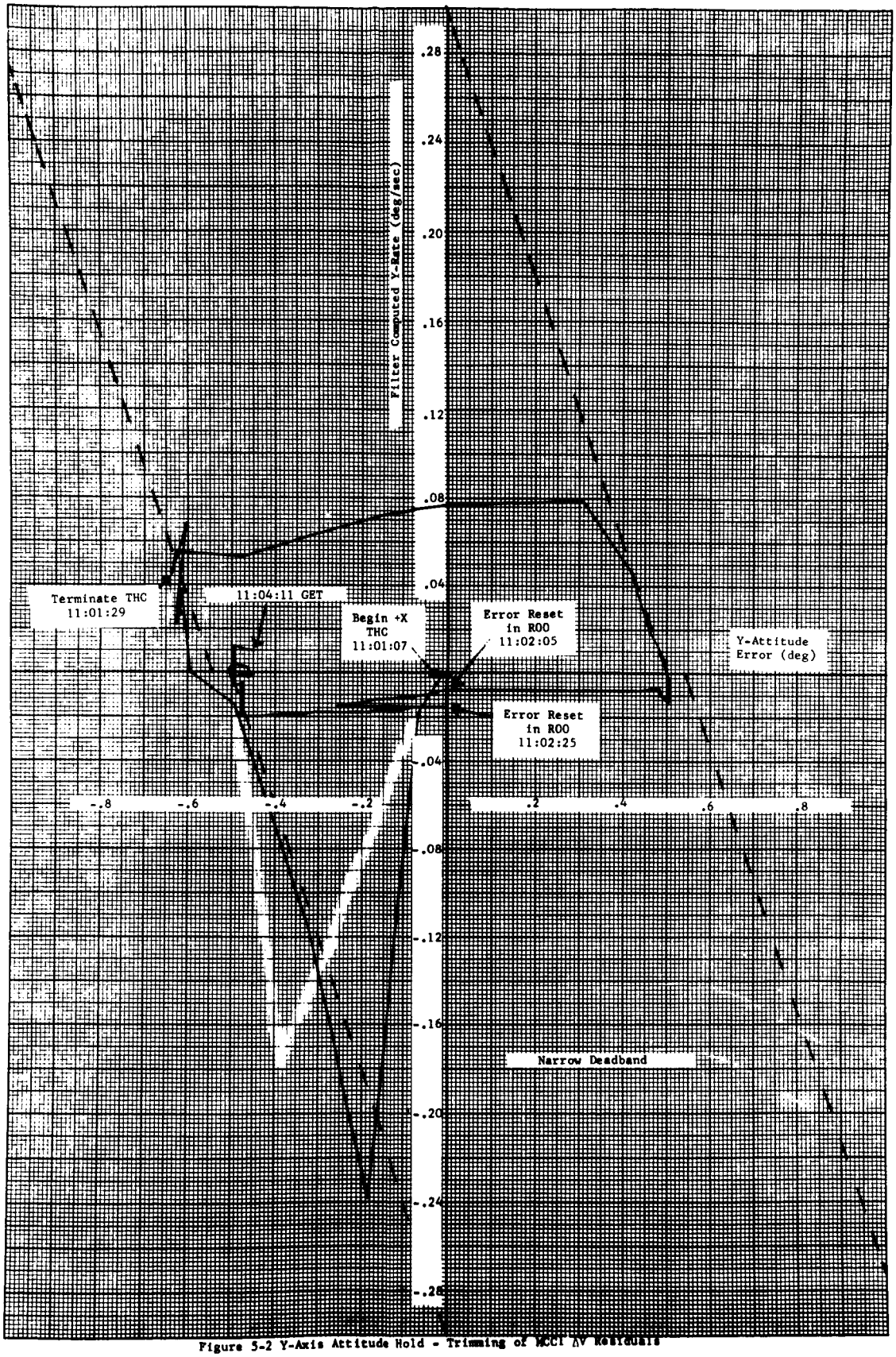

Figure 5-2 Y-Axis Attitude Hold - Trimming of MCC1 ΔV Residuals

5-7

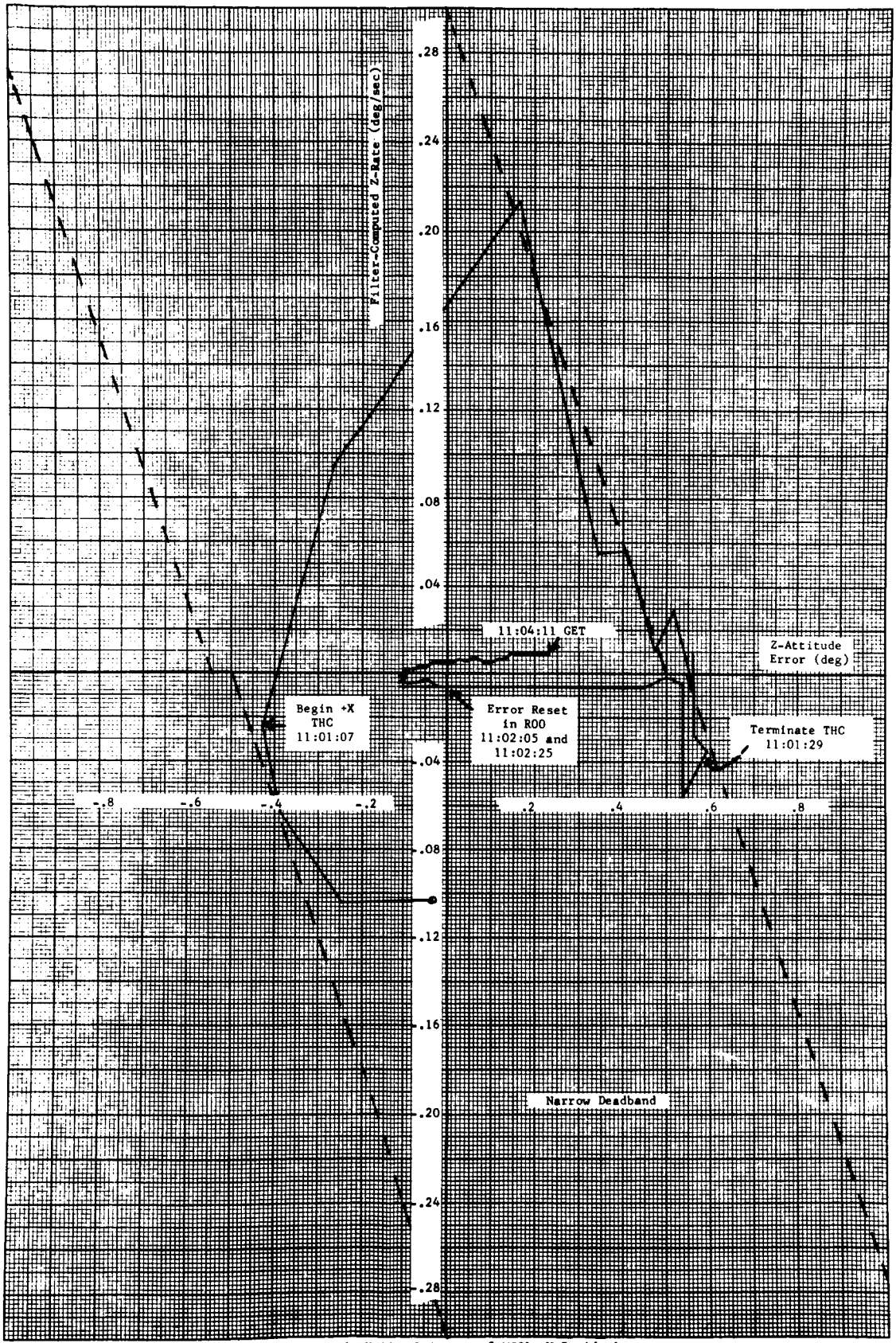

Figure 5-3 Z-Axis Attitude Hold - Trimming of MCC1 ΔV Residuals

5-9

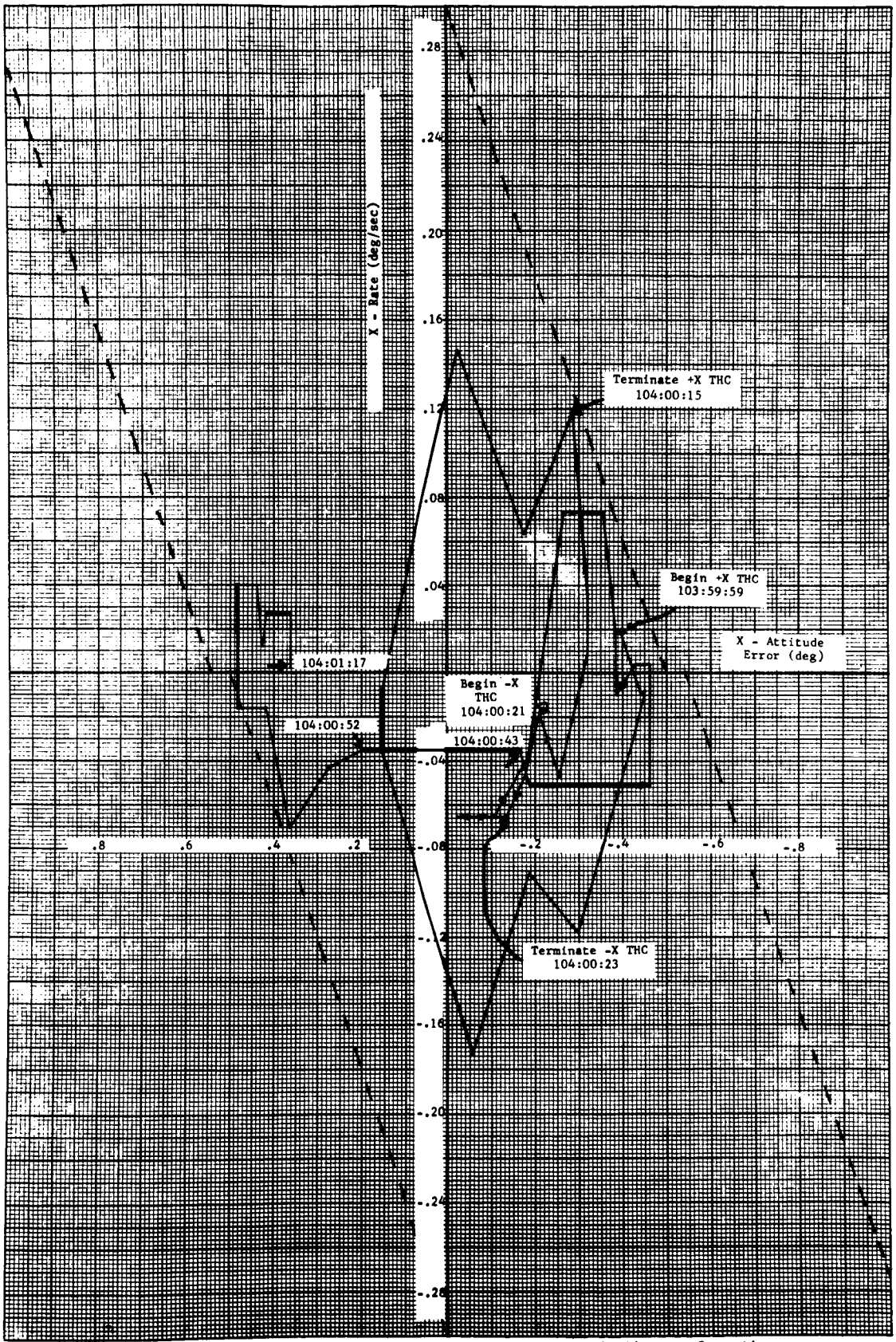

Figure 5-4 X - Axis Attitude Hold - Transearth Mid-course Correction

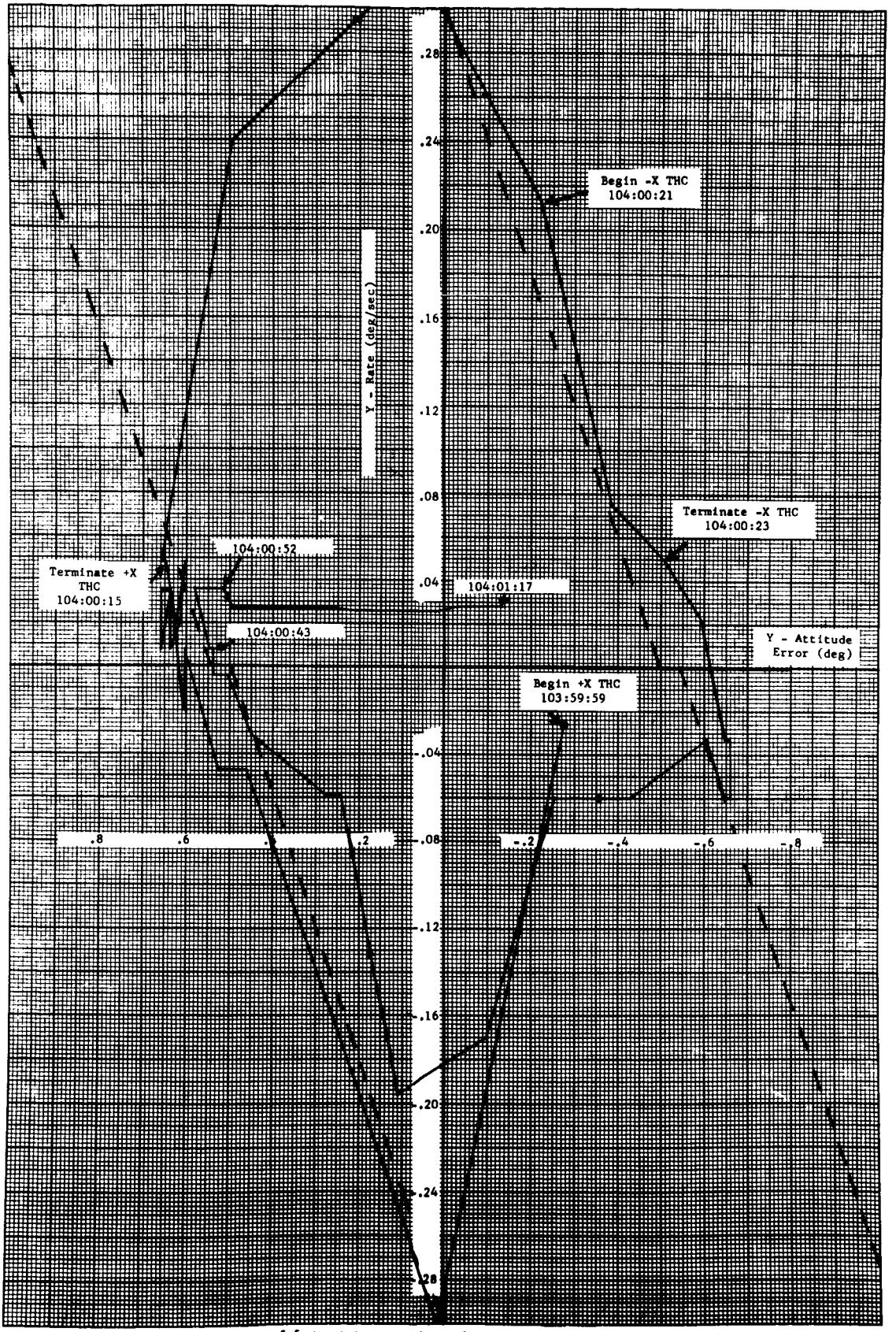

Figure 5-5 Y - Axis Attitude Hold - Transearth Mid-course Correction

5-13

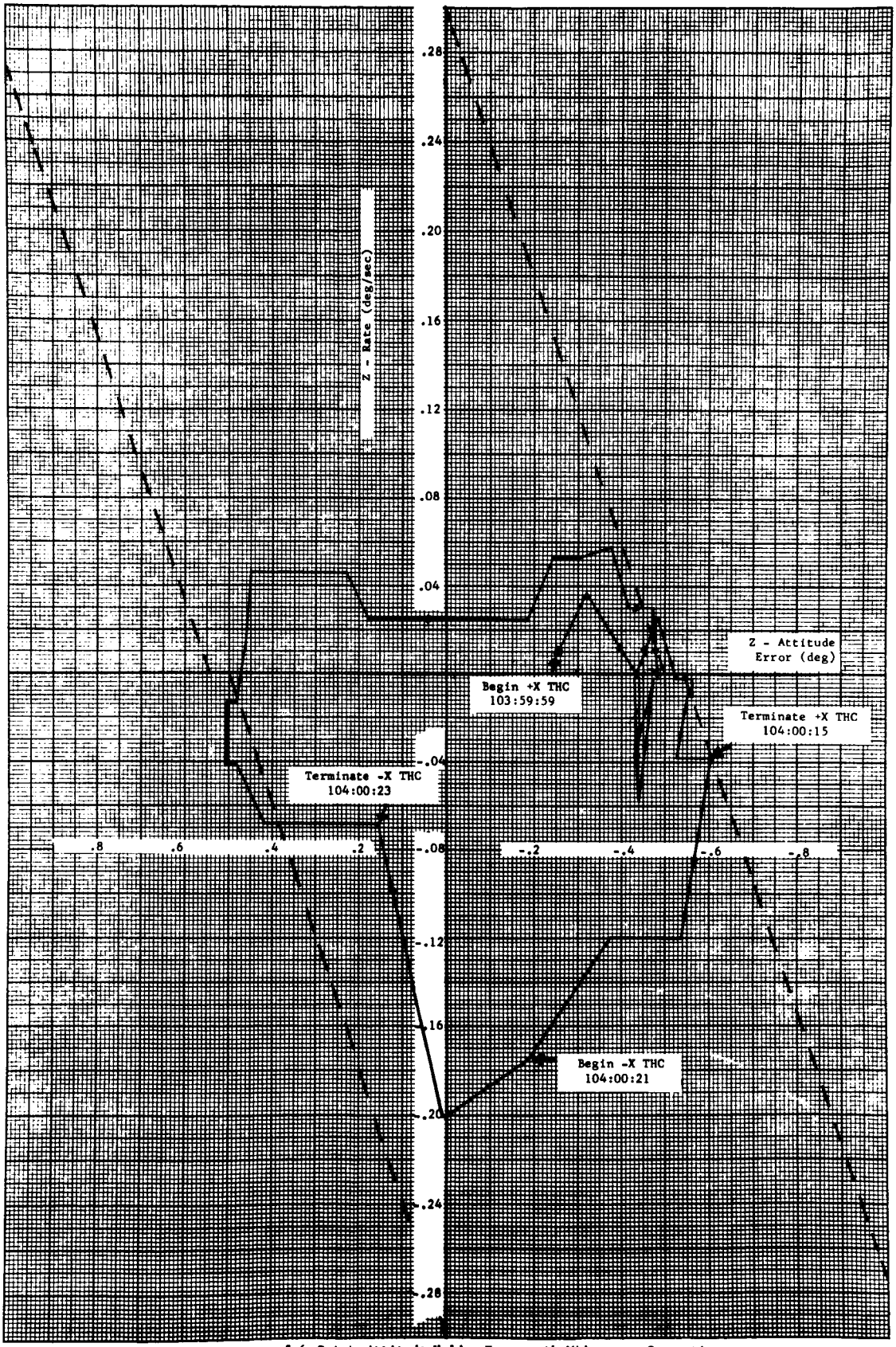

Figure 5-6 Z-Axis Attitude Hold - Transearth Mid-course Correction

5-15

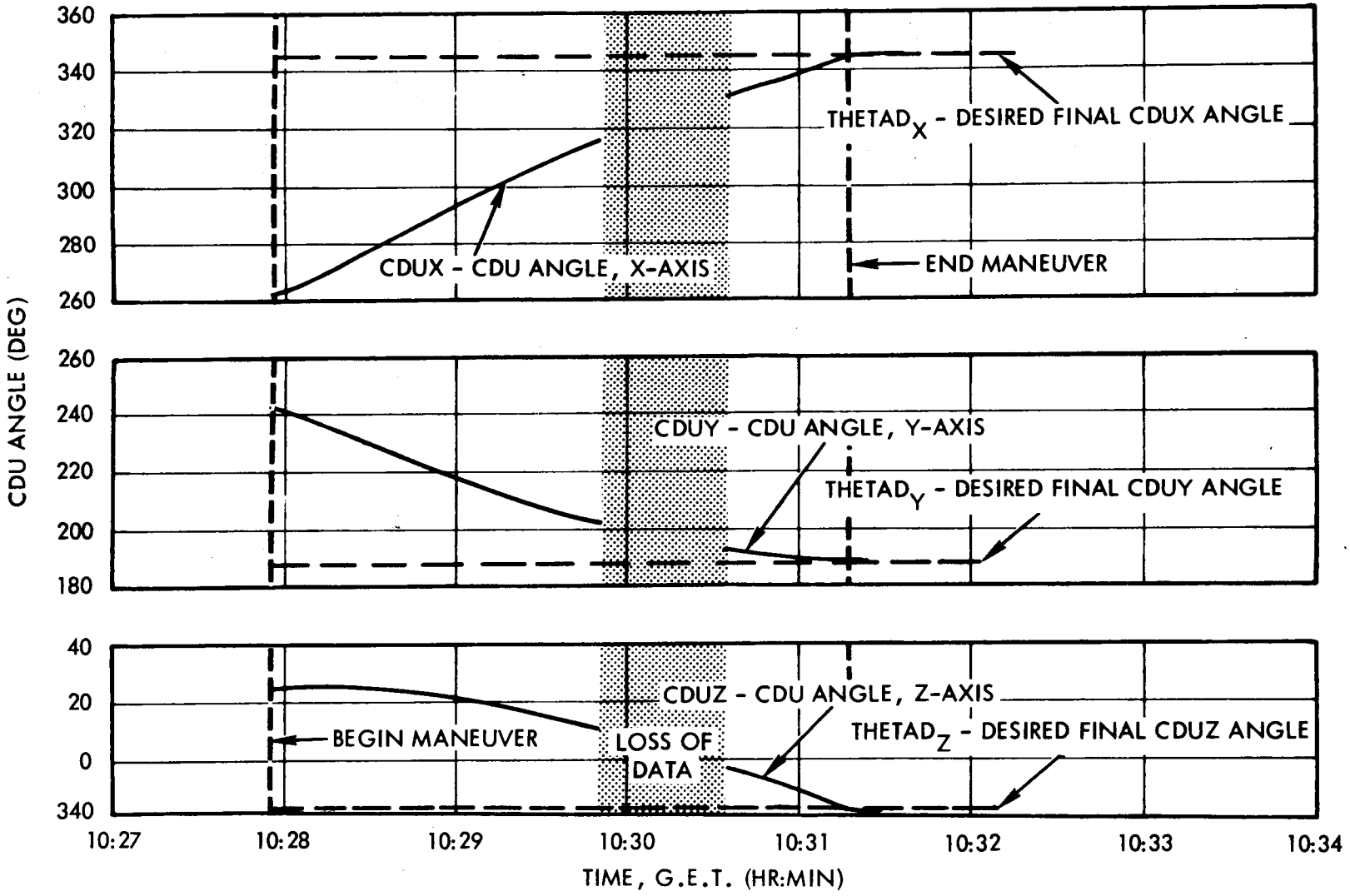

Figure 5-7. Automatic Maneuver, 0.5 deg/sec CDU Angle

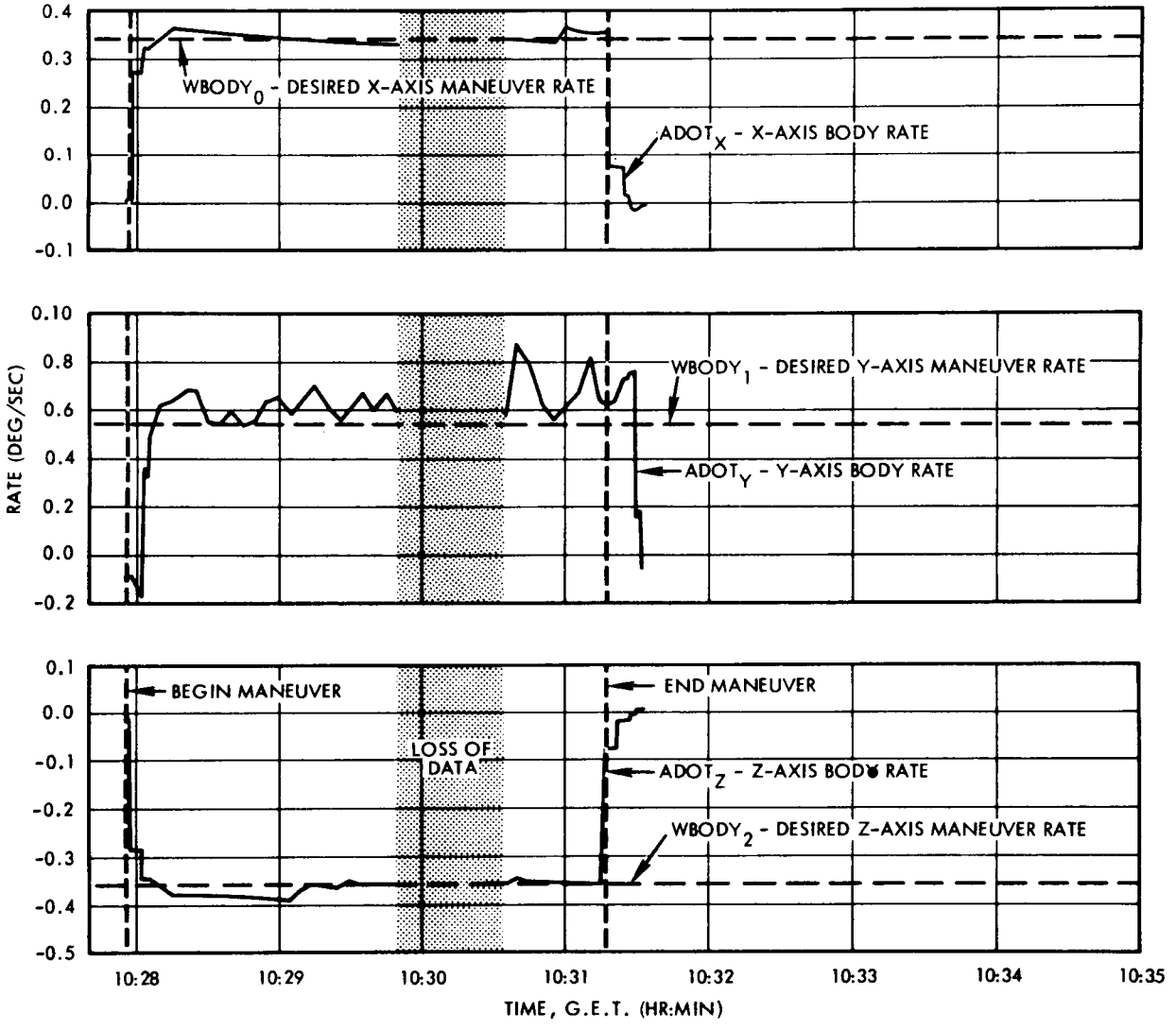

Figure 5-8. Automatic Maneuver, 0.5 deg/sec, Body Rates

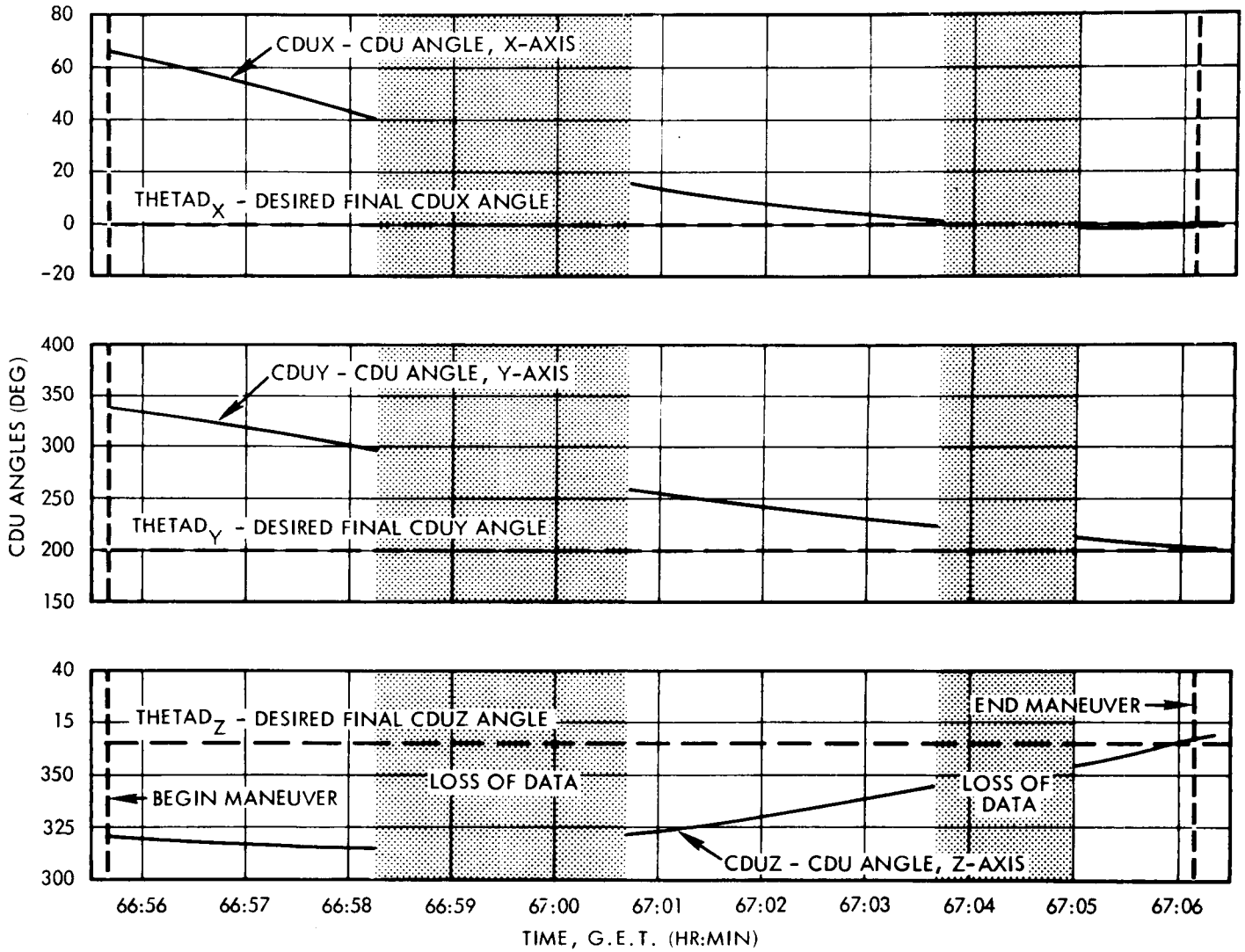

Figure 5-9. Automatic Maneuver, 0.2 deg/sec, CDU Angles

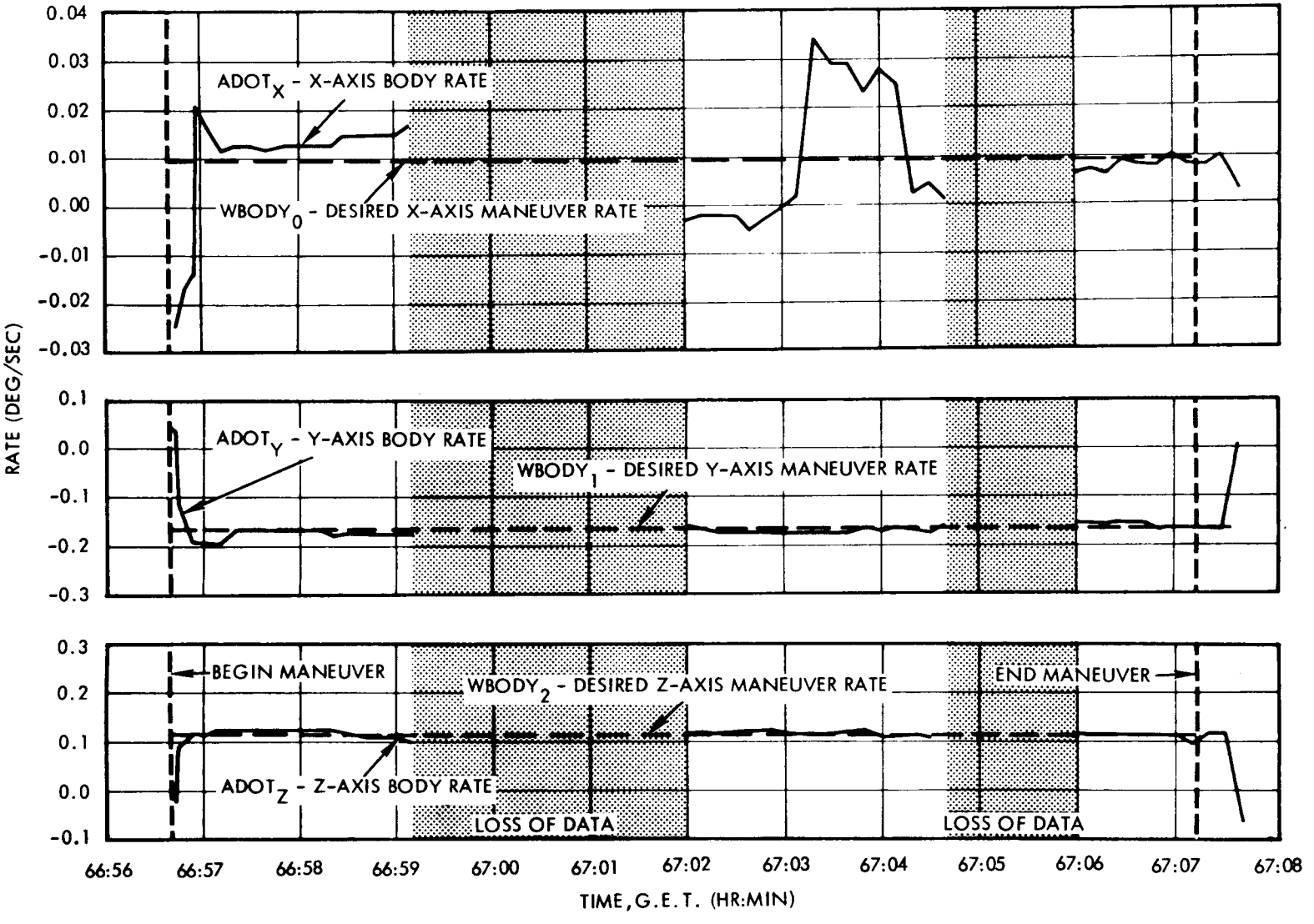

Figure 5-10. Automatic Maneuver, 0.2 deg/sec Body Rates

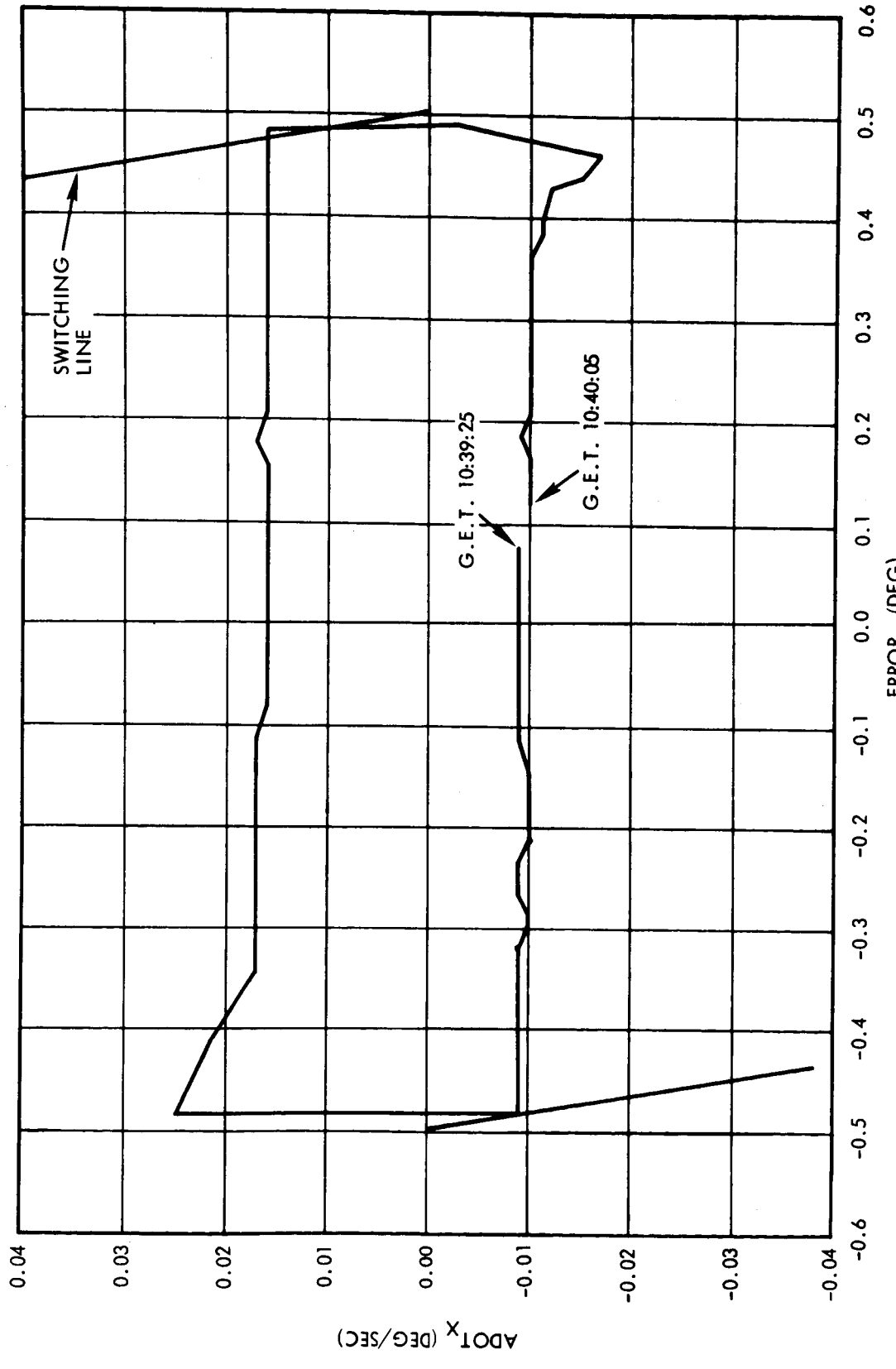

Figure 5-11. DAP Attitude Hold - X-Axis (Narrow Deadband)

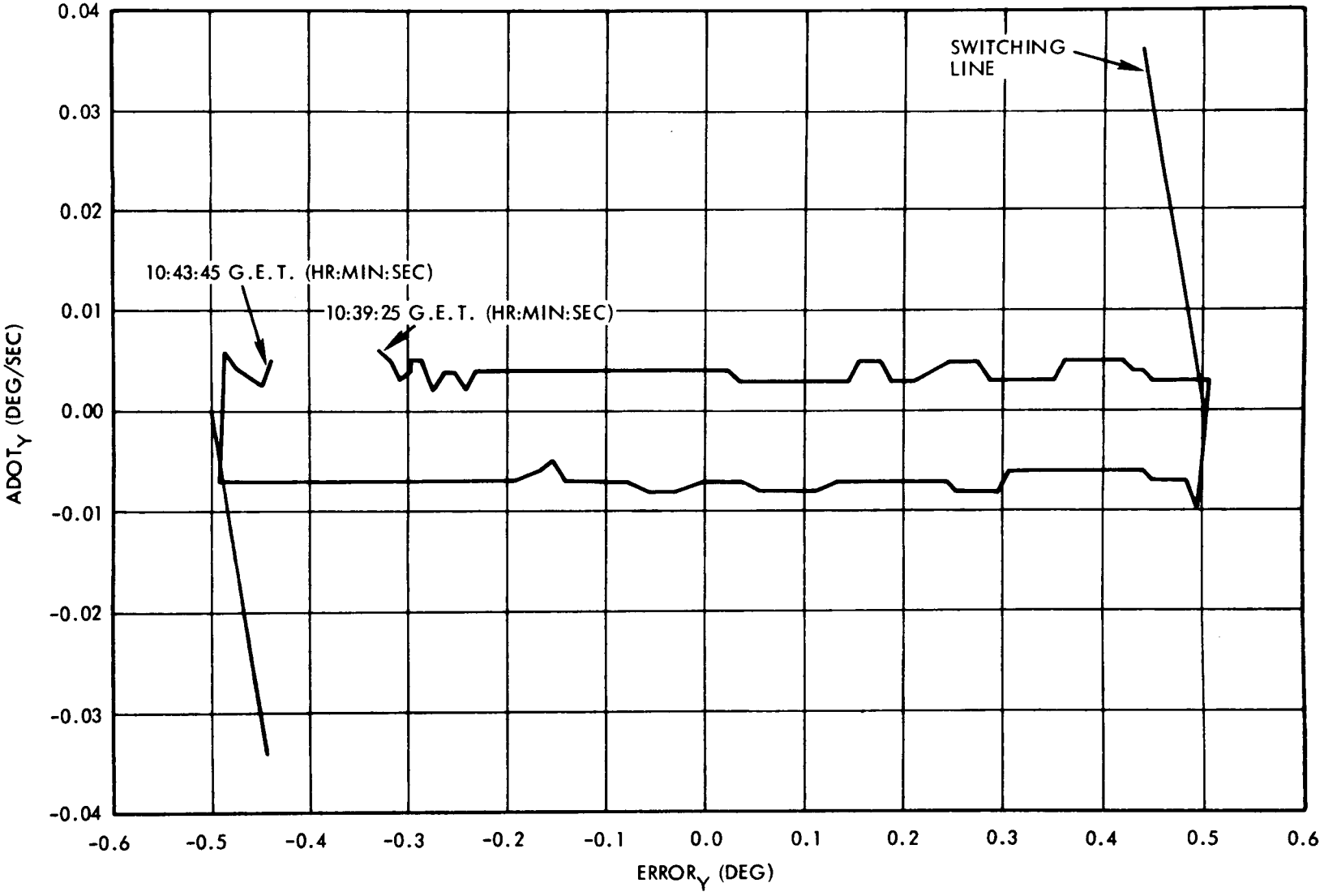

Figure 5-12. DAP Attitude Hold -Y Axis (Narrow Deadband)

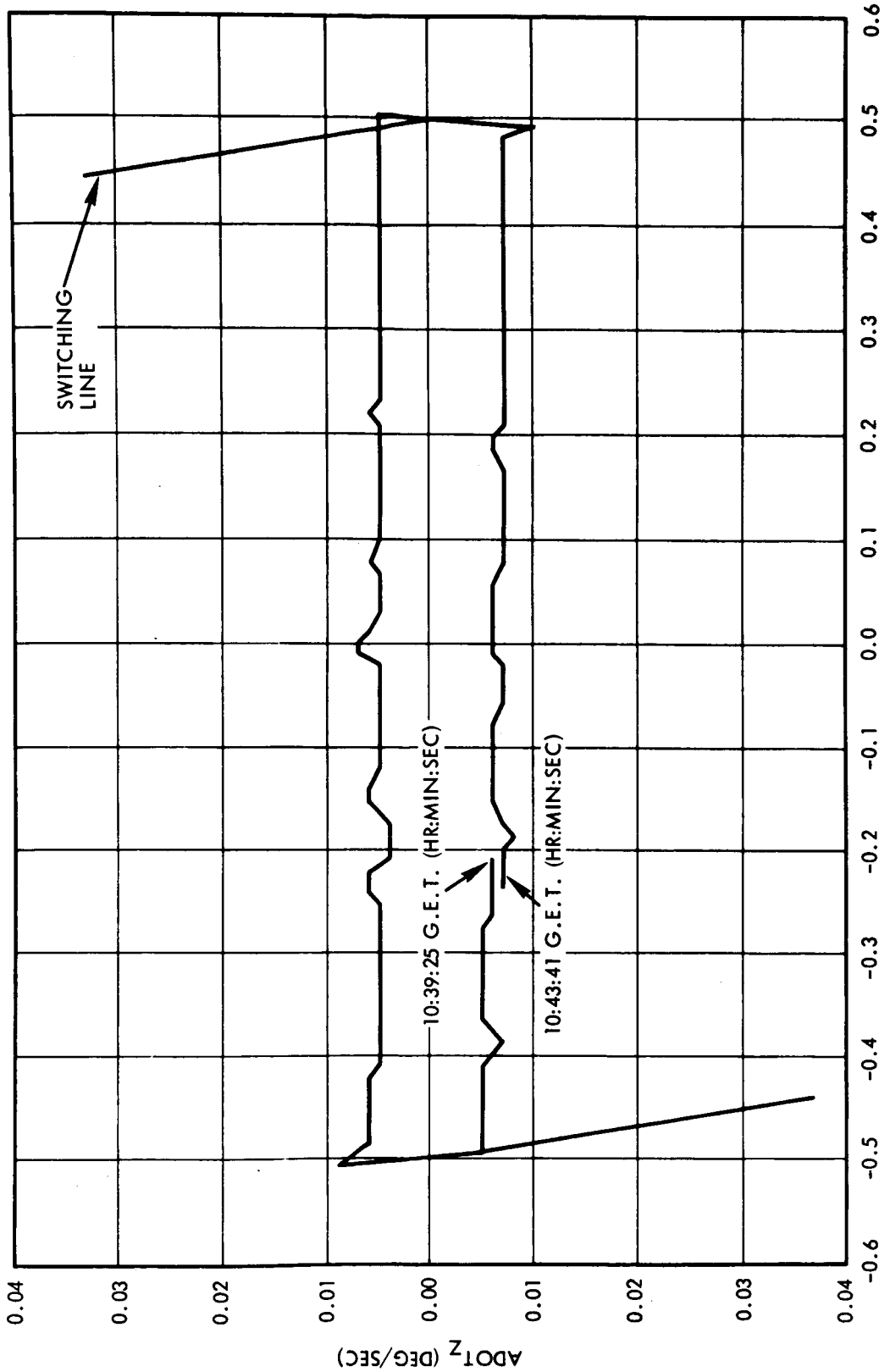

Figure 5-13. DAP Attitude Hold -Z Axis (Narrow Deadband)

6.0 PASSIVE THERMAL CONTROL

Three periods of passive thermal control were examined. Coning angles during the periods are shown in Figures 6-1, 6-2 and 6-3. Cone angle is defined as the deviation of the spacecraft X axis from the PTC initialization direction. The figures present cone angle (radial coordinate) as a function of roll angle.

Figure 6-1 shows the coning angles during PTC initiated at g.e.t. 11 hr 13 min 14 sec. Prior to initiation of PTC, the SCS was configured in the minimum impulse mode in all axes at g.e.t. 11 hr 5 min 57 sec and g.e.t. 11 hr 13 min 14 sec, a large number of pitch and yaw jet firings were executed in an attempt to null pitch and yaw body rates. PTC roll rate was introduced by five minus roll axis firings between g.e.t. 11 hr 13 min 38 sec and 11 hr 13 min 40 sec.

Between twenty and thirty minutes after initiation of PTC, the coning angle reached a maximum value of 27-1/2 degrees. Twenty-seven pitch and yaw axis firings were made during the interval to bring the X axis to the PTC orientation. However, rates were not nulled as the X axis approached PTC attitude and the coning angle rapidly diverged to over 95 degrees. A large number of pitch and yaw axis firings was again required to bring the X axis to PTC attitude. SCS attitude hold in pitch and yaw was initiated 2745 seconds after start of PTC.

An additional period of PTC with the SCS in the minimum impulse mode in all axes was attempted beginning at g.e.t. 112 hr 17 min 15 sec and coning angles during the period are shown in Figure 6-2. During the 40 minute period the coning angle reached a maximum value of 17.2 degrees and ninety-four minimum impulse firings were required to maintain PTC attitude.

In contrast to PTC attempted with the SCS in minimum impulse mode in all axes, coning angles for PTC with the SCS in maximum deadband high rate attitude hold in pitch and yaw are shown in Figure 6-3. This mode was employed for PTC during most of the flight apparently as consequence of the difficulty of maintaining PTC attitude in the SCS free mode.

The excessively large numbers of minimum impulse firings during PTC with the pitch and yaw axes in the minimum impulse mode will be of interest for RCS budgeting and mission planning. The large number of firings required to maintain PTC attitude in the SCS minimum impulse mode and the apparent difficulty of maintaining PTC attitude in this mode indicates that the SCS free drift mode has little or no advantage over the SCS attitude hold in pitch and yaw mode for passive thermal control.

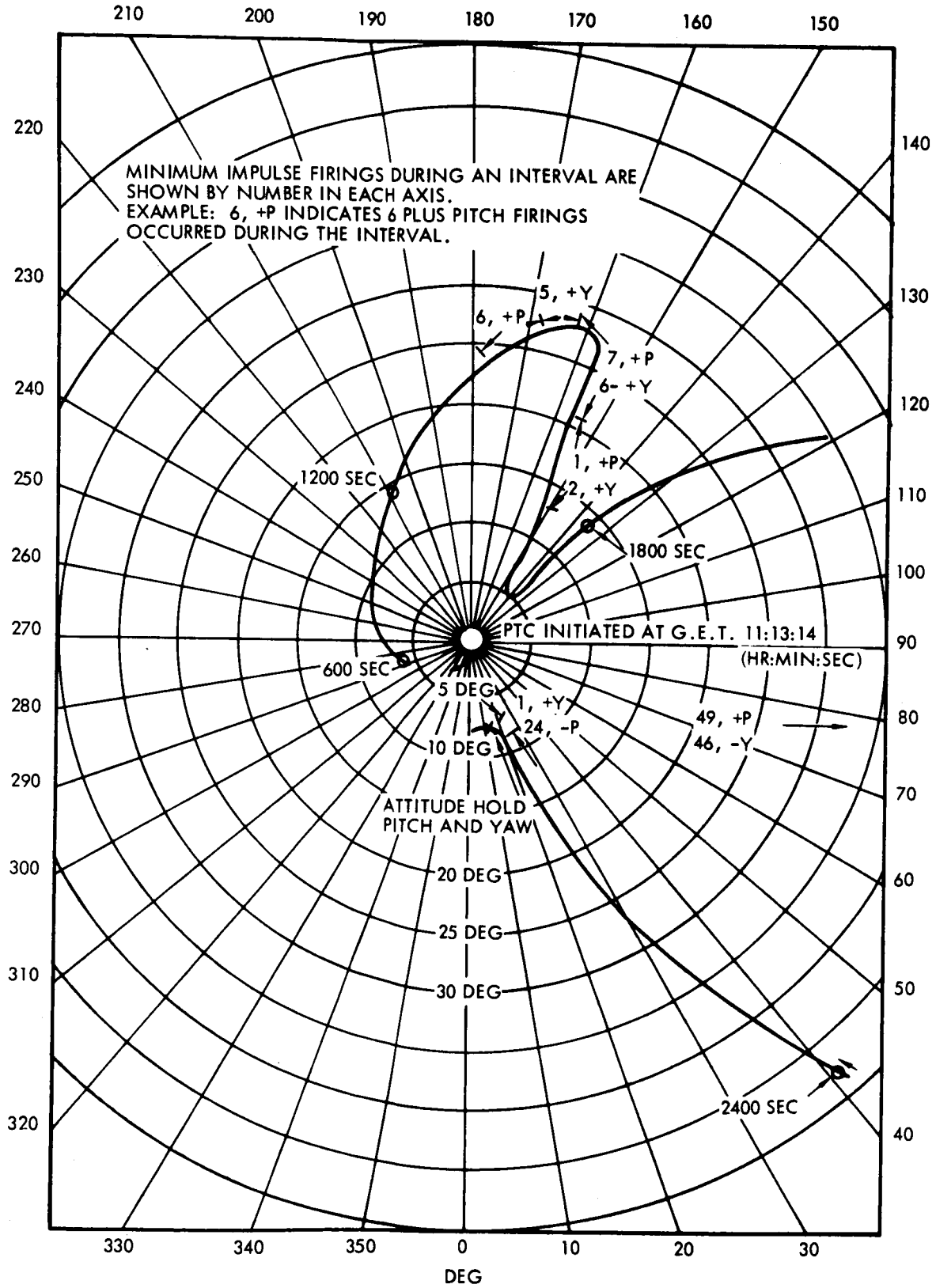

Figure 6-1. Coning Angles During PTC, Pitch and Yaw Axes Free

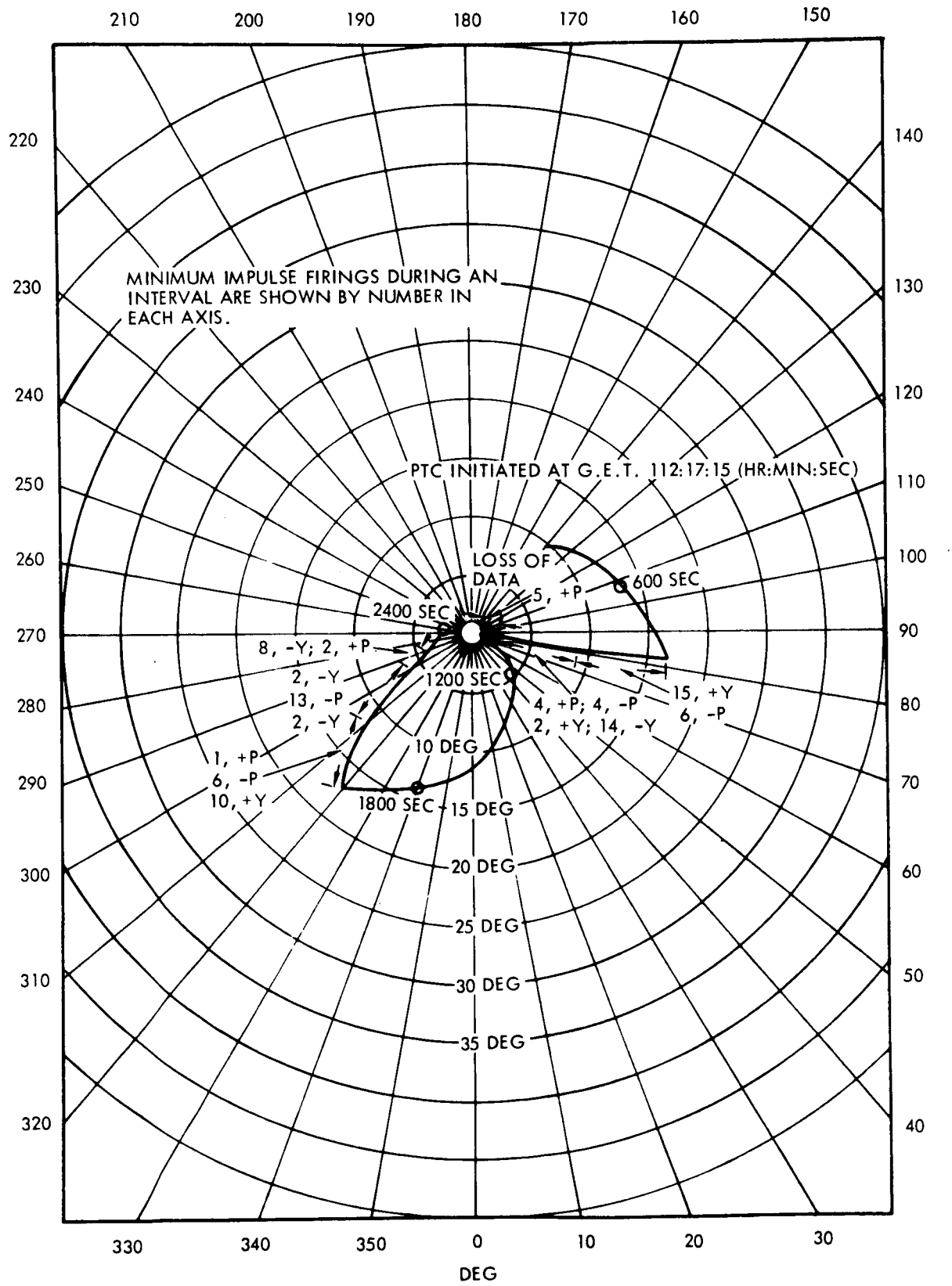

Figure 6-2. Coning Angles During PTC, Pitch and Yaw Axes Free

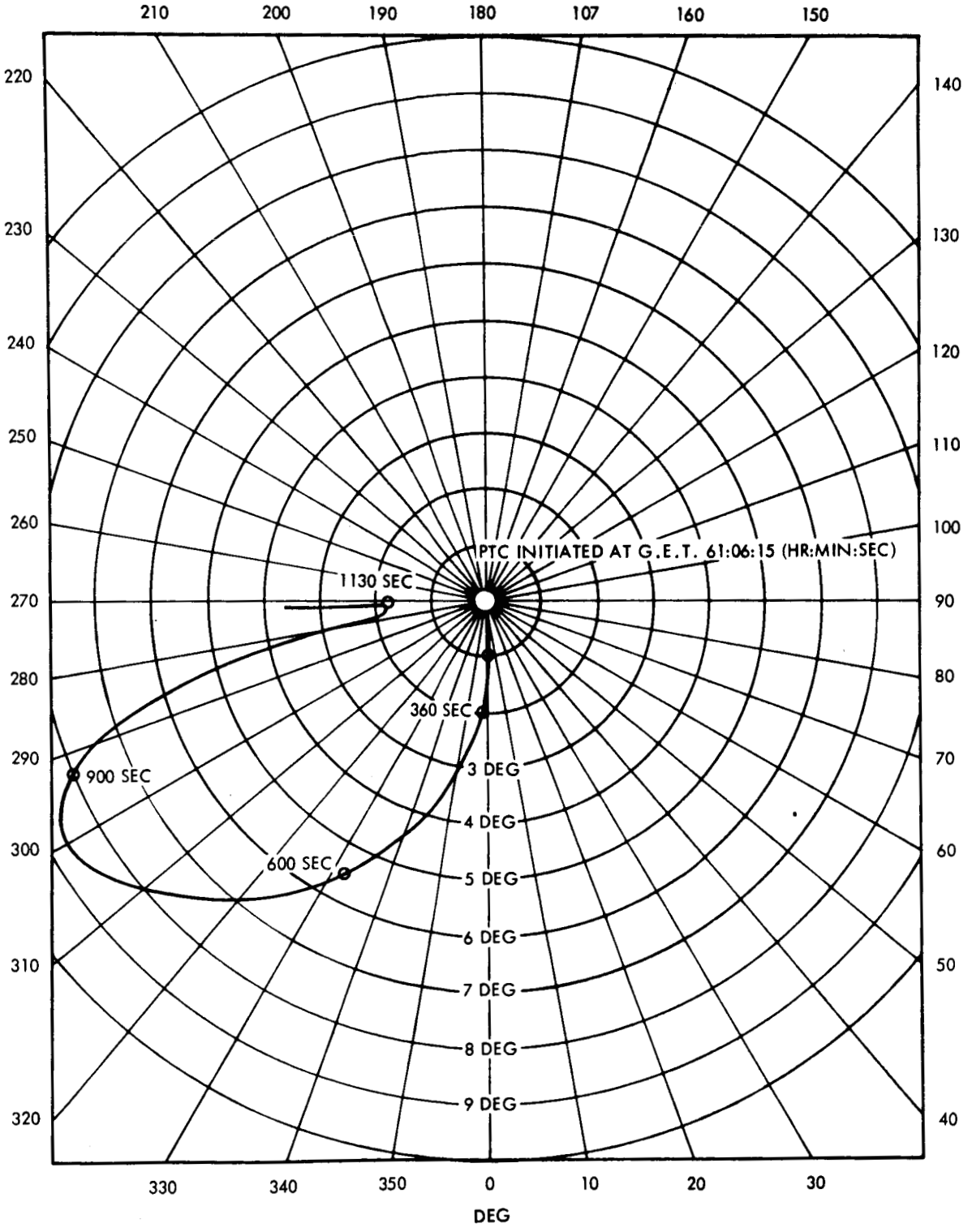

Figure 6-3. Coning Angles During PTC, Pitch and Yaw Axes Maximum Deadband, High Rate Attitude Hold

7.0 ONBOARD NAVIGATION/OPTICS

7.1 MIDCOURSE NAVIGATION

Star/horizon measurements were accomplished on Apollo 8 during the translunar and transearth mission phases. Both the earth and lunar horizons were used and in addition the sightings were made on both the near horizon and the far horizon of the body being viewed. Earth horizon data were evaluated for measurements obtained from geocentric attitudes of ≈20,000 n mi to ≈167,000 n mi. Lunar horizon data were evaluated for measurements obtained from lunar altitudes of ≈5500 n mi to ≈122,500 n mi.

Star/earth horizon measurement data indicated a mean bias error of 0.003 degrees and a random error of:

$$\text{Near earth horizon/star} = 0.007^{\circ}\ (1\sigma)$$
$$\text{Far earth horizon/star} = 0.004^{\circ}\ (1\sigma)$$

The earth horizon data included an earth horizon bias compensation value of 59,055 ft or 9.7 nautical miles.

Star/lunar horizon measurement data indicated a mean bias error of -0.022° and a random error of:

$$\text{Near lunar horizon/star} = 0.015^{\circ}\ (1\sigma)$$
$$\text{Far lunar horizon/star} = 0.006^{\circ}\ (1\sigma)$$

No lunar horizon bias compensation was used in determination of residuals.

The mean error on the earth horizon measurements is probably attributable to error in the assumed horizon bias and vehicle state vector errors. The mean error on the lunar sightings appears high and an error in the assumed lunar radius for each sighting is suspected. Studies are continuing to determine whether or not a mean lunar bias exists.

The random errors are considered to fall in the range of 0.004° to 0.007°. The lunar near horizon error is considered questionable due to large numbers of suspected invalid data points in that sample. The 0.004° to 0.007° range is a reasonable error and is equivalent to a 1.3 to 2.4 sigma number relative to the MEI 201-5000 specification value of 0.003°.

For the transearth star/horizon measurements, studies are being conducted wherein the measurements are to be incorporated post flight into onboard vehicle state vectors and the trajectories propagated to entry interface. Preliminary results indicate the onboard state vectors were sufficiently accurate after measurement incorporation that the CMC could have autonomously guided the spacecraft to a safe entry.

The star brightness appeared to have some affect on the measurement accuracy. Accuracy of the measurements on stars brighter than 1.5 magnitude improved by a factor of two over measurements on dimmer stars. At the same time a deterioration of RMS residuals occurred over the last five batches of data by about the same factor of two and may possibly be a measure of fatigue on the part of the astronaut.

Analysis of the star/horizon measurements was accomplished by determining the differences between the actual onboard measurements and calculated measurements (measured minus computed) using the TRW Program HOPE. HOPE is a second generation Editing and Special Perturbation Oribt Determination (ESPOD) Program which can generate dummy data from onboard optic instruments based on the input trajectory. The trajectory is a best fit least squares trajectory which is derived from input data derived from ground based sensors and onboard instruments using the TRW NAT Program.

The data were processed by taking a NAT state vector just prior to the start of a batch of measurements and propagating it by use of HOPE over the time interval required to complete the batch of measurements. At each mark time a computed trunnion angle was differenced with the measured trunnion angle and the residuals tabulated. Table 7-1 is a list of star/horizon sightings in chronological order by batches with time of mark, horizon identification, star number, brightness and distance from the earth for the first mark.

There are several ways of looking at the data in Table 7-1. For instance the first batch of data indicates an RMS residual of 0.008 degrees. The remainder of the translunar data, without regard to the body being sighted, (through batch 6) indicates an RMS residual of 0.003 degrees. Transearth data (batch 7 through batch 12) indicates an RMS residual of 0.004 degrees. The remainder of the data (batch 13 through batch 17) gives an RMS residual of 0.013 degrees.

The sightings on star number 1 contained in batch 7 are far out of line with the rest of the data taken during that batch. Perhaps a wrong star was used for the six marks. The RMS residual for the six marks identified as star 1 is 0.028 degrees. These six data points were not used to compute the RMS residuals quoted in the preceding paragraph. In batch 14 the same star indicated residuals of about the same magnitude; however, other residuals were also larger than those noted before and after batch 7.

For all measurements evaluated, the star brightness was anywhere from -1.6 magnitude to 2.8 magnitude. The -1.6 magnitude star is Sirius, the brightest navigational star and the 2.8 magnitude star was Menkar, approximately one/fifty-eighth (1/58) the brightness of Sirius. From the data evaluated, it appears that the accuracy of the measurement is somewhat a function of the star brightness; viz, RMS residual of 154 sightings on stars of magnitude less than 1.5 is 0.006 while RMS residuals of 63 sightings on stars of magnitude greater than 1.5 is 0.011.

7.2 LUNAR LANDMARK TRACKING

A lunar landmark tracking study was conducted under Task E-72 A Navigation Analysis. The results of the study indicate that the RMS residual noise is the same for both the sextant and the scanning telescope, 0.6 mr per axis. Using the sightings postflight a landmark location was derived for each set of sightings. The RMS change in landmark locations was 2000 ft in latitude, 1600 ft in longitude and 2390 ft in altitude. (Where the first location was the CMC solution based on the first mark.) A procedural error resulted in the marks being obtained with less than the recommended 20 seconds of separation between marks. The average time separation was 12 seconds. The closeness of the measurements would have had an effect on the accuracy of the sightings and these results may not be totally representative of onboard navigation capability. A more detailed presentation

of the methods used and the data processed are presented in Reference 2.

Rather than repeat the study conducted for Task E-72A, the Task E-38 effort consisted of using the TRW HOPE Program to provide a completely independent check on the landing site coordinates established by E72 studies. The excellent agreement between the two programs lends credence to the results of both studies.

On a revolution by revolution basis the differences (HOPE - Reference 2) in the two program results are as follows:

LANDMARK B1 (LANDING SITE)

	Δ Latitude	Δ Longitude	Δ Altitude
Revolution 5	-.001 deg	+.004 deg	+ 800 ft
Revolution 6	-.003 deg	-.007 deg	- 50 ft
Revolution 7	+.006 deg	+.007 deg	+ 135 ft

*1 degree is approximately 16 n mi.

TABLE 7-1

STAR-HORIZON SIGHTINGS

OBSERVATION TIME GMT TIME (day/Hr/min/sec)	BODY	HORIZON	MEASUREMENT ERROR	STAR NUMBER	STAR MAGNITUDE	APPROXIMATE GEOCENTRIC ALTITUDE (NM)
BATCH #1						
21/18/49/35.57	Earth	Far	.009	S13	-1.6	24,000
53/35.72			.004	S13	-1.6	
56/34.65			.007	S13	-1.6	
19/01/1.04			.007	S14	0.5	
03/27.35			.004	S14	0.5	
38/42.23			.006	S13	-1.6	
40/16.89			- .001	S13	-1.6	
43/35.26			.003	S13	-1.6	
47/51.44			.018	S14	0.5	
49/23.40			.010	S14	0.5	
51/23.00			.008	S14	0.5	
BATCH #2						
22/06/25/54.8	Earth	Far	.001	S14	0.5	79,000
31/5.510			.002	S14	0.5	
35/52.87			.004	S14	0.5	
39/15.240			.003	S14	0.5	
42/20.82			.006	S14	0.5	
44/20.25			.003	S14	0.5	
46/39.85			.001	S14	0.5	
49/19.99			.004	S14	0.5	
51/33.98			.002	S14	0.5	
55/35.61			- .003	S18	1.3	
57/53.87			.002	S18	1.3	
07/00/58.71			.001	S18	1.3	
03/41.69			.004	S18	1.3	
06/29.83			.002	S18	1.3	
BATCH #3						
22/17/16/34.39	Earth	Far	.003	S14	0.5	114,000
19/5.83			.001	S14	0.5	
21/21.65			.001	S14	0.5	
24/7.37			.001	S14	0.5	

TABLE 7-1

STAR-HORIZON SIGHTINGS (Continued)

OBSERVATION TIME GMT TIME (day/hr/min/sec)	BODY	HORIZON	MEASUREMENT ERROR	STAR NUMBER	STAR MAGNITUDE	APPROXIMATE GEOCENTRIC ALTITUDE (NM)
26/12.25			- .001	S14	0.5	
28/21.21			- .001	S14	0.5	
32/7.31	Earth	Far	.005	S18	1.3	
34/52.42			.003	S18	1.3	
37/34.19			.003	S18	1.3	
39/44.26			.002	S18	1.3	
41/14.25			.004	S18	1.3	
43/7.4			.003	S18	1.3	
46/51.13			.002	S17	2.2	
50/3.61			.005	S17	2.2	
53/7.29			.003	S17	2.2	
BATCH #4						
23/01/21/15.63	Earth	Near	- .004	S22	1.2	135,000
23/25.60			.000	S22	1.2	
25/31.37			- .002	S22	1.2	
28/34.24			- .002	S22	1.2	
30/5.65			- .002	S22	1.2	
32/22.62			0	S22	1.2	
36/56.22	Earth	Far	.001	S14	0.5	
39/2.53			.001	S14	0.5	
40/58.33			.001	S14	0.5	
BATCH #5						
23/09/53/47.11	Moon	Near	.007	S27	1.2	155,000
57/21.43			.004	S27	1.2	
10/01/40.02			- .002	S27	1.2	
10/12.29	Moon	Far	- .003	S28	1.9	
12/45.05			- .004	S28	1.9	
15/10.51			- .005	S28	1.9	
18/8.67			.001	S28	1.9	
22/29.48			- .004	S28	1.9	
26/40.66			- .003	S28	1.9	
31/12.47	Moon	Near	- .001	S32	0.9	
33/21.24			.001	S32	0.9	
35/49.23			- .001	S32	0.9	

TABLE 7-1

STAR-HORIZON SIGHTINGS (Continued)

OBSERVATION TIME GMT TIME (day/hr/min/sec)	BODY	HORIZON	MEASUREMENT ERROR	STAR NUMBER	STAR MAGNITUDE	APPROXIMATE GEOCENTIRC ALTITUDE (NM)
38/17.11			0	S32	0.9	
39/49.99			- .004	S32	0.9	
41/57.82			.003	S32	0.9	
BATCH #6						
23/16/58/59.81	Moon	Near	.005	S27	1.2	169,000
17/1/23.59			.002	S27	1.2	
3/25.26			.003	S27	1.2	
6/32.02			.001	S27	1.2	
8/16.2			.001	S27	1.2	
10/1.44			.007	S27	1.2	
12/26.451			.004	S27	1.2	
14/31.59			.006	S27	1.2	
17/34.770			.001	S27	1.2	
23/10.27	Moon	Far	.003	S28	1.9	
25/24.21			- .002	S28	1.9	
27/53.82			.002	S28	1.9	
31/51.91	Moon	Near	- .004	S32	0.9	
35/4.64			- .006	S32	0.9	
37/30.44			.008	S32	0.9	
BATCH #7						
25/07/25/23.7	Moon	Near	.032	S01	2.1	200,000
28/11.05			.026	S01	2.1	
31/5.72			.026	S01	2.1	
34/37.96			.028	S01	2.1	
37/25.20			.022	S01	2.1	
40/44.21			.030	S01	2.1	
45/35.79			- .009	S02	2.2	
48/38.45			- .006	S02	2.2	
50/18.23			- .001	S02	2.2	
52/47.78			- .004	S02	2.2	
55/27.43			.001	S02	2.2	
57/49.49			.002	S02	2.2	

TABLE 7-1

STAR-HORIZON SIGHTINGS (Continued)

OBSERVATION TIME GMT TIME (day/hr/min/sec)	BODY	HORIZON	MEASUREMENT ERROR	STAR NUMBER	STAR MAGNITUDE	APPROXIMATE GEOCENTRIC ALTITUDE (NM)
BATCH #8						
25/17/05/42.28	Moon	Near	.004	S02	2.2	177,000
07/23.80			- .001	S02	2.2	
09/17.59			0	S02	2.2	
12/14.71			.002	S02	2.2	
13/44.51			0	S02	2.2	
16/2.77			.001	S02	2.2	
19/10.94	Moon	Far	- .010	S07	2.8	
21/55.12			- .005	S07	2.8	
24/32.43			- .005	S07	2.8	
27/31.42	Moon	Near	.006	S01	2.1	
29/33.80			.004	S01	2.1	
31/44.01			.004	S01	2.1	
BATCH #9						
25/22/11/5.27	Earth	Far	- .001	S18	1.3	164,000
13/14.27			.003	S18	1.3	
15/15.36			.001	S18	1.3	
17/48.90			.000	S18	1.3	
19/22.28			.001	S18	1.3	
21/28.37			.001	S18	1.3	
25/33.34	Earth	Near	- .004	S22	1.2	
31/34.01			- .001	S22	1.2	
34/17.77			- .005	S22	1.2	
38/13.44			- .005	S25	0.2	
39/31.52			- .003	S25	0.2	
41/0.52			- .004	S25	0.2	
43/24.60			- .003	S25	0.2	
44/34.67			- .001	S25	0.2	
46/5.57			.002	S25	0.2	
BATCH #10						
25/23/04/35.910	Moon	Near	- .006	S02	2.2	162,000
06/12.44			- .007	S02	2.2	
08/7.33			- .004	S02	2.2	
12/8.64	Moon	Far	- .004	S09	1.1	
13/51.03			- .007	S09	1.1	

TABLE 7-1

STAR-HORIZON SIGHTINGS (Continued)

OBSERVATION TIME GMT TIME (day/hr/min/sec)	BODY	HORIZON	MEASUREMENT ERROR	STAR NUMBER	STAR MAGNITUDE	APPROXIMATE GEOCENTRIC ALTITUDE (NM)
15/45.610			- .002	S09	1.1	
BATCH #11						
26/01/25/38.85	Earth	Far	- .001	S18	1.3	156,000
27/36.11			.001	S18	1.3	
29/27.12			- .001	S18	1.3	
35/3.31	Earth	Near	- .002	S22	1.2	
36/45.14			.006	S22	1.2	
38/45.28			- .002	S22	1.2	
41/20.72			.004	S22	1.2	
44/19.96			- .001	S22	1.2	
46/13.29			- .001	S22	1.2	
50/3.67			.000	S25	0.2	
55/6.99			.000	S25	0.2	
56/17.83			.000	S25	0.2	
57/56.78			- .003	S25	0.2	
59/30.76			- .003	S25	0.2	
02/01/5.42			- .003	S25	0.2	
BATCH #12						
26/02/23/15.91	Moon	Near	- .003	S02	2.2	154,000
28/10.47			- .002	S02	2.2	
29/38.55			- .003	S02	2.2	
31/20.01			- .001	S02	2.2	
32/23.81			- .008	S02	2.2	
33/50.93			- .004	S02	2.2	
36/14.52	Moon	Far	- .003	S09	1.1	
38/34.20			- .009	S09	1.1	
40/21.10			- .012	S09	1.1	
43/21.10			- .006	S09	1.1	
45/21.04			- .004	S09	1.1	
46/34.90			- .006	S09	1.1	

TABLE 7-1

STAR-HORIZON SIGHTINGS (Continued)

OBSERVATION TIME GMT TIME (day/hr/min/sec)	BODY	HORIZON	MEASUREMENT ERROR	STAR NUMBER	STAR MAGNITUDE	APPROXIMATE GEOCENTRIC ALTITUDE (NM)
BATCH #13						
26/12/56/51.55	Earth	Far	.007	S18	1.3	124,000
59/5.99			.009	S18	1.3	
13/0'/43.46			.007	S18	1.3	
31/ .36			.007	S18	1.3	
04/ 2.07			.007	S18	1.3	
05/14.17			.006	S18	1.3	
07/38.92	Earth	Near	-.013	S22	1.2	
08/51.90			-.009	S22	1.2	
10/59.76			-.012	S22	1.2	
12/37.90			-.009	S22	1.2	
14/31.290			-.011	S22	1.2	
17/2.44			-.012	S22	1.2	
20/25.23			.011	S25	0.2	
22/04.15			.010	S25	0.2	
23/25.65			.009	S25	0.2	
BATCH #14						
26/15/49/12.30	Moon	Near	-.025	S02	2.2	115,000
51/4.04			-.028	S02	2.2	
52/29.21			-.028	S02	2.2	
54/12.35			-.028	S02	2.2	
56/22.69			-.030	S02	2.2	
57/21.69			-.031	S02	2.2	
16/00/48.96			.019	S01	2.1	
03/7.38			.020	S01	2.1	
04/16.93			.020	S01	2.1	
BATCH #15						
26/16/27/20.27	Earth	Far	.007	S18	1.3	113,000
29/19.97			.006	S18	1.3	
30/54.52			.004	S18	1.3	
32/27.10			.006	S18	1.3	
34/23.34			.005	S18	1.3	
36/15.28			.005	S18	1.3	

TABLE 7-1

STAR-HORIZON SIGHTINGS (Continued)

OBSERVATION TIME GMT TIME (day/hr/min/sec)	BODY	HORIZON	MEASUREMENT ERROR	STAR NUMBER	STAR MAGNITUDE	APPROXIMATE GEOCENTRIC ALTITUDE (NM)
38/42.71	Earth	Near	- .013	S22	1.2	
39/55.05			- .011	S22	1.2	
41/0.22			- .010	S22	1.2	
44/18.24			.007	S25	0.2	
46/20.43			.005	S25	0.2	
47/42.27			.007	S25	0.2	
49/23.53			.010	S25	0.2	
51/22.34			.008	S25	0.2	
52/50.63			.008	S25	0.2	
BATCH #16						
26/22/43/09.51	Moon	Near	- .021	S02	2.2	91,000
47/3.63			- .018	S02	2.2	
48/58.31			- .020	S02	2.2	
52/7.01			.009	S01	2.1	
54/0.80			.013	S01	2.1	
55/41.96			.010	S01	2.1	
57/18.59			.011	S01	2.1	
58/40.01			.009	S01	2.1	
23/00/22.62			.009	S01	2.1	
BATCH #17						
26/23/16/52.72	Earth	Far	.009	S18	1.3	89,000
18/27.05			.007	S18	1.3	
19/49.69			.013	S18	1.3	
21/21,83			.012	S18	1.3	
22/55.93			.010	S18	1.3	
24/34.49			.011	S18	1.3	
28/1.14	Earth	Near	- .013	S22	1.2	
29/31.46			- .015	S22	1.2	
31/2.58			- .011	S22	1.2	
32/19.24			- .015	S22	1.2	
33/42.02			- .012	S22	1.2	
35/29.38			- .013	S22	1.2	
39/8.85			.005	S25	1.2	
40/39.32			.005	S25	1.2	
42/2.95			.004	S25	1.2	

TABLE 7-1

STAR-HORIZON SIGHTINGS (Continued)

OBSERVATION TIME GMT TIME (day/hr/min/sec)	BODY	HORIZON	MEASUREMENT ERROR	STAR NUMBER	STAR MAGNITUDE	APPROXIMATE GEOCENTRIC ALTITUDE (NM)
44/4.87			.003	S25	1.2	
46/13.36			.006	S25	1.2	
48/1.99			.004	S25	1.2	

8.0 ENTRY EVALUATION

This section presents results of an evaluation of the performance of the entry digital autopilot (DAP) and Entry Monitor System (EMS) during the Apollo 8 Mission. Data of interest for this postflight analysis were obtained from the onboard Data Storage Equipment (DSE). This information consists of command module computer (CMC) words and various other measurements, such as gyro display coupler (GDC) body rotation rates.

8.1 ENTRY DAP PERFORMANCE

CM/SM separation occurred approximately 17 minutes prior to entry. After separation the commander manually tracked the horizon with the S/C under SCS minimum impulse control until 146 hrs 45 min 28 sec g.e.t., when S/C control was given to the CMC. For approximately 1 min and 15 sec, attitude hold was maintained in pitch and yaw while the 2 second predictive DAP provided roll axis control. A drag level of .05 g was sensed by the CMC at 146:46:42 g.e.t. and the atmospheric entry DAP assumed control, changing the pitch and yaw functions to rate damping. The DAP remained in control of the S/C throughout the entry phase, using the single "A" ring for all jet firings. Drogue chutes deployment occurred at 146:54:48 g.e.t., and shortly thereafter the entry DAP was disabled by keying in PROCEED on the DSKY.

8.1.1 Preentry Phase - Exoatmospheric Entry DAP

The S/C was under DAP control for approximately 1 min and 15 sec prior to .05 g. During this time the 2 second predictive DAP controlled S/C roll while attitude hold about the desired entry orientation was maintained in pitch and yaw (side-slip angle ≈ 0 and angle of attack ≈ -20 deg). Operation of the exoatmospheric entry DAP appeared nominal; however, little activity was required during this period, because the vehicle was essentially in the desired entry attitude before the CMC assumed S/C control.

8.1.2 Entry Phase (Post .05 g) - Atmospheric Entry DAP

After .05 g, S/C control consisted of the 2 second predictive DAP in roll and rate damping in pitch and yaw. The function of the atmospheric entry DAP is to follow the roll commands issued by entry guidance, while maintaining coordinated roll.

Figure 8-1 presents time histories of roll command and roll angle. They agree closely, indicating that the roll DAP performed as desired.

The conditions for coordinated roll are $\dot{\alpha} = \dot{\beta} = \beta = 0$, where the angles R, β, α specify the transformation from the trajectory triad (TT) coordinate frame to the S/C body system. The TT system is defined as follows:

X_{TT} along negative relative velocity direction $(-\vec{V}_{rel})$

Z_{TT} along $\vec{V}_{rel}$ X$(\vec{r}$ X $\vec{V}_{rel})$ direction (lift up)

Y_{TT} completing the right-handed coordinate set.

The entry DAP computes body rotation rates p, q, and r by differencing gimbal angle measurements every .01 second and resolving the resultant gimbal angle rates along the S/C body axes. If the rotation of the TT system wrt the reference inertial system is neglected; then $\beta = \dot{\beta} = 0$ results in the condition $r = p \tan \alpha$ for coordinated roll. Rotation of the TT system is not negligible at lower speeds, where the effect is seen principally as a change in flight-path angle (Y). Accordingly, DAP computations for coordinated roll incorporate corrections due to TT frame rotations whenever $\dot{Y}$ exceeds .05 deg/sec. The resulting control quantities are denoted by p rel, q rel, and r rel, where q rel is damped to 0 $\pm$ 2 deg/sec and r rel is controlled to within $\pm$ 2 deg/sec of (p rel)(tan α).

At high speeds the CM is so stable that the pitch and yaw rates rarely exceed the 2 deg/sec deadbands, and little RCS activity is seen. For Apollo 8, at vehicle speeds above approximately Mach 2, pitch and yaw jet firings were required only during periods of significant roll jet activity such as roll reversals.

RCS fuel usage during the entry phase of Apollo 8 is summarized in Table 8-1. Pitch and yaw jet firings increased dramatically in the final two minutes before drogue chutes deployment - after the vehicle velocity dropped below approximately Mach 2. This phenomenon has been noted on previous flights. Figure 8-2 illustrates this increased jet activity. Values of GDC and CMC pitch rates are presented for a 7.5 sec time interval. Jet-on times are also shown. Because the CMC p rel, q rel, and r rel are

saved for downlink every .02 sec, only half of the computed rate data is available. Significant differences are seen between the GDC and DAP pitch rate values. These differences arise because the DAP takes account of the rotation of the TT frame, through corrective terms in Y. The time period presented in the figure occurred near the end of the Apollo 8 entry, when Y effects were significant. CDU sampling effects can also contribute to these differences, because the CDU's , for gimbal angle rates above approximately 4 deg/sec,alternate between a high and low following rate. This results in noise on the order of 1 deg/sec. Yaw rate control data resembles that of Figure 8-2 and plots of yaw control activity would be similar to this figure. An additional factor when considering yaw rate damping is the fact that the DAP uses its variable measured value of α in the computation of p rel and r rel and also in the control equation r rel = p rel tan α $\pm$ 2 deg/sec. Summarizing, in the final 2 minutes of entry there is a marked increase in jet activity for pitch and yaw rate damping. Significant differences are seen between GDC and CMC rates. They are attributable to CDU noise and, more significantly, effects of a variable α and $\dot{Y}$ corrections which are used in CMC computations.

Where CMC data are available, all jet firings for pitch and yaw rate control have been verified as occurring when CMC rate measurements were outside the 2 deg/sec control deadbands. While CMC data verifies the correctness of this RCS activity, the number of jet firings was significantly greater than predicted by pre-flight entry simulations. This represents a simulation problem and not a vehicle control problem. Attempts are being made to duplicate this increased jet activity at low Mach numbers by incorporating atmospheric winds data into available entry simulations.

8.2 ENTRY MONITOR SYSTEM

Figure 8-3 presents the EMS G/V trace for Apollo 8. For this mission, the splashdown target range from EI was rather short, approximately 1300 n mi. This range was chosen to insure that entry guidance would not attempt to "skip" the S/C out of the atmosphere and below .05 g after its initial plunge. For maximum safety, the non-exit EMS pattern was chosen for use in Apollo 8, because the skip monitoring lines on this scroll are more conservative than those on the other available EMS pattern (3500 n mi range limiter).

The vehicle G/V profile as computed by the CMC is also presented in Figure 8-3. The two traces agree closely, indicating that the EMS provided an excellent monitor of the S/C entry trajectory.

The G/V trace became tangent to a skipout monitoring line shortly after pullup. This constituted a "violation" of the monitoring lines. In such a situation, the crew is prepared to take over spacecraft control and manually roll the lift vector to 180 degrees (lift down). This action was not required in this instance because the violation occurred at a time when the CMC roll command and vehicle bank angle were already 180 degrees. Such a situation had been seen in pre-flight similations; the crew was aware of this possibility; and they correctly allowed the CMC to continue controlling the spacecraft.

CMC values of target range (THETA) are placed at 10 second intervals beneath the EMS scroll pattern in Figure 8-3. The values are consistent with the range potential lines, shown dashed in the Figure. The S/C commander, in his technical debriefing, commented that when the G/V trace crossed the 50 mile line, the EMS range counter had also counted down to 50, as desired. The CMC value at this time is approximately 35 n mi; however, at low velocities the CMC range is simply a great circle length between two geographic positions, while the range potential lines and counter values are inertial quantities. The consistency that is seen between the EMS and CMC range indicators demonstrates that the EMS could be used with confidence as a backup system for ranging to the splashdown target, if a CMC failure required that the entry phase be controlled manually.

TABLE 8-1

RCS Fuel Consumption for Apollo 8 Entry

Engine	RCS Fuel (lbs) After .05 g	Final 2 Minutes Before Drogues
+ Roll	10.19	
- Roll	11.71	
Total Roll	21.90	
+ Pitch	.76	.73
- Pitch	1.97	1.97
Total Pitch	2.73	2.70
+ Yaw	3.20	2.85
- Yaw	1.32	1.11
Total Yaw	4.52	3.96

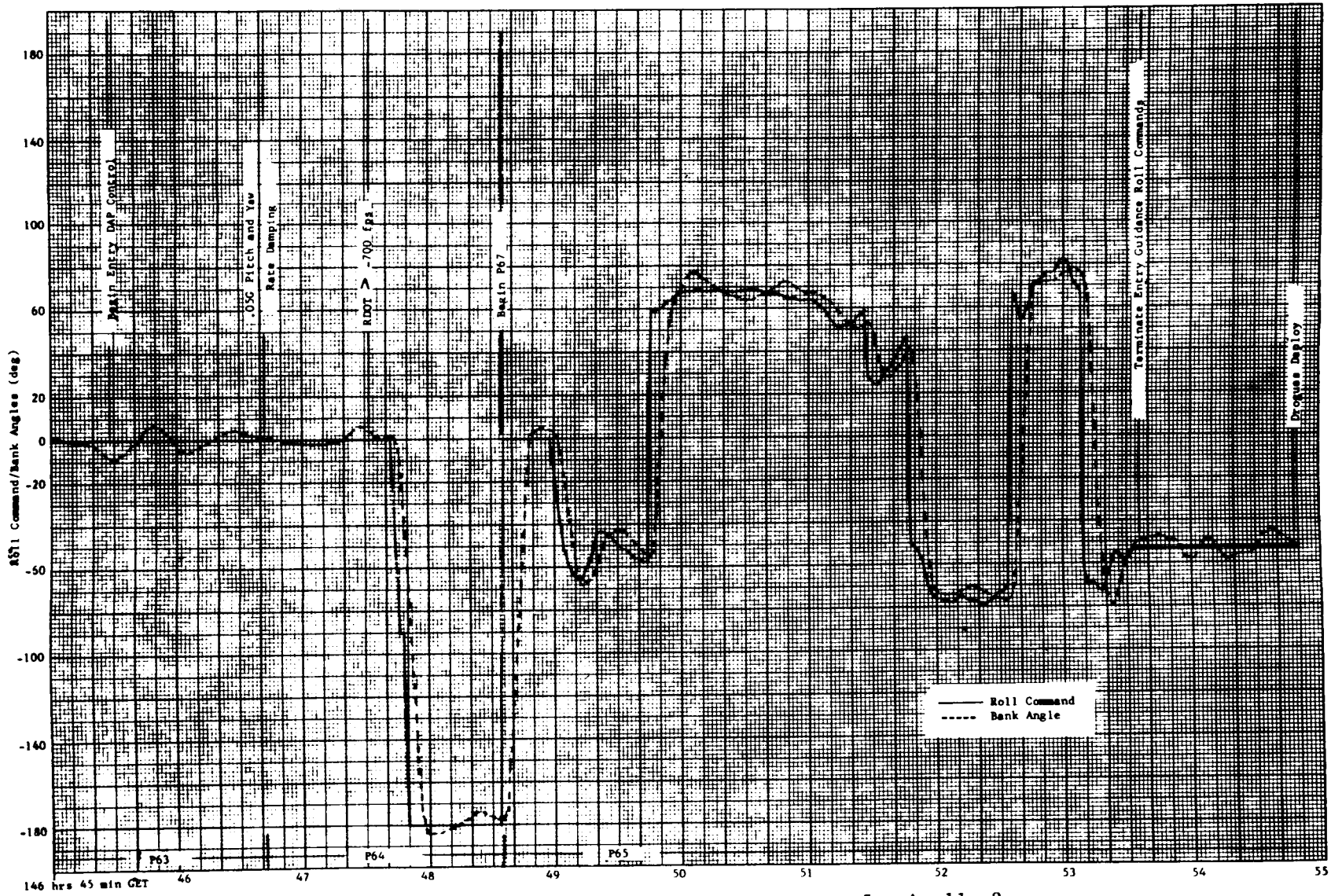

Figure 8-1 Roll Command/Roll Angle Histories for Apollo 8

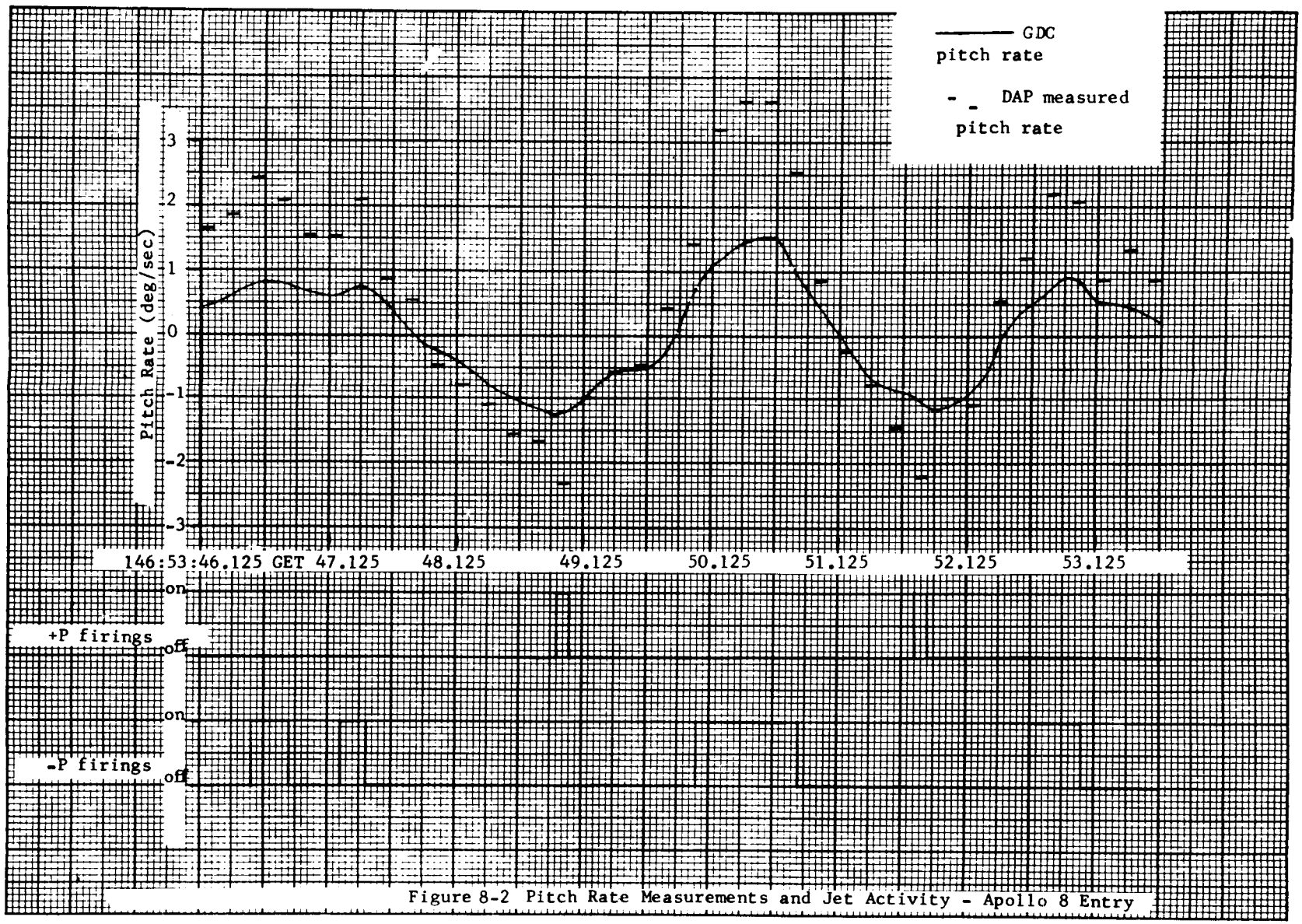

Figure 8-2 Pitch Rate Measurements and Jet Activity - Apollo 8 Entry

FIGURE 8-3 ENTRY MONITOR SYSTEM G/V TRACE FOR APOLLO 8

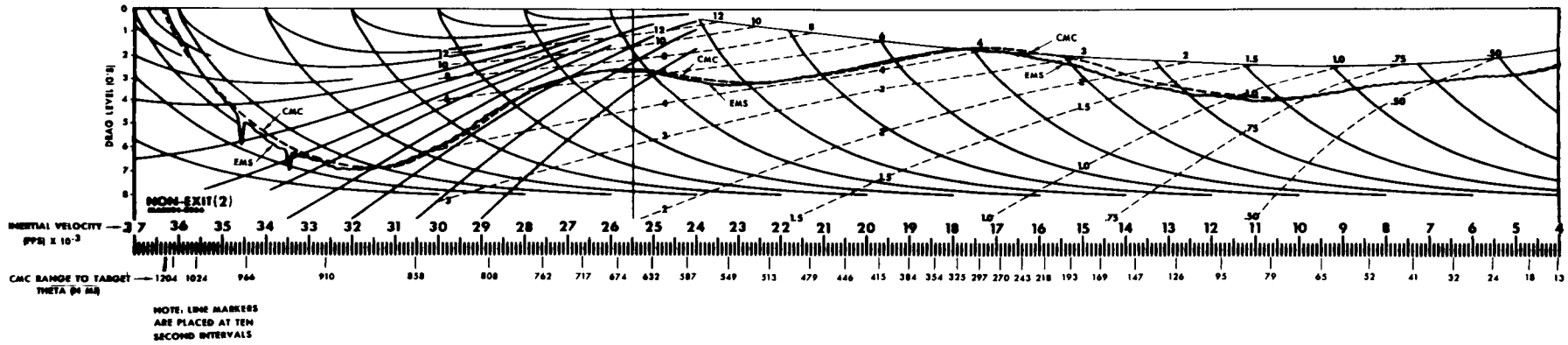

APPENDIX A

ANALYTIC METHODOLOGY

APPENDIX A

METHODOLOGY

1. METHODOLOGY

1.1 Trajectory Reconstruction

There are two available measures of G&N performance which have cardinal significance in the spacecraft (S/C) postflight error analysis. During non-G&N controlled mission phases (GRR and Boost through Coast: S-IVB attached), the measurement of greatest significance is the accuracy with which the S/C IMU and CMC sense and record actual trajectory parameters. During G&N controlled phases, focus shifts to a measure of the accuracy with which targeted trajectory parameters (the nominal trajectory) are attained by the spacecraft. For both situations, reliable knowledge of the actual trajectory is an essential tool. To this end, analysis is centered on a reconstructed, best estimate trajectory (BET). This trajectory was obtained via a working interface between this task and Task A-50 (Trajectory Reconstruction, MSC/MPAD). The reconstruction and related error analysis proceed as follows.

a) Basic Data Processing and EAP

Before trajectory reconstruction or IMU error analysis can be undertaken, the basic data tapes must be edited and processed so that they are compatible with the trajectory computing programs. The configuration for the processing of the basic data sources, and the production of an EAP tape, is shown in Figure A-1 This is a straightforward procedure, and the function of each of the four programs involved is explained in the following subsections.

b) G&N Processor Program

The G&N Processor reads total position, total velocity, incremental PIPA counts, and time ($\vec{P}_T$, $\vec{V}_T$, ΔN, t) from the input CMC telemetry tape. The program editing capability provides for correcting data in individual records, deleting records, inserting new records, and reconstructing lost data by interpolating between the values of $\vec{P}_T$ and $\vec{V}_T$ bounding the specified dropout interval.

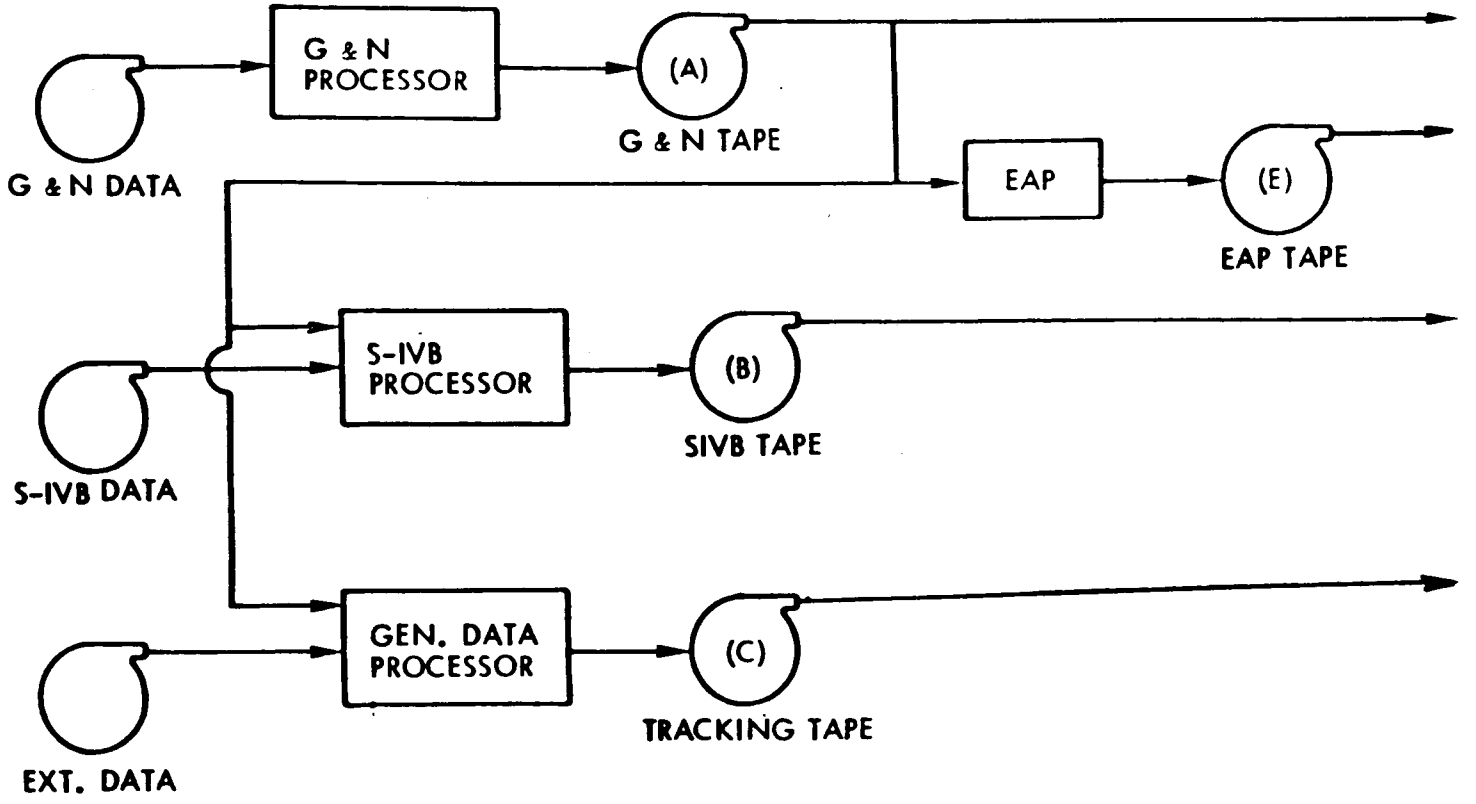

Figure A-1. Configuration for Processing Basic Data Sources

Processing of the edited data proceeds in two phases:

1) Phase I

The incremental PIPA counts, ΔN, are used to compute sensed position, velocity, and acceleration ($\vec{P}_s$, $\vec{V}_s$, $\vec{A}_s$). The desired values of each PIPA scale factor and bias may be loaded into the program for this computation. Total position and velocity are rotated into ECIG coordinates.

2) Update Phase

If desired, a total position and velocity may be specified at any time in the trajectory, and the program will re-compute the trajectory from this "update state vector" and the incremental PIPA counts. This capability is useful for reconstructing short burns. The following quantities are computed:

a) $\vec{P}_T$, $\vec{V}_T$ in G&N coordinates

b) $\vec{P}_T$, $\vec{V}_T$, $\vec{A}_T$ in ECIG coordinates

c) $\vec{G}$ - acceleration due to gravity in G&N coordinates.

c) S-IVB Processor Program

The S-IVB Processor reads sensed velocity and acceleration, total inertial position and velocity, and time

$$\vec{V}_s(\text{S-IVB}),\ \vec{A}_s(\text{S-IVB}),\ P_T(\text{S-IVB}),\ V_T(\text{S-IVB}),\ t(\text{S-IVB})$$

from the S-IVB telemetry tape, and G&N time, T_{GN}, from the G&N coordinate frame and interpolated to the G&N time base. The time history (G&N time) of the following quantities are computed:

1) $\vec{V}_s$, $\vec{A}_s$ in G&N coordinates

2) $\vec{P}_T$, $\vec{V}_T$ in G&N coordinates

3) $\vec{P}_T$, $\vec{V}_T$ in ECIG coordinates

d) General Data Processor Program

The General Data Processor, as used in Apollo postflight evaluation, reads position and velocity (usually RAE or XYZ surface fixed) and time from a tracking data tape,

and G&N time from the G&N processor tape. The tracking data is transformed into a Cartesian coordinate frame and interpolated to the G&N time base. The output tape contains the following trajectories in the G&N time base.

1) Total position, velocity, and acceleration in ECIG coordinates.

2) Position, velocity, and acceleration in the tracking system coordinates.

c) Position, velocity, and acceleration in an ESF coordinate frame (ENU or Downrange-Crossrange-Up).

e) Apollo IMU Error Analysis Program (EAP)

The EAP Program reads sensed acceleration, $\vec{A}_s$, in guidance coordinates, and time, T, from the G&N processor tape. The output program is position and velocity error partial derivatives (in guidance coordinates) with respect to each of 40 IMU error sources. These error sources are defined in Table A-1.

If the guidance coordinates are not coincident with the accelerometer coordinates, $\vec{A}_s$ is rotated into accelerometer coordinates, and acceleration errors, $\partial\vec{A}/\partial e_i$, are computed for each of the 40 error sources, e_i. These acceleration errors are then trapezoidally integrated to obtain velocity and position errors which are rotated back into guidance coordinates and written on the output tape. The values of each e_i are input to any of the programs which employ an EAP output to construct a corrected trajectory.

f) Boost Phase Trajectory Reconstruction

The configuration for computing corrected G&N trajectories, and comparing G&N with other trajectory data is shown below and in Figure A-2.

The Velocity Comparison Program (VELCOMP) corrects the G&N trajectory using the EAP partials and the values of IMU errors input by load sheet. The corrected G&N trajectory is differenced in both sensed and total "coordinates" with either S-IVB or high speed tracking data.

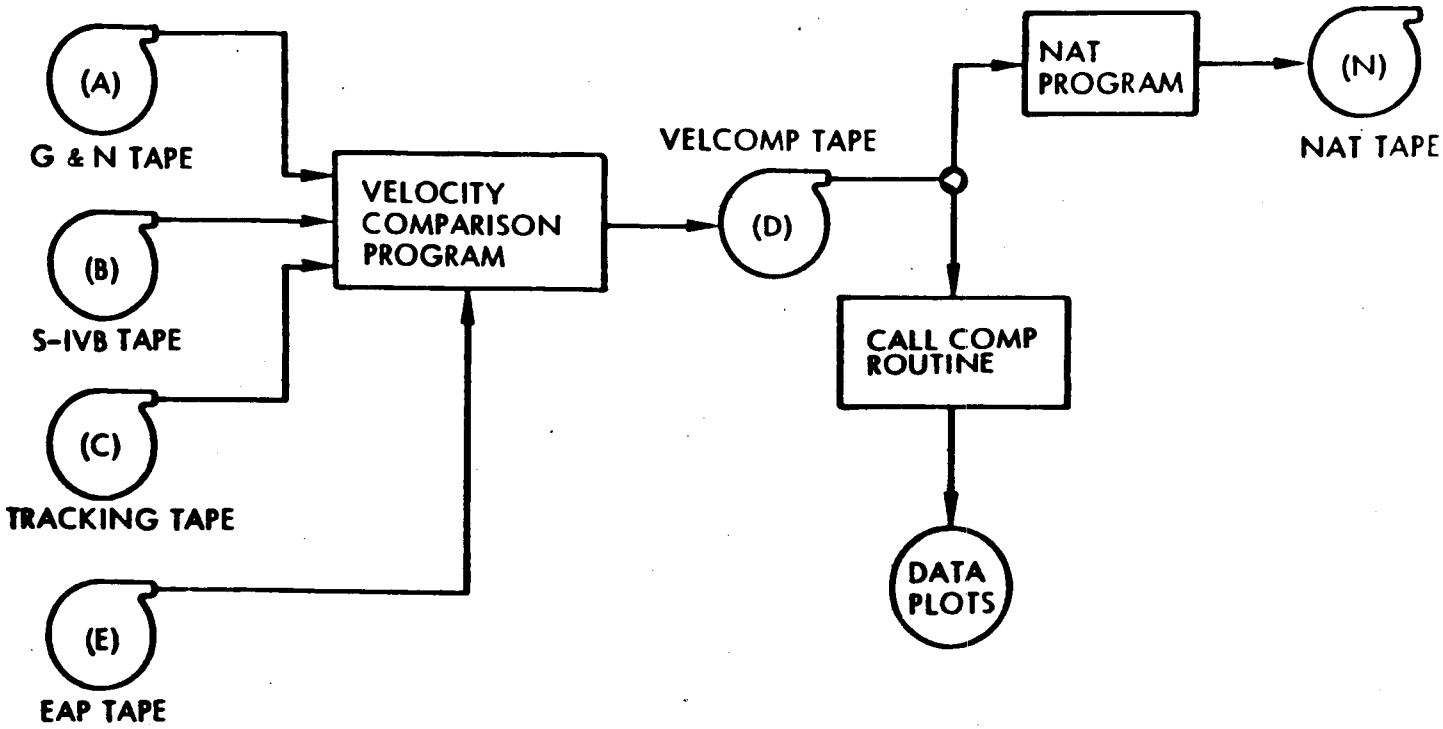

Figure A-2. Configuration for Correcting, Comparing and Analyzing Boost Guidance Data

The configuration of Figure A-2 can also be used to reconstruct burns, provided accurate, high speed position data is available throughout the burn.

The VELCOMP program may be used in several configurations (selected by load sheet options) in correcting and reconstructing the G&N trajectory. The following diagram shows the general configuration.

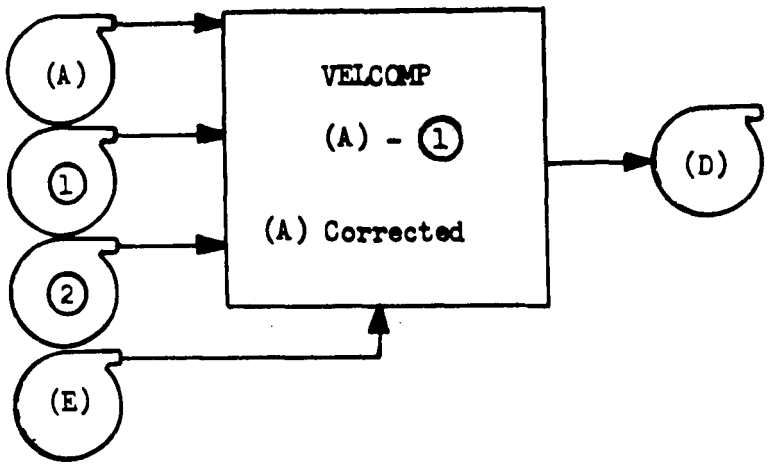

A minimum of two tapes are required as input.

- (A) - Sensed position and velocity and total position and velocity (P_s, V_s, V_T) in G&N coordinates are read from the G&N Processor output.
- ① - The tape ① may be an output from either the S-IVB Processor or the General Data Processor. The program reads total position and velocity in ECIG coordinates from this tape.

Generally, an EAP output, (E), will also be included, in which case the program reads the position and velocity partials for each of the IMU error sources. The values of the errors themselves are input to the VELCOMP program via load sheet.

If neither of the tapes (A) or ① being compared contains accurate position information, another tape, ②, may be input. The program reads total position in ECIG coordinates from this tape and uses this information only in computing the gravity profile.

In the discussion of the computations made by the VELCOMP program, the following notation will be used:

$\vec{P}$, $\vec{V}$ are position and velocity data from the G&N tape;

$T\vec{P}$, $T\vec{V}$ are position and velocity data from tape (1);

M is the matrix which transforms from ECIG to G&N coordinates;

$\vec{P}_I$, $\vec{V}_I$ are initial conditions in ECIG coordinates.

Each of the following quantities are computed and written on the VELCOMP output tape.

Guidance Computations

$$[\delta\vec{P}_s]_{G\&N} = \sum_i \frac{\partial\vec{P}_s}{\partial e_k} e_k$$

$$[\delta\vec{V}_s]_{G\&N} = \sum_i \frac{\partial\vec{V}_s}{\partial e_k} e_k$$

Gravity Profile

$[\vec{P}_G, \vec{V}_G, \vec{A}_G]_{ECIG}$ - These quantities are computed from total position data on any of the tapes, (A), (1), (2), for any specified segment of the trajectory. The gravity model assumes the Fisher Ellipsoid.

"Tracking" Data (Tape (1)) in Sensed Coordinates

$$[T\vec{P}_S, T\vec{V}_S]_{G\&N} = M \left\{ [T\vec{P}_T, T\vec{V}_T]_{ECIG} - [\vec{P}_G, \vec{V}_G]_{ECIG} - [\vec{P}_I, \vec{V}_I]_{ECIG} \right\}$$

"Tracking" Data (Tape (1)) in Total Coordinates

$$[T\vec{P}_T, T\vec{V}_T]_{G\&N} = M [T\vec{P}_T, T\vec{V}_T]_{ECIG}$$

Sensed Position and Velocity Comparison

Note: Let the compensated G&N data be represented by

$$\vec{P}_s' = \vec{P}_s - \delta\vec{P}_s \qquad \vec{V}_s', \ \vec{V}_s' = \vec{V}_s - \delta\vec{V}_s$$

$$[\Delta\vec{P}_s, \ \Delta\vec{V}_s]_{G\&N} = [\vec{P}_s', \ \vec{V}_s']_{G\&N} - [T\vec{P}_s, \ T\vec{V}_s]_{G\&N}$$

Total Position and Velocity Comparison

Note: "Compensated" total G&N data is defined by

$$\vec{P}_T' = \vec{P}_T - \delta\vec{P}_s \qquad \vec{V}_T' = \vec{V}_T - \delta\vec{V}_s$$

$$[\Delta\vec{P}_T, \ \Delta\vec{V}_T]_{G\&N} = [\vec{P}_T', \ \vec{V}_T']_{G\&N} - [T\vec{P}_T, \ T\vec{V}_T]_{G\&N}$$

Delta of Delta Comparison

$$[\Delta^2\vec{P}, \ \Delta^2\vec{V}]_{G\&N} = [\Delta\vec{P}_T, \ \Delta\vec{V}_T]_{G\&N} - [\Delta\vec{P}_s, \ \Delta\vec{V}_s]_{G\&N}$$

Reconstructed G&N Trajectory

The total corrected G&N trajectory in ECIG coordinates is computed from

$$[\vec{P}_{TC}, \ \vec{V}_{TC}]_{ECIG} = M^{-1}\,[\vec{P}_s', \ \vec{V}_s']_{G\&N} + [\vec{P}_G, \vec{V}_G] + [\vec{P}_I, \ \vec{V}_I]$$

g) Orbital Maneuver Reconstruction

Since continuous (and accurate) high speed tracking is not expected during the orbital maneuvers, the configuration of Figure A-2 cannot be used to compensate and reconstruct the G&N trajectory. The trajectory reconstruction program has the capability of reconstructing an entire G&N trajectory using only sensed velocity (and EAP partials) as an input. The configuration for reconstructing burns (and entry if applicable) is shown in Figure A-3.

If tracking is available over segments of a burn, position and velocity comparisons may be generated with the VELCOMP program using the configuration shown in Figure A-3. The Trajectory Reconstruction Program output (which contains corrected total position

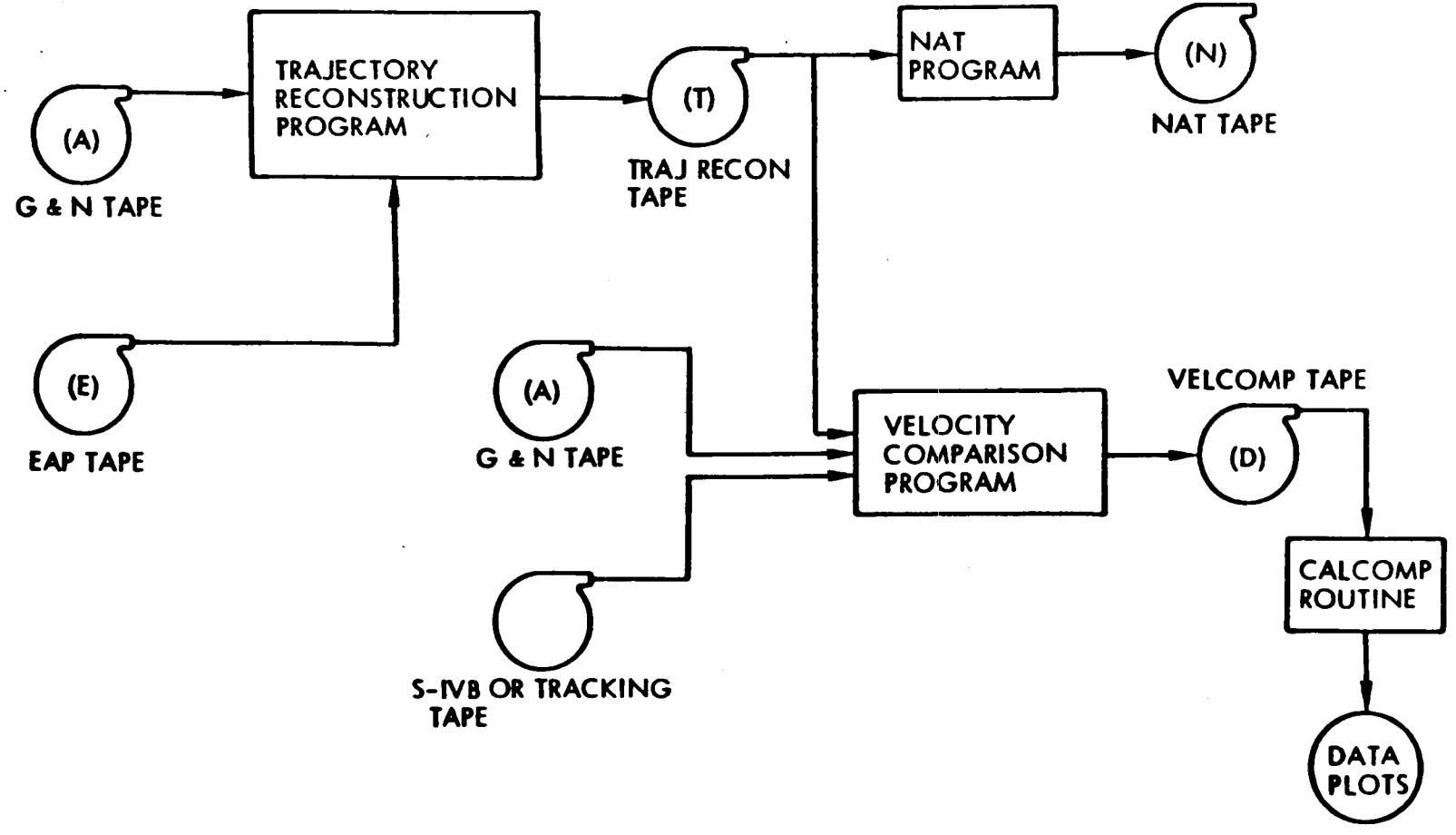

Figure A-3. Configuration for Correcting, Comparing and Analyzing Burn Data

data) is used to generate the gravity profile, and the comparisons are made as explained earlier.

The trajectory reconstruction program utilizes two input tapes: sensed velocity is read from the G&N processor tape; $\partial V_s/\partial e_k$ is read from the EAP tape.

The error magnitudes, e_k, initial position and velocity, P_I and V_I in ECIG coordinates, and the Matrix, M, which transforms from ECIG to G&N coordinates are input to the program via load sheet.

The program output consist of the following quantities:

- P_T V_T A_T in ECIG coordinates. This is the reconstructed trajectory which is computed as follows: The sensed velocity corrections are computes from

$$\delta V_s = \sum_k \frac{\partial V_s}{\partial e_k} e_k$$

Total velocity at time "i" is computed from

$$V_{Ti} = V_I + M^{-1} (V_{Si} - \delta V_{Si}) + V_{Gi}$$

Where $V_{Gi} = V_{Gi-1} + \frac{A_{Gi-1} + A_{Gi}}{2}$ and

$$A_{Gi} = A_{Gi} (P_{Ti-1} \cdots P_{Ti-4})$$

Total position is computed from $P_{Ti} = P_I + \frac{V_{Ti-1} + V_{Ti}}{2} \delta t$

Total acceleration is computed from $A_{Ti} = \frac{V_{ti} - V_{Ti-1}}{\delta t}$

- P_T, V_T rotated into G&N coordinates.
- Several NAT output quantities, viz., Nos. 9, 10, 11, 12, 13, 14, 15, 16, 19, 20, 21, 50 - 55.

h) NAT Program

The NAT (NASA Apollo Trajectory) Program accepts the output tapes from the G&N Processor, VELCOMP Program, Trajectory Reconstruction Program, and ESPOD. The program also accepts input tables of atmospheric data which is used for computation during entry. The output tape contains 112 parameters which are listed in the NAT Index.

1.2 IMU Evaluation

The VELCOMP program was a basic tool used in arriving at a set of "most probable" IMU errors. Trial values of the error quantities were loaded into this program and the output for each trial was examined for conformance with the BET. That set of errors which reduced the "corrected" G&N trajectory residuals to a minimum for all accurate BET intervals was postulated as the most probable set of error values. Prelaunch G&N calibration data provided a source of most probable errors for initial trial values. Subsequent trial errors were selected based upon an examination of the preceding VELCOMP position and velocity residuals (deltas with respect to the BET). A final most probable set of error values was obtained from the earlier estimates using a Kalman filter technique.

The boost phase of any mission is most important for determining IMU errors because acceleration levels are high and good high speed tracking is available. For this reason, comparisons of "corrected" (trial) G&N trajectories with the boost phase BET will yield the most reliable estimates of IMU errors.

2. ESPOD

As will be noted, the principal source referred to for trajectory data during coasting phases of the flight is ESPOD. ESPOD denotes "Editing and Special Perturbation Orbit Determination." This program is a comprehensive model of the principal and perturbing accelerations which act on a vehicle during free fall (non-thrusting, exo-atmospheric flight). As such, it is used to generate a continuous estimate of the free fall trajectory of an orbiting spacecraft based upon radar data and models of the earth's potential field, aerodynamic drag, lunar, solar, and planetary perturbations, and radiation pressure.

Table A-1. IMU Error Sources

Apollo Mnemonic	EAP Mnemonic	Accelerometer Errors	Apollo Mnemonic	EAP Mnemonic	Gyro Errors
ACBX	BX		ADIAX	XADIA	
ACBY	BY	Bias	ADIAY	YADIA	Drift rate sensitivity to acceleration along input axis.
ACBZ	BZ		ADIAZ	ZADIA	
SFEX	XSF		ADSRAX	XADSR	
SFEY	YSF	Scale Factor	ADSRAY	YADSR	Drift rate sensitivity to acceleration along spin axis.
SFEZ	ZSF		ADSRAZ	ZADSR	
NCXX	XQUAD	SF sensitivity to	ADOAX	XADOA	
NCYY	YQUAD	input acceleration	ADOAY	YADOA	Drift rate sensitivity to acceleration along output axis.
NCZZ	ZQUAD	supared.	ADOAZ	ZADOA	
	XYMSL		ADSXX	XIASQ	
	XZMSL	IKMSL is the misalign-	ADSYY	YIASQ	Drift rate sensitivity to
	YXMSL	ment of accelerometer "I"	ADSZZ	ZIASQ	acceleration squared along
	YZMSL	toward the "K" the plat-			the spin reference axis.
	ZXMSL	form axis.			
	XYMSL				
(not modeled)	XICRO	SF sensitivity to coupling	NBDX	XGCDR	
	YICRO	of acceleration along input	NBDY	YGCDR	Constant drift rate
	ZICRO	and output axes (ppm/g)	NBDZ	ZGCDR	
		Platform Errors			
	PHIX				
	PHIX	Platform misalignment			
	PHIZ				
	DT	Timing Error			
	VOX				
	VOY	Velocity Offset			
	VOZ				

REFERENCES

1. TRW Report 11176-H095-R0-00, "Apollo 7 Guidance, Navigation and Control Performance Analysis-Final Report," dated 20 December 1968.

2. TRW Memo 69:7252.2-7, "Preliminary Analysis of Apollo 8 Landmark Optical Sightings," dated 7 February 1969.

3. TRW Report 05952-H546-Ro-00, "Apollo 6 Guidance and Navigation Error Analysis - Final Report," dated 28 June 1968.